Numerical Groundwater Flow and Solute Transport Modelling -

A Case Study of Sardon Catchment in Spain

R. R. G. Ruwan Rajapakse

February, 2009

Numerical Groundwater Flow and Solute Transport Modelling: A Case Study of Sardon Catchment, Spain

by

R. R. G. Ruwan Rajapakse

Thesis submitted to the International Institute for Geo-information Science and Earth Observation in partial fulfilment of the requirements for the degree of Master of Science in Water Resources and Environmental Management, Specialisation: Groundwater Assessment and Management

Thesis Assessment Board

Prof. Dr. Bob Su, ITC (Chair)
Prof. Dr. Okke Batelaan, Vrije Universiteit Brussel (External Examinar)
Dr. Ir. Maciek W. Lubczynski, ITC (1st Supervisor)
Drs. R. Becht, ITC (2nd Supervisor)
MSc. Alain Pascal Francés (Advisor)

INTERNATIONAL INSTITUTE FOR GEO-INFORMATION SCIENCE AND EARTH OBSERVATION
ENSCHEDE, THE NETHERLANDS

Disclaimer

This document describes work undertaken as part of a programme of study at the International Institute for Geo-information Science and Earth Observation. All views and opinions expressed therein remain the sole responsibility of the author, and do not necessarily represent those of the institute.

To my parents and family

Abstract

The fully transient models are data intensive but more reliable in exploring the groundwater flow regimes than steady state models due to spatio-temporal nature of flux input. However even those models suffer non-uniqueness of solutions due to the several possible combinations between fluxes and system parameters. The coupling of solute transport models with flow models enables to explore the complexity of the flow regime better. This study focused to improve the reliability of the existing fully transient flow model in Sardon catchment through: (i) improvement of the model input data set; (ii) validation of the steady state flow model by solute transport model of chloride considered as natural tracer; (iii) recalibration of the fully transient model using improved input data set (the transient solute transport model could not be performed due to insufficient chloride concentration records).

The intensive field tests and processing techniques were used to assess the parameters and fluxes; ADAS data acquisition, borehole drilling , sampling and analysis of chloride in groundwater, forced gradient tracer tests with automated plume monitoring and Electrical Resistivity Tomography (ERT) survey, soil sampling, slug test and differential GPS surveys were performed. The spatio-temporal distribution of groundwater fluxes (recharge and groundwater evapotranspiration) was assessed through pyEARTH-1D model. Chloride Mass Balance (CMB) and well hydrograph analysis were also employed to obtain the recharge. The qualitative zoned maps developed by integration RS-GIS techniques were used to delineate the spatially distributed fluxes in each stress period in the transient model.

The largest improvement as compared to the existing model used as starting point of this work was in reformulation of the topological surfaces used in the former model as a consequence of the high-precision differential GPS survey carried over the entire Sardon study area. This survey not only improved the layer boundaries but also the potentiometric surface that was used in the new calibration of the steady state flow MODFLOW model.

The local scale dispersivity obtained by numerical model was regionalized and applied in the solute transport MT3D model to validate the steady state flow model using chloride tracer in groundwater. The validation revealed the calibrated steady state flow model was satisfactorily reliable even improvement is still necessary. The solute transport model i.e. chloride concentration distribution in groundwater showed to be insensitive to dispersivity change.

The fully transient model was developed for years 2003-2008 and in general its results are in good agreement with previously calibrated model. The average recharge is 0.38 mm/d (24.1 % of annual rainfall) while the groundwater evapotranspiration indicated 0.14 mm/d (8.2 of annual rainfall) in average for the simulated period. The groundwater outflow through the drain along Sardon fault zone is apparently uniform and it is 0.24 mm/d (15.2 % of annual rainfall).

Acknowledgements

I would like to express my sincere gratitude towards the Netherlands Government for providing me a scholarship through Netherlands Fellowship Programme (NFP) to follow this Master of Science programme at ITC. I am grateful to my employer, Water Resources Board in Sri Lanka for allowing me this opportunity to pursue my higher studies. Also, I would like to thank all who helped me through out this programme.

I am greatly indebted to my supervisors Dr. Ir. M. W. Lubczynski, Drs. Robert Becht, and specially the advisor Alain Pascal of ITC for proper guidance, suggestions and their encouragement throughout the study.

Undoubtedly my sincere gratefulness should go to all the ITC staff specially Ir. Arno Van Lieshout, Dr. A. S. M. Ambro Gieske, Ir. G. N. Gabriel Parodi and Dr. J. B. Boudewijn de Smeth for supporting and giving valuable suggestions in the difficult times during the work.

I greatly appreciated Prof. Jose Martinez Fernandez and staff of the CIALE Institute, University of Salamanca, Spain for sharing their brand new installations and laboratory. I also thank Michel Groen, Free University of Amsterdam, for his great support through out the tracer test and ERT survey.

I do my extended appreciation to Alain Pascal who did an enormous support during the hard field work and also Leonardo, Guido, Ricardo and Michael who worked together helped a lot when ever I needed. Further, my thanks should go to all the colleagues working with me during the WREM programme who shares their thoughts in our academic or non-academic discussions; yet however it was a nice time out there in the MSc. Cluster.

Many thanks to all the Sri Lankan friends with whom I had always a wonderful time to cherish my memories. We had full of fun and joy throughout this period, whatever the workload on us.

Finally, I have always kept a special place in my heart for my family; their inspirations, unwillingness support, patience, care and tenderness on me throughout this hectic study was unmatchable to none.

Table of contents

1. Introduction 1
   1.1. Background of the study 1
   1.2. Research problem statement 1
   1.3. Research questions 2
   1.4. Objectives 2
   1.5. Hypothesis 3
   1.6. Assumptions 3
   1.7. Literature Review 3
      1.7.1. Previous studies 3
      1.7.2. Groundwater modeling 4
   1.8. Methodology 6
      1.8.1. Field activities, laboratory analysis and data processing 6
      1.8.2. Assessment of recharge and groundwater evapotranspiration 6
      1.8.3. Dispersivity assessment 6
      1.8.4. Steady state model calibration and validation 7
      1.8.5. Transient model 7
2. General characteristics of the study area 9
   2.1. Location and accessibility 9
   2.2. Topography and geomorpholgy 10
   2.3. Climate and hydrology 10
   2.4. Soil and Geology 10
   2.5. Land cover and land use 11
   2.6. Hydrogeology 11
3. Field work and data processing 13
   3.1. Monitoring network 13
   3.2. Raw data processing 14
      3.2.1. Time series 14
      3.2.2. Spatio - temporal data 15
   3.3. Auxiliary data 15
   3.4. Field investigations 16
   3.5. Reference evapotranspiration 16
   3.6. Hydraulic head 18
   3.7. Augering piezometers 19
   3.8. Chloride analysis 19
   3.9. Soil sample analysis 20
   3.10. Differential GPS 21
   3.11. Inverse auger tests (slug tests) 21
   3.12. Tracer tests 22
4. Assessment of recharge and groundwater evapotranspiration 23
   4.1. Recharge evaluation 23
      4.1.1. Recharge by Chloride Mass Balance (CMB) 23
      4.1.2. Recharge by well hydrograph analysis 25

4.1.3. Temporal recharge by pyEARTH-1D model ... 25
4.1.4. GIS map modelling for spatial distribution of recharge ... 32
4.2. Evapotranspiration - groundwater interaction ... 33
4.2.1. Temporal ET_g assessment ... 34
4.2.2. Spatio-temporal ET_g map preparation ... 34
5. Dispersivity assessment by tracer tests ... 35
5.1. Tracer tests ... 35
5.2. Tracer test setup preparation ... 36
5.2.1. Site selection ... 36
5.2.2. Piezometer constructions ... 37
5.2.3. Geophysics ... 37
5.3. Forced Gradient Tracer test with pumping test ... 37
5.3.1. Pumping test ... 37
5.3.2. Tracer injection ... 37
5.3.3. Geophysics ... 38
5.3.4. Plume monitoring in piezometers ... 38
5.4. Numerical modeling ... 40
5.4.1. Conceptual model ... 40
5.4.2. Model setup and model boundaries ... 41
5.4.3. Calibration of flow model and solute model ... 41
5.4.4. Model results ... 42
6. Groundwater model development ... 43
6.1. Conceptual groundwater model ... 43
6.1.1. Hydrostratigraphic units and groundwater flow network ... 43
6.2. Numerical groundwater model ... 44
6.3. Steady state flow model ... 44
6.3.1. Boundary conditions ... 45
6.3.2. Hydraulic heads ... 45
6.3.3. Groundwater fluxes ... 46
6.3.4. Model parameterisation ... 47
6.4. Steady state solute transport model ... 47
6.4.1. Effective porosity and dispersivity ... 48
6.4.2. Regionalisation of the dispersivity ... 48
6.4.3. Chloride concentrations ... 49
6.5. Transient flow model ... 49
6.5.1. Hydraulic head data ... 50
6.5.2. Storage coefficient (S) ... 50
6.5.3. Time discretization ... 50
6.5.4. Recharge and groundwater evapotranspiration (ET_g) ... 51
7. Model calibration ... 53
7.1. Steady state flow model calibration ... 53
7.1.1. Head calibration target ... 53
7.1.2. Hydraulic conductivity ... 54
7.1.3. Recharge and ET_g ... 55
7.1.4. Water budget ... 55

7.2. Steady state solute transport model 56
7.2.1. Calibration result 57
7.2.2. Sensitivity analysis 58
7.3. Transient model calibration 59
7.3.1. Hydraulic heads 59
7.3.2. Hydraulic conductivity and specific yield 62
8. Discussion, conclusions and recommendations 65
8.1. Discussion 65
8.1.1. Field tests and spatio-temporal data acquisition 65
8.1.2. Spatio-temporal recharge and ET_g 65
8.1.3. Steady state flow and solute transport models 67
8.1.4. Fully-transient model 68
8.2. Conclusions 69
8.3. Recommendations 70
References 71
Appendices I

Appendix A: Rainfall analysis data and statistics I
Appendix B: Correlation of rainfall at Trabadillo with surrounding stations for 2005-2008 III
Appendix C: The coordinates and technical details of the piezometers V
Appendix D : The average recharge and actual evapotranspiration estimated from the pyEARTH-1D model for each stress period of the transient model VII
Appendix E: Well hydrograph analysis used in the recharge assessment using head data IX
Appendix F : The description of modules in the EARTH model XI
Appendix G: The pumping test curves and VES, ERT survey of the Muelledes1 tracer test site XIII
Appendix H: Simulated heads at the observed locations by the steady state model XV
Appendix I: Simulated chloride concentrations at the measured locations by the steady state solute model XVI
Appendix J : First and final page of the weekly groundwater level used in the transient model calibration, 2003 - 2008 XVII
Appendix K: Field activities and characteristics of the study area XIX

List of figures

Figure 2:1 Location map of the Sardon catchment as part of the Sourthern Rio Tormes catchment 9
Figure 2:2 Geology, lineament and drainage map of the area (after Attanayake, 1999) 11
Figure 2:3 The schematic cross section of the Sardon catchment (Lubczynski and Gurwin, 2005) 12
Figure 3:1 The piezometric monitoring system and ADAS stations of the Sardon area 13
Figure 3:2 Correlation of rainfall calculated by station average and Normal ratio method with Trabadillo rainfall, 2005-2008. 15
Figure 3:3 Daily rainfall and reference evapotranspiration (ET_0) by Penman-Monteith method in mm (2003-2008). 17
Figure 3:4 Groundwater level fluctuations of piezometers in Sardon during the period of 2003-2008. 18
Figure 3:5 The time vs. water level in the two boreholes tested for drain conductance. 22
Figure 4:1 EARTH model represented by subsequent modules of subsoil, unsaturated zone followed the saturated zone (after Francés, 2008). 26
Figure 4:2 The results of pyEARTH-1D model calibration at piezometer Gejo. 29
Figure 4:3 The results of pyEARTH-1D model calibration at piezometer Gejuello. 30
Figure 4:4 The results of pyEARTH-1D model calibration at piezometer Muelledes1. 30
Figure 4:5 The results of pyEARTH-1D model calibration at piezometer Muelledes2. 31
Figure 4:6 The results of pyEARTH-1D model calibration at piezometer Sardon. 31
Figure 4:7 The results of pyEARTH-1D model calibration at piezometer Trabadillo. 32
Figure 4:8 Recharge zonation map by index-overlay procedure and evapotranspiration zonation map by SEBAL algorithm (After Worku, 2000) 33
Figure 5:1 The cross section of tracer test design 39
Figure 5:2 A conversion section processed by the 2-D ERT data obtained during the test in N-S longitudinal direction 39
Figure 5:3 The overview of the tracer test design 39
Figure 5:4 The EC variation with time at T2 piezometer and Pmu1 pumping well (bottom) respectively. 40
Figure 5:5 The calibrated hydraulic heads in *Figure 5:6 Simulated solute model for EC* 42
Figure 6:1 The boundary condition applied in the numerical model in the layer 1 and 2 respectively. 45
Figure 6:2 The regressions developed for elevation and water level of the Sardon catchment 46
Figure 6:3 Some relationships of longitudinal dispersivity in function of scale compared with the dataset of Gelhar et al. (1992) and plot of Muelledes site. 49
Figure 6:4 The defined stress periods for fully transient modelling. 51
Figure 7:1 (a) Scatter plot of steady state simulated vs. observed hydraulic heads and (b) Head residuals at calibration targets. 54
Figure 7:2 Steady state hydraulic head distribution in the calibrated model 55
Figure 7:3 The steady state water budget components 56
Figure 7:4 Scatter plot of observed chloride concentrations (in the second layer) compared to calculated values after 20 years simulation time. 57
Figure 7:5 The sensitivity analysis result on dispersivity parameters of the second layer 58
Figure 7:6 Simulated hydraulic heads of Gejo, Gejuello and Muelledes1 wells 60

Figure 7:7 Simulated hydraulic heads of Muelledes2 well and piezometers Sardon, Trabadillo..... 61
Figure 7:8 The average groundwater balance components of the transient model solution 63
Figure 7:9 The temporal variability of fluxes for the period of September 2003 -2008 December. 64

List of tables

Table 1-1: Maps/data available from the previous works done in Sardon catchment. 4
Table 3-1: Technical details of the piezometers constructed during the field work.....19
Table 3-2: The chloride analysis groundwater sample collected during June- September, 2008 20
Table 3-3: The soil samples analysed at Trabadillo and new piezometer locations from different depths of unsaturated and saturated zones 21
Table 3-4: Inverse auger results at Sardon river bed near to Pcl3 and Pcl7 piezometers locations....22
Table 4-1: Chloride concentration of the groundwater samples (September, 2008) used for point recharge calculation by CMB method and annual recharge as rainfall percentage. 24
Table 4-2: Recharge analysis results by well hydrograph method.....25
Table 4-3: Soil and aquifer parameters for pyEARTH-1D model and their derivations for the study 27
Table 4-4: Input parameters used in final calibration of pyEARTH-1D 28
Table 4-5: Mean daily and mean annual recharge summarized by the pyEARTH-1D model results...29
Table 5-1: Pumping test results for site selection.....36
Table 5-2: Technical details of the piezometers and depth of installed loggers 38
Table 5-3: The stress periods defined in the transient flow model.....41
Table 5-4 The parameter configuration applied in the model 42
Table 6-1: Stress periods defined for simulation in the transient model.....50
Table 7-1: The evaluated calibration statistics 54
Table 7-2: Recharge and ET_g used in steady state model.....55
Table 7-3: Steady state water balance of the model 56
Table 7-4 The parameter configuration applied in the solute model 57
Table 7-5 The error analysis statistics of the solute mode calibration 57
Table 7-6 : Water balance of the stress periods (September 2003 - December 2008) 62
Table 8-1 The recharge assessed by pyEARTH-1D, CMB and well hydrograph and ET_a by pyEARTH-1D 66
Table 8-2 The water balance of the previous model and recalibrated steady state model 67
Table 8-3 The comparison of average water balance of the previous and this work.....69

1. Introduction

1.1. Background of the study

The water demand in the world is rapidly increasing due to population growth, extensive industrialization and agricultural practices. Groundwater plays an important role in the supplying of this ever increasing water demand. Therefore, accurate estimation of groundwater resources is a prerequisite for any sustainable water management especially in water scarce (semi-) arid regions. Groundwater modeling is an essential tool in the evaluation of groundwater flow and quantification of resources. It enables to predict the behavior of the groundwater system in response to future stresses due to abstractions or land cover and climatic changes. Numerical groundwater flow models solve the distribution of hydraulic head and describe flow whereas numerical transport models solve the distribution of solute concentration due to advection, dispersion and chemical reactions.

The Sardon catchment is located in Salamanca province, central part of Spain. The study area is in semi-arid climatic condition and the environment is almost free from human population. The catchment discharges natural replenishment of water from the rainfall. However the river baseflow quantification is in doubt as Sardon river flows along the regional fault zone. The Sardon catchment has been used for ITC experimental studies since 1996. Several studies have been carried out in respect to groundwater recharge and groundwater balance through numerical modelling (Appiah Duah, 1999; Shakya, 2001; Uria Cornejo, 2000). This was concluded by Lubczynski and Gurwin (2005) who summarized the available knowledge but also emphasized the uncertainty in this study due to the complexity of the flow regimes and spatio-temporal flux variability in this area. This research work is another step forward in the groundwater modeling of the Sardon catchment which focused to constrain and validate the flow model by solute model to improve the reliability of flow model.

1.2. Research problem statement

Understanding the groundwater flow behaviour is always uncertain. The non-uniqueness of groundwater model solution is due to various combinations between hydraulic parameters and fluxes. This is additionally complicated by the spatio-temporal variability of recharge and evapotranspiration due to aquifer heterogeneity, anisotropy and unpredictable fluctuations of the driving forces such as rainfall. The proper parameters/fluxes evaluation by integration of data sources with different methods is essential to select an appropriate model or to develop a reliably calibrated model (Lubczynski and Gurwin, 2005).

The potential of groundwater resources in hard rock aquifers strongly depend on the hydrogeological and climatic conditions. However, the accurate assessment of spatial and temporal characteristics of an aquifer in semi arid hard rock regions is always difficult due to the aquifer heterogeneity and

unpredictable driving forces as stated above. Beside the recharge; transmissivity and storativity are also critically important parameters in the assessment of groundwater flow regimes and resources. All the aquifer responses for the sink/sources are influenced by transmissivity and storativity. Fully transient groundwater model can describe the groundwater flow regimes more reliably and accurately since the introduction of spatio-temporal fluxes constrain the model more effectively than steady state models (Lubczynski, 2000). Even in fully transient model, the non-uniqueness of the model solutions still exists because of uncertainty involved in the fluxes and parameter estimates.

In numerical transport model, the solute transport parameters (dispersivity and effective porosity) are used to calibrate the model in addition to the fluxes and parameters applied in flow model calibration. Therefore, the introduction of these additional parameters with sufficient number of spatio-temporal solute concentration observations in numerical transport model can be used to constrain and validate the flow model. Thereby the degree of freedom is reduced in the model thus improving the reliability of the model.

1.3. Research questions

Main research question

- How to improve the reliability of groundwater flow model?

Specific research questions

- Are the spatio-temporal methods to assess fluxes effective and reliable?
- Is the validation of flow model through the solute transport model effective?

1.4. Objectives

The general objective is to improve the reliability of groundwater flow model through its validation by solute transport model using spatio-temporal chloride concentrations as an additional calibration constrain.

The specific objectives are:

- Derive solute transport parameters by field experiments
- Estimate dispersivity of the regional model
- Evaluate spatio-temporal recharge and groundwater evapotranspiration (ET_g)
- Setup and calibrate regional scale steady state flow and solute transport model
- Setup and calibrate the fully transient model

1.5. Hypothesis

In the process of achieving the objectives, the following hypotheses were formulated.

- The measurements of tracer concentrations, site specific experiment with electrical resistivity tomography (ERT) and pumping test analysis can provide data for the assessment of solute parameters.

- The range of dispersivity expected in the solute model could be reliably estimated through the comparison and extrapolation of field scale derived dispersivity with the existing field datasets and literature.

- The only source of chloride in groundwater is from precipitation and chloride is naturally enriched in aquifers. The possible chloride sources from the dissolution of chloride rich rocks, agriculture or industrial pollution and mixing of saline water are at minimum level in the area. Therefore the assessment of groundwater flow behaviour through hydraulic head distribution and validation of flow model by spatial chloride sampling is justified.

1.6. Assumptions

The following assumptions were primarily made in the work.

- During dry season, the actual evapotranspiration (ET_a) is equal to the evapotranspiration from the groundwater reservoir (referred as groundwater evapotranspiration, ET_g)

- The transport and redistribution of chloride in groundwater is resulted primarily due to the processes of advection and dispersion. The adsorption, biodegradation and chemical reactions are considered negligible.

- The equivalent porous media (EPM) concept (Anderson and Woessner, 1992) applies for weathered and fractured granite in Sardon.

1.7. Literature Review

1.7.1. Previous studies

Number of studies has been carried out in the Sardon catchment purely on scientific research basis since it is an area where the human influences on groundwater are at the minimum level. During the start of these experimental studies in 90's, rain gauges were installed at six locations in the Sardon catchment and the results indicated an uniform rainfall distribution since the catchment is spread out in a relatively small area (app. 80 km^2). Groundwater sensor loggers and micro-climatic stations were established during this period to acquire the groundwater head variations and climatic data. These loggers have been shifted in time to time to obtain the maximum spatial resolution and to avoid data redundancy.

The previous studies focused on geology and structure of the catchment (Attanayake, 1999; Tesfai, 2000), groundwater balance, geochemistry and recharge and ET_g assessment (Shakya, 2001; Uria Cornejo, 2000). The subsurface structure and characterization of the Sardon granitic basement was assessed by Tesfai (2000) and he reported that the top most soil layer is followed by weathered fractured granitic layer. This upper layer varies the thickness from 0.0 to 40.0 m, depending on the local and regional geological and structural influences. The basement rock is massif granite. The maps of geology, lithology, landuse, vegetation cover, drainage system and fault pattern prepared during these previous studies provided the background information for this research work (*Table 1-1*)

Table 1-1: Maps/data available from the previous works done in Sardon catchment.

Maps/ Data	Locations	Source
Geological, fracture distribution, outcrop maps	Digital	Attanayake, MSc. 1998 ITC
Thickness maps of weathered and fractured layer	Digital	Tesfai, MSc. 2000 ITC
Evapotranspiration maps	Digital	Worku, 2000
Recharge attribute maps	Digital	Dan Ratna Shakya, MSc. 2001 ITC
Chloride concentrations data	Digital	Uria, MSc. 2000 ITC
Steady state flow model*	Digital	Lubczynski and Gurwin, 2005 ITC

In previous groundwater balance studies, spatio-temporal variability of recharge and ET_g fluxes have been assessed through the combination of various techniques (Shakya, 2001). It involves the application of GIS modeling and remote sensing, sap flow measurements, chloride mass balance, well hydrograph, 1-D recharge model, geophysics and other in-situ and laboratory experiments.

The various approaches such as GIS, remote sensing, automated monitoring systems, geophysics and pumping test have been integrated in a study carried in the Sardon catchment by Lubczynski and Gurwin (2005). These authors present a fully transient groundwater flow model of the Sardon catchment for the 1996-2000 period. That model indicated an average recharge of 0.3- 0.5 mm/d in the wet season and no recharge in dry period. The ET_g has been estimated as 0.55-0.80 mm/d in dry season and <0.05 mm/d in wet seasons. The water budget of the steady state model assessed the recharge in the order of approximately 56 mm/yr (11 % of annual rainfall) as equal to the sum of ET_g (20 mm/yr) and groundwater outflow of the Sardon catchment (36 mm/yr). This result is comparable with the transient model developed by Dan Ratna (2001) for his MSc. study. As indicated by the authors, the calibrated model involves a spatial and temporal non-uniqueness, mainly due to uncertainty between groundwater evaporation and groundwater outflow which could not be measured (Lubczynski and Gurwin, 2005). This research work aims to improve the reliability of that model by upgrading the steady state flow model and later validating through solute transport model by chloride measurements. The transient flow model was finally developed for the period of 2003-2008.

1.7.2. Groundwater modeling

The reliability of the numerical model solution depends on number of criteria: code selection, implications of simplifying assumptions in conceptualization, spatio-temporal resolution and accuracy of data and fluxes (Anderson and Woessner, 1992).

In quantitative groundwater modeling, the model algorithm is based on groundwater flow equation developed with combination of Darcy's law and continuity of mass equation (Anderson and Woessner, 1992) . The behavior of groundwater flow system could be described by several techniques which have developed to solve the partial differential equations. In MODFLOW (Harbaugh and Mc Donald, 1988), this is simulated by finite difference method. The transport models are simulated by advection and dispersion equation based on conservation of mass (Freeze and Cherry, 1979).

Transient flow models are far better reliable in exploring the groundwater flow behavior compared to steady state models since the transient models can incorporate the spatio-temporal variations of fluxes and the steady state models have a higher degree of freedom in the calibration process (Lubczynski and Gurwin, 2005). However the transient flow models still involve non-uniqueness between fluxes and parameters when the data are scarce. There are different techniques that have been applied in the previous studies to determine the spatio-temporal fluxes more accurate and reliably as explained in the section 1.7.1. In this research work, the assessed spatio-temporal fluxes by chloride mass balance (CMB), well hydrograph methods and pyEARTH-1D modelling were integrated using the remote sensing and GIS. The steady state flow model was validated by chloride concentrations in solute transport model to improve the reliability of flow model and developing the fully transient model.

The solute transport models are mainly focused on the hydrogeological problems dealing with spreading of contaminants in agricultural, industrial and urban activities (Vandenbohede and Lebbe, 2003). Despite this, the solute transport model with flow model is increasingly applied in recent scientific research works since it enables to explore the flow regime behavior in deep. Effective porosity and dispersivity are the additional parameters required for solute modeling. Tracer test is by far more reliable and efficient method to derive these parameters compared to laboratory scale tests. The combined hydrogeological analysis with information obtained from tracer test data allows for an improved groundwater flow modeling (Onnis et al., 2007). Further, the tracer tests are useful tool in understanding broad fundamental processes of recharge and solute dispersion in fractured rock aquifers (Craig and Jeffrey, 2005).

The transport modeling with flow model has been used for different scientific approaches in the recent groundwater studies. For instance, the groundwater flow model developed by Mattle et al. (2001) in Swiss pre-Alpine river (north-eastern Switzerland) has been constrained by solute transport modeling of 3He for detail exploration of the aquifers. In that study, the tracer has been used to determine the age distributions and mixing ratios of two types of waters in the model area. The natural tracer distribution has considered at steady state and the solute parameters have estimated using the field experiments data of Gelhar (1992) in the model calibration.

The steady state transport model has been used to validate and improve the flow model in a groundwater resources study in well field at Khurutshe and Palla Road (Leif, 1993). In the study, the recharge has been optimized through steady state flow and solute transport model calibrated with total dissolved solids (TDS) in groundwater.

1.8. Methodology

The methods to be followed in this research work are based on the objectives formulated in section 1.4. During the study, spatial model parameters and spatio-temporal fluxes were acquired and processed using remote sensing and GIS to use as inputs for the groundwater flow model. MODFLOW software was used to model the groundwater flow system in PMWIN 5.3 interface. The steady state model was recalibrated after the layer elevation corrections and input of additional data obtained during this field work. The steady state flow model was validated through solute transport model simulating advection and dispersion in MT3D using the chloride concentrations in groundwater. Finally, the transient ground water flow model was developed and calibrated for five years (2003-2008) with hydraulic head data of the existing piezometers and the wells in the Sardon catchment.

1.8.1. Field activities, laboratory analysis and data processing

Several field work activities were carried out to obtain the necessary data and to perform the field tests. The chloride concentrations of groundwater samples were analyzed during four different time steps starting from June 2008 to December 2008. New piezometers were constructed in June 2008 and September 2008 to assess the spatial chloride concentrations of groundwater and obtain additional hydraulic head data. The forced gradient tracer test was carried out at Muelledes site after construction of observation piezometers. The plume was monitored by EC loggers in the piezometers and cross-checked with electrical resistivity tomography (ERT) surveys during the test. The obtained tracer test data were used to evaluate the local scale dispersivity. The soil sampling and logging was performed at new piezometers and analyzed to assess the soil properties such as porosity, field capacity, hydraulic conductivity. ADAS climatic data were processed to obtain the reference evapotranspiration that used in the assessment of recharge and actual evapotanspiration through pyEARTH-1D modeling (Chapter 4.1.3). The location and elevation of the piezometers/wells were obtained through high-precision differential GPS survey and obtained data were used to correct the steady state model geometry. In addition, the slug tests at two sites were carried out to estimate the river bed conductance. The processed hydraulic heads and chloride concentrations were used as calibration targets in the flow and solute transport model calibrations.

1.8.2. Assessment of recharge and groundwater evapotranspiration

The point recharge at 27 locations were calculated by chloride mass balance (CMB) method and the spatio-temporal recharge was assessed through pyEARTH-1D model and well hydrograph analysis. The actual evapotranspiration calculated by pyEARTH-1D model was considered as ET_g during dry season since unsaturated zone was completely depleted. The spatial zoned maps of recharge and ET_g prepared by GIS cross overlay index procedure in the previous study (Lubczynski and Gurwin, 2005) were used to construct the spatio-temporal maps for each stress period defined in the transient model 2003-2008.

1.8.3. Dispersivity assessment

The forced gradient tracer test was simulated in the numerical local scale model to determine the dispersivity and effective porosity. The results were used to estimate the dispersivity in the regional

scale solute model after comparing with Gelhar's (1992) field test data plots and suggested values by literature (ASTM, 1995) at the scale of regional model.

1.8.4. Steady state model calibration and validation

The layer elevations of the steady state model developed by Lubczynski and Gurwin (2005) was corrected by 64 differential GPS data points and recalibrated with new hydraulic heads at 37 locations, drain conductance obtained by slug tests, long term recharge obtained from CMB method. The calibrated steady state model was validated by solute transport modelling with spatial chloride concentrations in groundwater.

1.8.5. Transient model

The fully transient model was developed using the validated steady state model and calibrated with hydraulic head data of 2003 - 2008 period at six locations (see Chapter 3.6 for hydraulic head data availability).

2. General characteristics of the study area

2.1. Location and accessibility

The Sardon catchment is located in the central-western part of the Spain in the Salamanca province between the geographical co-ordinates of 6°07'- 6°13' W longitudes and 41°01' - 41° 08' N latitudes. The area is situated in lower part of the Rio-Tormes basin as a sub-catchment (*Figure 2:1*). The Sardon catchment is more elongated towards North-South direction having total area of approximately 80 km^2. The major river is intermittent which coalescence to perennial river Rio–Tormes. The area can be accessed by Ledesma which is located in east and could also reach through Villaseco de los Reyes from north. The population is very low and sparsely distributed. The most of villages are nearly abandoned such as Tremedal, Sardon, Penalbo and Villosino.

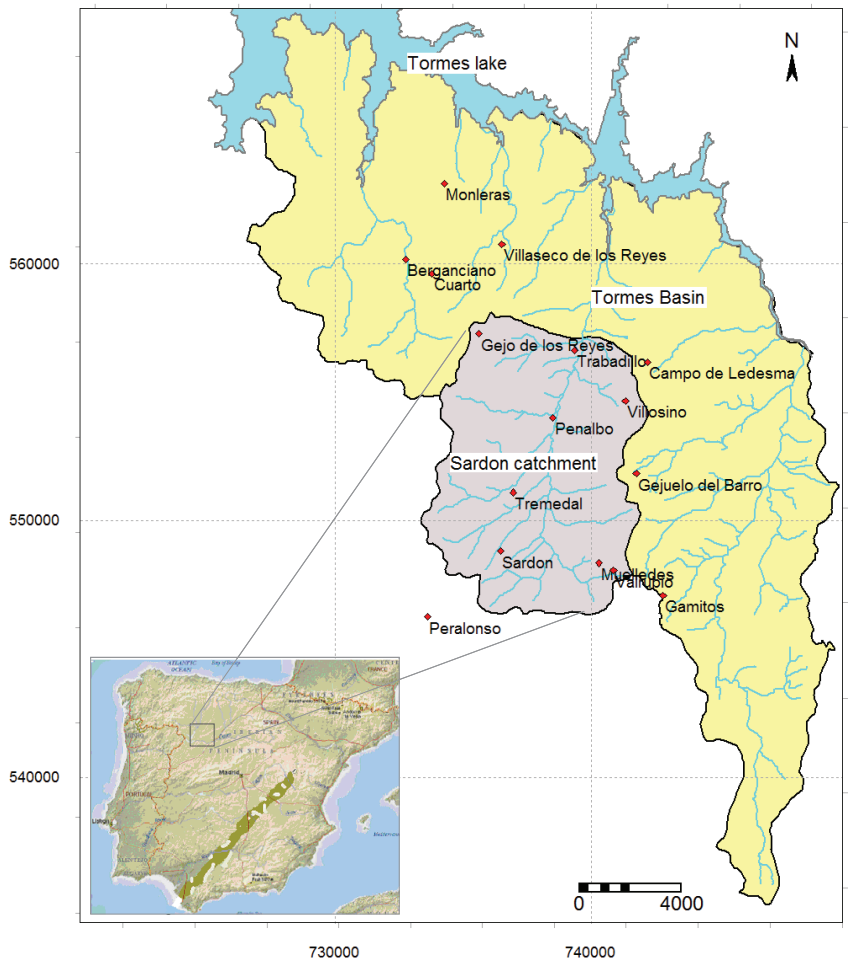

Figure 2:1 Location map of the Sardon catchment as part of the Sourthern Rio Tormes catchment

2.2. Topography and geomorpholgy

The study area has a gentle undulating topography mainly controlled by geological structure and subsequent interactive weathering processes. This is obviously evident by alternative series of valleys and ridges resulted by weathering along weak structural lineament or intense joint network systems. The higher relief is comprised of quartzite dykes, massive or fractured granitic outcrop with large boulders and capped by thin in-situ soil overburden in certain parts. The depression valleys possess higher thickness of alluvial and colluvial materials. The elevation varies within 730- 870 meters above mean sea level and the highest level is reported at southern boundary of the catchment.

The landscape of the catchment is characterized by semi-arid woody shrubs with deciduous broad-leafed vegetation. The western flank of the catchment is existed with broader weathered granitic zone compared to east, which is influenced by structural and geological setup in the area. The surface runoff could be observed only in wet season and consists with poorly defined drainage systems in most part of the area. The morphology of the catchment seems to be largely controlled by the Sardon brittle shear zone (Tesfai, 2000).

2.3. Climate and hydrology

Groundwater recharge in hard rock aquifers are strongly controlled by hydrogeology and climatic conditions of the area. The area is semi-arid and the rainfall analysed for a period of 1962 to 1996 indicated mean of approximately 480 mm/yr (Appiah Duah, 1999). In general, July & August are the warmest & driest months with average temperature of 22^0 C, potential evapotranspiration (PET) of 5 mm/d and the average rainfall of 20 mm/month. The wettest months November & December have average temperature 5^0C, potential evapotranspiration of 0.5 mm/d with 100 mm of monthly rainfall. The rainfall, temperature, relative humidity and other climatological data acquired by automatic micro-climatic stations at Trabadillo and Muelledes in the study area is discussed in chapter 3.1.

The central part of the area is the major drainage channel where the Sardon river flows towards north direction. The drainage network is dense and largely influenced by Sardon river which flows into Tormes river, a perennial river. The river is dry from June to October and during the wet period; the flow is mainly occurred as direct runoff due to rainfall. The flow pattern follows the regional Sardon fault zone in the area. Geomorphologically, the area shows two distinct units with gently undulating western part and steeper undulating eastern part, divided by the Sardon regional fault (Attanayake, 1999). The runoff processes are typical for semi-arid hard rock catchments. The thin, highly permeable upper unconsolidated layer with low retention capacity results in rapid direct run off responses to high-intense rainfalls (Dan Ratna, 2001).

2.4. Soil and Geology

The study area lies in the Central Iberian Zone (CIZ) of the Iberian Massif in Moncorvo-Vitigudino metamorphic belt. The Iberian Massif is generally underlain by granitic rocks belongs to the CIZ with intrusions of quartz dykes (Lopez and Carnicero, 1987). The major lithological units identified are megacrystic granite, microgranite and two varieties of mica rich granites (Attanayake, 1999). The

tectonic processes are dominantly affected on lithological units of the area and it is important in hydrogeological point of view as porosity and permeability of geologic materials are changed. The area consists of massive granite with intermittent highly fractured and weathered granitic areas. The thickness of this weathered granite zone is varied place to place.

In regional scale, the folding axes are oriented along NW-SE direction with several ductile shear zones, one of which is located along the Sardon river resulting subsurface flow though this shear zone. A NNE-SSW fracture system is persistently occurred in the area and it can be clearly seen on outcrops which plunge almost vertical.

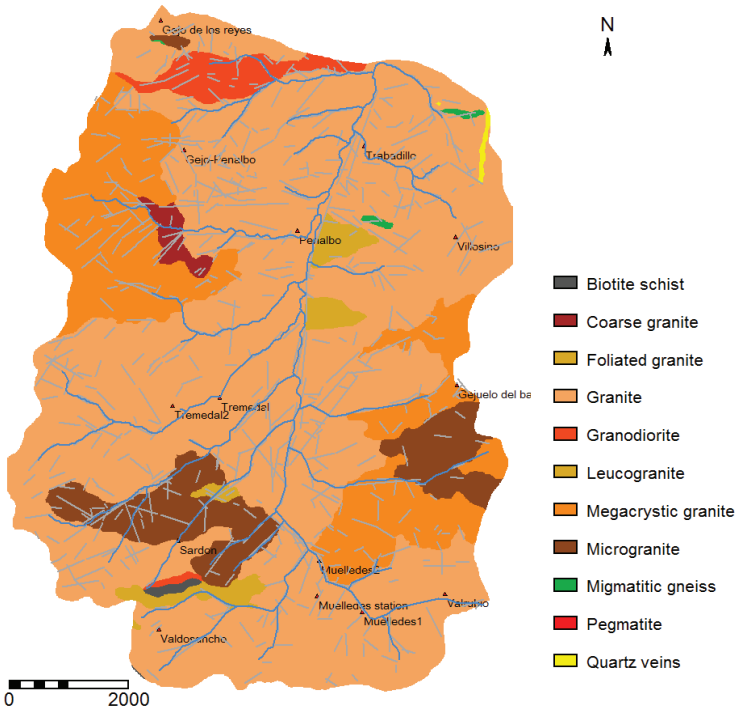

Figure 2:2 Geology, lineament and drainage map of the area (after Attanayake, 1999)

2.5. Land cover and land use

The Sardon area is characterized by natural vegetation of mainly two tree species, *Quercus pyrenaica* and *Quercus ilex*. These are sparsely distributed and remaining land is covered by *Cytisus scoparius* shrub and short grass in the area. The agricultural practises are rarely used in the area due to most part of the topsoil is weathered rock. These land areas are covered by grass and weed typical in semi-arid savannah areas (Dan Ratna, 2001).

2.6. Hydrogeology

The groundwater flow is towards the central regional drainage line of Sardon fault, which extends towards the northern outlet of the study area (*Figure 2:2*). The hydrogeology of the study area is mainly influenced by the weathering and fracturing of the granitic basement rock. Three layers have

been identified in the area from top to bottom: (i) top layer, consisted of weathered granitic rocks and alluvial deposits; (ii) fractured granitic rock of varying depth from few meters to approximately 60 mbgl (Attanayake, 1999); (iii) massive impermeable rock with gneissic inclusions at the basement underneath represents the bottom layer.

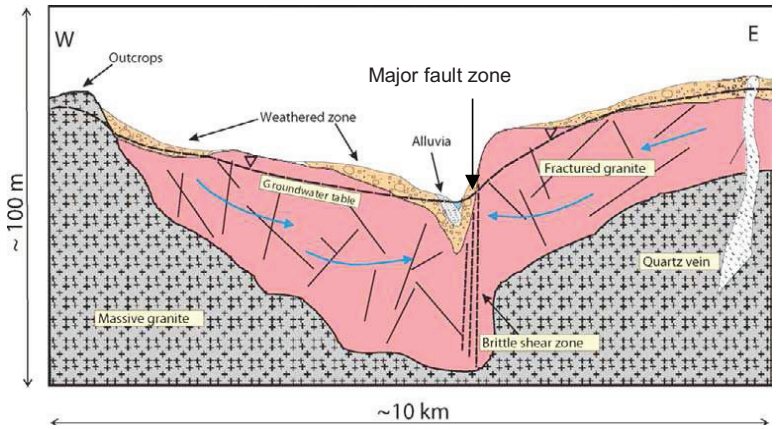

Figure 2:3 The schematic cross section of the Sardon catchment (Lubczynski and Gurwin, 2005)

The groundwater table shows a concentric pattern influenced by the fault zone which lies along the river drainage (*Figure 2:3*). The groundwater pattern is in natural condition as there is limited extraction of groundwater in the area. The baseflow measured at the river outlet is uncertain because part of the groundwater outflow is drained and move out of the study are under the surface along the fault zone (*Figure 2:3*). Therefore, only a part of the total outflow is possible to measure at the river outlet where flume has built in.

3. Field work and data processing

The data acquisition was performed in two phases of the study i.e. (a) primary data during the field work and (b) secondary data from the previous studies (see Chapter 1.7.1). The processing of raw data is explained in the first part of the chapter. The main field activities are summarized in the next section. Finally the subsequent data compilation, processing and interpretation of field activities are explained. This chapter is focused in overall to deliver the input data for the assessment of recharge and evapotranspiration as explained in Chapter 4. In addition, the calibration targets of hydraulic heads and chloride concentrations in groundwater were also obtained for flow and solute transport models. The purpose of the data integration and processing was mainly focused on to deliver:

- Time series data: (i) Driving forces - rainfall and reference evapotranspiration (ET_0)
  (ii) State variables - hydraulic heads and chloride concentrations
- Spatial data: soil hydraulic properties, river conductance and hydraulic conductivity of the aquifers

3.1. Monitoring network

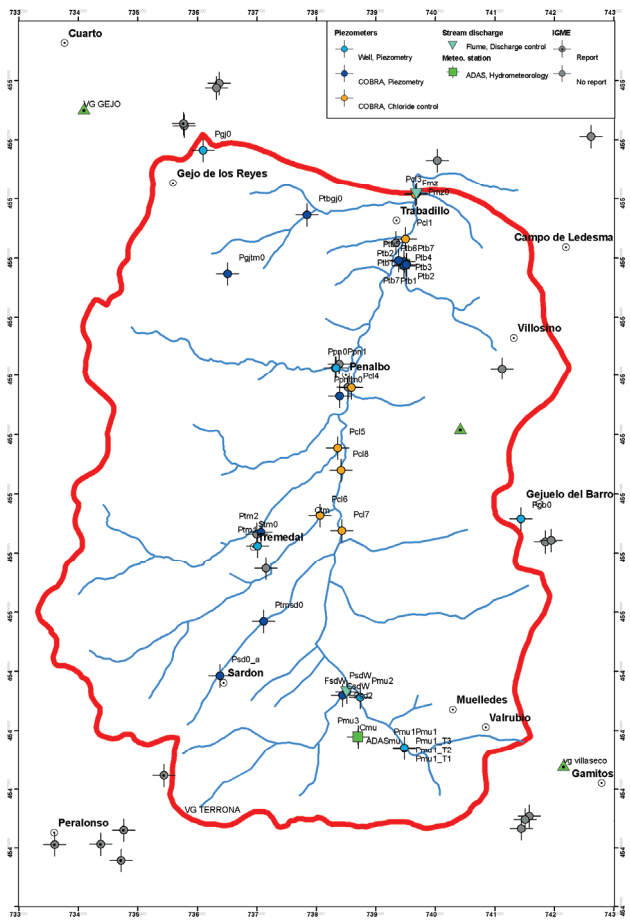

Figure 3:1 The piezometric monitoring system and ADAS stations of the Sardon area

The automated data monitoring was performed by number of automated groundwater level recorders and by two ADAS stations at Muelledes and Trabadillo (*Figure 3:1*). The hourly climatic data including rainfall was measured by these multi-sensor stations. The hydraulic head variation was measured by the automated groundwater head monitoring loggers at six locations from 2003 to 2008. Additionally, new loggers were installed at seven locations in June 2008 (see *Figure 3:1*).

3.2. Raw data processing

Extensive data is required to accurately characterize a hydrogeologic system for the groundwater model setup design. The data requirement is particularly demanding in fully transient model with additional solute transport modeling. During the calibration stage of the model, more data of hydraulic heads and groundwater chloride concentrations are important to improve the model calibrations. The following temporal, spatio-temporal and spatial data was reviewed and processed to achieve the objectives of the study.

3.2.1. Time series

3.2.1.1. Rainfall

The rainfall is monitored on hourly basis in the study area at the two ADAS micro-climatic stations, Muelledes in the upper southern part of the catchment and Trabadillo in the lower northern part of the catchment. The rainfall is quite uniform throughout the entire catchment since the catchment area is relatively small (approximately 80 km^2) and not highly varying in topography.

The Trabadillo rainfall is considered as representative for the study area and in general covers the assessment years 2003 to 2008. Through that period there were some data gaps due to malfunction of the tipping buckets. Therefore continuous data stream was processed using the surrounding station rainfall data of Berrocol, Fresno, Iruelos, Ledesma and Villar obtained from the Meteorological office, Ledesma (See appendix B for details of these stations). The Trabadillo rainfall behavior and amount of annual precipitation is almost similar as in the surrounding stations. Normal ratio and station average methods (Dingman, 2002) were adopted and the calculated rainfall data was correlated with the existing rainfall at Trabadillo. The calculated rainfall by normal ratio method was used since it showed a better correlation with Trabadillo (*Figure 3.2*). The extrapolated Trabadillo rainfall is presented in Figure 3.3.

The Muelledes ADAS station has stopped the measuring the climatic data when it was damaged in 2001. It has been reinstalled in June, 2008 and therefore only six months climatic data exists.

3.2.1.2. Temperature, wind speed, relative humidity and solar radiation

The sensors and equipment which measured temperature, relative humidity and wind speed are hourly monitored at Trabadillo. The daily average of solar radiation, soil heat flux and wind speed

were processed by the hourly basis measurement. The minimum and maximum daily temperature and relative humidity was obtained to calculate the daily reference evapotranspiration.

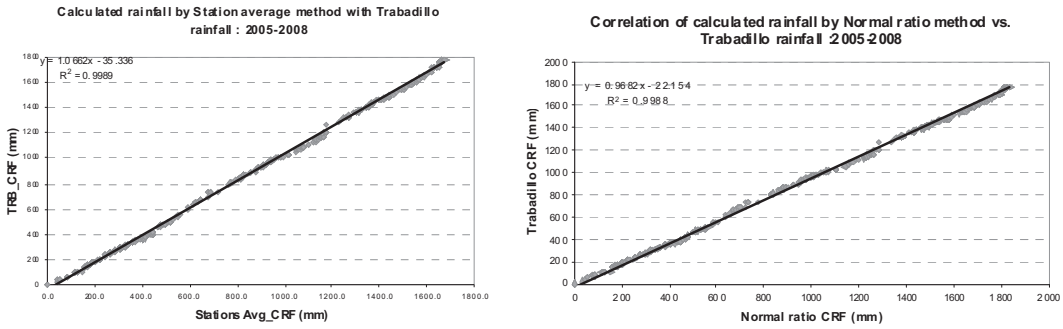

Figure 3:2 Correlation of rainfall calculated by station average and Normal ratio method with Trabadillo rainfall, 2005-2008.

3.2.2. Spatio - temporal data

3.2.2.1. Hydraulic head data

The groundwater levels variations were measured by logger based water level recorders such as Tirta and Nivolog in the existing piezometers and wells. These hourly records cover the years 2003 to 2008 at six locations with some data gaps and rests were included only six month data of 2008, where the loggers were installed very recently. These loggers recorded absolute pressure above logger. The atmospheric pressure was also measured at Trabadillo station with an automated logger on hourly basis. The subtraction of measured atmospheric pressure from the logger reading in the piezometer represents the barometrically corrected data of water column height above the logger. The final groundwater level in meters above mean sea level was computed based on the altitude measurement. The processed data in these six locations were used in pyEARTH-1D model to evaluate recharge and to calibrate the transient flow model (Chapter 4.1.3 and Chapter 7).

3.2.2.2. Chloride

The chloride concentration of groundwater was analysed by water sampling at the piezometers and well locations for the period of June 2008 to December 2008 in four time intervals (see Chapter 3.8). The sampling locations are shown in the *Figure 3:1*.

3.3. Auxiliary data

The available maps of digital elevation, landuse, vegetation, soil-geology and structural maps from the previous studies (Shakya, 2001; Tesfai, 2000) were used during the main spatio-temporal fluxes of recharge and groundwater evoptranspiration assessment processing. The additional data of storage parameters from previous works were also used in calibration of the groundwater flow model.

3.4. Field investigations

Several field programmes were carried out to obtain the required data and to perform the field tests from June to December 2008 as a co-work with Alain Francés for his PhD work. During the field, the following major activities were carried out;

- ADAS installation in Muelledes;
- Installation of head monitoring loggers to compare the spatial coverage of the monitoring network;
- ADAS climatic data downloading from two stations at Muelledes and Trabadillo;
- Download hydraulic head data from the monitoring loggers installed in piezometers and wells;
- Construction of new piezometers to;
    - determine the chloride concentration in groundwater where additional chloride concentrations are required in solute transport model.
    - for implement the observation piezometers at Muelledes site to perform forced gradient tracer test.
- Chloride sampling and analysis of groundwater at piezometer locations;
- Soil sampling and analysis of unsaturated and saturated zone where the new piezometers were constructed;
- Differential GPS survey at piezometers and wells;
- Slug tests in Sardon river bed to obtain the river conductance;
- Forced gradient tracer test with ERT survey to determine the solute parameters at local scale.

The each task carried out during these field works are explained in following sections with the primary data processing and analysis (sections 3.5 to 3.12).

3.5. Reference evapotranspiration

Evapotranspiration plays an important role in groundwater balance as its direct and indirect impact on groundwater resources. The ET_g influenced by deep root systems is considered as direct impact and evaporation from surface water resources and unsaturated zones term as indirect impact. These direct and indirect impacts are significant in the overall groundwater balance specially in (semi-) arid areas.

The modified Penman-Monteith method following the FAO Irrigation and Drainage Paper No. 56 (1998) was used to evaluate the reference evapotranspiration (ET_0) as its simplicity and reliability compared to other methods. The wind speed, relative humidity, solar radiation daily minimum and maximum temperature data was acquired from automatic data acquisition systems installed at Trabadillo station from September 2003 to December 2008. The hourly data was processed into daily basis to calculate the ET_0. In general, net radiation is calculated from the solar radiation *in* and *out* measured at the station, In Muelledes the solar radiation *out* from the soil was not available, therefore the net radiation was calculated using the following equation.

$$R_{ns} = (1-\alpha)R_s \qquad (3\text{-}1)$$

Where R_{ns} is net solar or shortwave radiation [MJ m-2 day-1], α is albedo (0.23 for grass reference crop) and R_s is incoming solar radiation [MJ m-2 day-1].

$$U_z = U_z \frac{4.87}{\ln(67.8z - 5.42)} \qquad (3\text{-}2)$$

Where U_z is wind speed at 2 m above ground surface [ms-1], U_z is measured wind speed at z m above ground surface [ms^{-1}] and z is the height of measurement above ground surface [m]. The temporal ET_0 was calculated using the Penman equation with the use of Excel spreadsheets.

$$ET_0 = \frac{0.408\Delta(R_n - G) + \gamma \frac{900}{T+273} u_2 (e_s - e_a)}{\Delta + \gamma(1 + 0.34u_2)} \qquad (3\text{-}3)$$

Where ET_0 is reference evapotranspiration [$mmday^{-1}$], R_n - net radiation at the crop surface [MJ $m^{-2}day^{-1}$], G - soil heat flux density [MJ m^{-2} day^{-1}], T - air temperature at 2 m height [°C], u_2 - wind speed at 2 m height [ms^{-1}], e_s - saturation vapour pressure [KPa], e_a - actual vapour pressure [KPa], $(e_s - e_a)$ - saturation vapour pressure deficit [KPa], Δ – slope vapour pressure curve [KPa°C^{-1}] and γ is psychometric constant [KPa°C^{-1}]

The above parameters required to calculate ET_0 in Penman equation were obtained from the relevant equations developed in the FAO-56 paper with the use of microclimatic daily data. The calculated ET_0 is varied within 0.2 - 7.0 mm/d range at Trabadillo station during the period 2003-2008 (*Figure 3:3*).

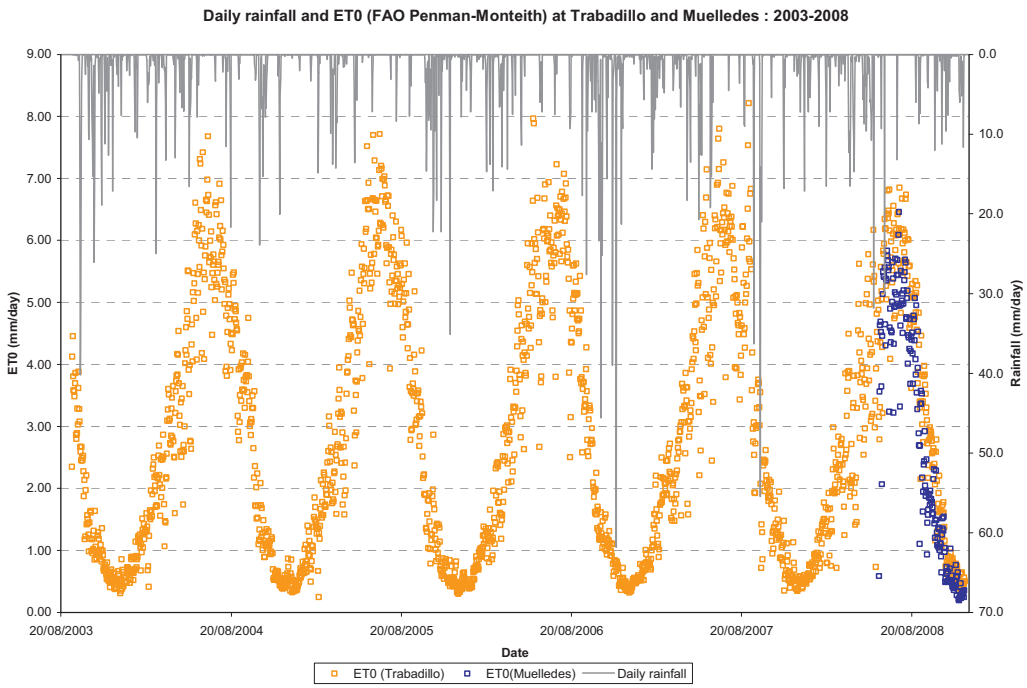

Figure 3:3 Daily rainfall and reference evapotranspiration (ET_0) by Penman-Monteith method in mm (2003-2008).

ET_0 was calculated only for June-December of 2008 at Muelledes ADAS station. Even though the stations are located at more or less north and south corners of the catchment (*Figure 3:3*), the temporal behaviour of ET_0 shows an approximately similar and systematic pattern.

The temporal actual evapotranspiration was determined by approach based on groundwater level fluctuations and temporal soil moisture data with the use of one dimensional (1-D) lumped parameter model EARTH modified (Vander Lee and Gehrels, 1990). This is explained in the Chapter 4.1.3.2.

3.6. Hydraulic head

The two wells Gejo and Gejuello (see the location map *Figure 3:1*) have continues time series hydraulic head data from September 2003 to December 2008 measured by Tirta logger. Muelledes1 and Muelledes2 wells have data strating from September 2003 but the recording have terminated during 2004 in Muelledes2 well as it reflects the similar pattern as Muelledes1. Muelledes1 has no hydraulic head data in year 2005 to 2007 due to the loss of the recording device and thereafter continues again up to now. Sardon piezometer was established again in June 2008 after it has collapsed. Data stream of September 2003 to December 2008 was available in Sardon piezometer with one year (2003-2004) data gap.

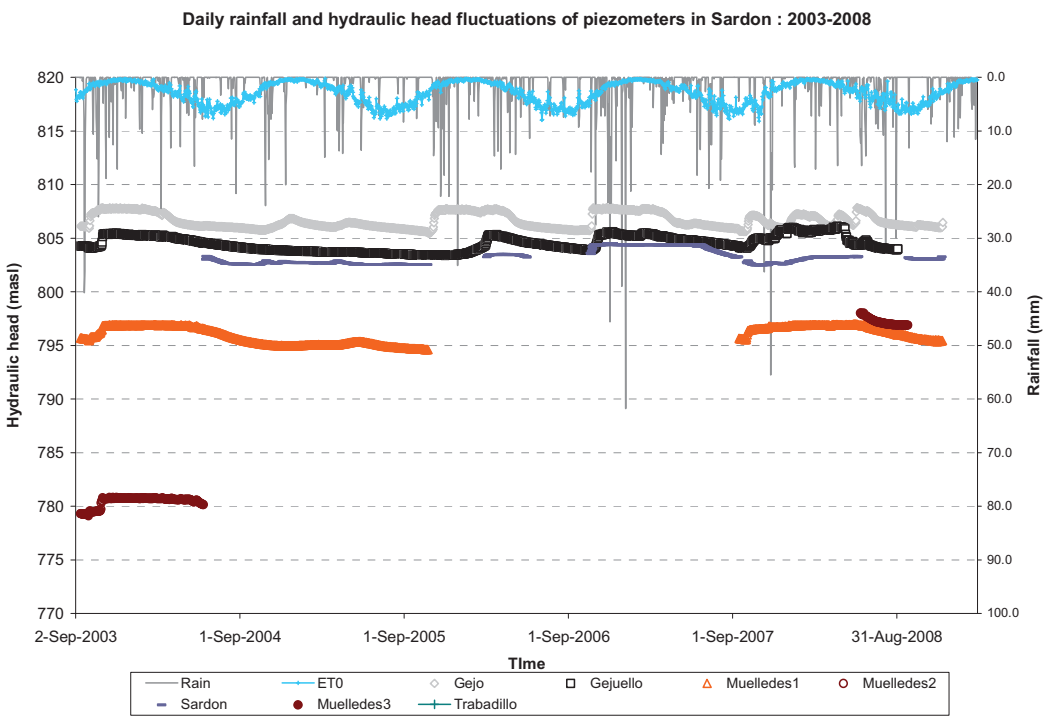

Figure 3:4 Groundwater level fluctuations of piezometers in Sardon during the period of 2003-2008.

The automated monitoring of other eight locations (wells/piezometers) was started in June 2008 and comprised only six months data. The most of the wells are few meters in depth and the deepest is around 18 meters below ground level at Muelledes2. Hydraulic heads are strongly fluctuated following the rainfall and recess until the next recharge episode takes place.

3.7. Augering piezometers

Eleven piezometers have been constructed at each sub-catchment close to the main Sardon river to obtain the hydraulic heads and chloride concentration in groundwater in addition to the existing wells (see *Figure 3:1* indicated as Pcl1, Pcl2 etc. and *Table 3-1*). The chloride concentrations provided the groundwater flow characterization of each sub-catchment which was of critical importance in calibration of the solute transport model.

Table 3-1: Technical details of the piezometers constructed during the field work

Piezometer/well	Depth (mbgl)	Diameter (cm)	Screen depth range (m)	ISWL(mbgl)
T1	2.00	5.0	1.60 - 2.00	1.27
T2	1.57	5.0	0.67 - 1.57	1.28
T3	1.68	5.0	0.78 - 1.68	1.33
Pcl1	1.80	5.0	0.90 - 1.80	0.65
Pcl3	0.96	5.0	0.50 - 0.96	0.76
Pcl4	1.76	5.0	0.66 - 1.76	1.13
Pcl5	2.51	5.0	1.61 - 2.51	1.19
Pcl6	2.14	5.0	1.24 - 2.14	1.57
Pcl7	1.53	5.0	0.63 - 1.53	1.11
Pcl8	1.59	5.0	1.61 - 2.51	1.18
Sardon	1.47	5.0	0.57 - 1.47	1.25

Auguring of piezometers was performed by Cobra percussion hammer and it was restricted only to the first 2-3 meters depth due to difficulty of drilling where boulder terrain, hard weathered rock and collapsing soils were encountered. The soil samples have been analysed in the laboratory to acquire the soil hydraulic properties (specific capacity, porosity, hydraulic conductivity etc.) of both unsaturated and saturated zones of the upper layer (Francés, 2008). The technical details of the piezometers constructed are included in the *Table 3-1*.

3.8. Chloride analysis

The chloride sampling and analysis were carried out at four instances during the period of June 2008 to December 2008. In June 2008 and in December 2008, the sampling and analysis were carried out by Alain Francés (2008a). The rest of the analysis was performed during field work carried out in September 2008. Electrical conductivity and temperature of the samples were also measured at the site. The locations of piezometers and wells are indicated in *Figure 3:1*. The analysis was performed with the chloride ISE sensor WQ-CL from Nexsens since its simplicity and environmental friendly nature (no toxic chemicals usage) over other conventional methods of spectrophotometer and digital titration and still maintaining the same accuracy level. The duplicate samples from the same location were analyzed to check the accuracy and frequent sensor calibration for every 4-6 readings were maintained.

The primary objective of the chloride analysis was to monitor the temporal variability of chloride concentration in groundwater and to apply in the solute transport model. In addition, the annual recharge estimation was evaluated through Chloride Mass Balance (CMB) method described in Chapter 4.1.1. The analyzed chloride concentrations of groundwater during these three time phases are tabulated below. The higher chloride concentration of Pmu1 in December 2008 analysis is due to

the injection of Tracer during the tracer test carried out in September 2008. The temporal variability of chloride concentration of the piezometers and wells indicated approximately negligible in this monitoring period, June 2008 to December 2008.

Table 3-2: The chloride analysis groundwater sample collected during June- September, 2008

	10-Jun-2008		1-Sep-2008		23-Sep-2008		10-Dec-2008
ID	**Cl**	**EC**	**Cl**	**EC**	**Cl**	**EC**	**Cl**
Fmz	13.93						
FsdW	8.10	82.42					
Pcl1*					23.19	222.99	22.40
Pcl3*					19.78	270.32	15.25
Pcl4*					13.52	139.07	15.11
Pcl5*					19.57	217.65	20.85
Pcl6*					26.01	191.38	24.04
Pcl7*					13.47	169.54	14.50
Pcl8*					20.83	262.52	21.93
Pgb0	11.67	196.90	9.84	187.80	11.92		13.06
Pgj0	17.84	208.69	18.62	198.30	18.93	191.17	21.56
Pgjtm0	4.96						
Pmu1	16.05	154.60	15.97	132.70	16.37	98.94	74.39
Pmu1_t1*					14.26	157.29	
Pmu1_t2*					15.04	141.84	
Pmu1_t3*					14.50	104.88	
Pmu2	12.40	142.61	12.77	155.20	14.03	87.49	18.11
Pmu3	17.79	121.48	26.74	144.20	29.01	149.88	36.70
Ppn0	16.15			433.00			
Ppn1			15.00	520.90	16.67	282.35	16.83
Psd0					33.10	1086.15	29.83
Psd2	9.70	120.28					
Ptb1	7.23	44.20					
Ptb2	8.50	49.40					
Ptb3	27.15	169.80					
Ptb6	9.85	104.50					
Ptb7	5.98	123.20					
Ptbgj0	9.83		10.74	188.80			
Ptm1	38.44	754.56	53.91	753.10	55.38	87.49	61.04

* constructed in Sept. 2008; Cl in ppm; EC (Elelctrical conductivity) in uS/cm

3.9. Soil sample analysis

The soil samples were collected at different depth in unsaturated zones at Trabadillo station in June 2008 by Francés (2008a). In addition, the samples were also obtained from both saturated and unsaturated zones during the new piezometers construction in September 2008 (see *Figure 3:1* as indicated Pcl1, Pcl2 etc). These samples were analysed by Francés (2008a) tested to acquire hydraulic properties such as porosity, specific yield, specific retention and saturated hydraulic conductivity (*Table 3-3*). The saturated hydraulic conductivity was determined by falling head method using laboratory permeameter “Eijkelkamp” (Francés, 2008a). These properties were used in the calibration of pyEARTH-1D recharge model to evaluate the temporal point recharge at the piezometers and wells.

Table 3-3: The soil samples analysed at Trabadillo and new piezometer locations from different depths of unsaturated and saturated zones

Soil type	ID	Depth	ρ (mg/cm^3)	N (%)	S_r (%)	S_y (%)	K (mm/day)
Silty soil	C_25_ILEX_0A	25	1.66	37	29	9	4229
Silty soil	outC_25_ILEX_2A	25	1.48	40	31	9	6122
Silty soil	C_25_PYR	25	1.40	43	37	6	3596
Weathered granite	C_50_ILEX_0B	50	1.48	30	24	6	5158
Weathered granite	outC_50_ILEX_2B	50	1.70	30	25	5	3650
Dark clayey soil	Ptrab6_50	50	1.63	32	26	6	1889
Weathered granite	C_50_PYR	50	1.42	38	30	8	4014
Sandy-silty	Pmu1_T1_65	65	1.43	37	34	3	6920
Sandy soil	Pcl4_70	70	1.47	32	28	5	15173
Sandy-silty soil	Pcl5_70Kh	70	1.56	36	34	2	133
Weathered granite	C_75_ILEX_3A	75	1.70	27	23	4	3903
Weathered granite	outC_75_ILEX_5A	75	1.86	24	22	2	448
Weathered granite	C_75_PYR	75	1.70	27	21	6	5368
Silty-sandy soil	Pcl5_80Kv	80	1.66	32	32	1	671
Compacted weathered granite	outC_110_ILEX_5B	110	1.84	25	20	4	9
Sandy soil	Pcl4_120	120	1.74	32	30	2	22800
Sandy soil	Pcl6_140	140	1.52	31	28	4	53404
Sandy soil	Pcl5_150	150	1.66	34	32	2	11669
Soil, transition with weathered granite	Ptrab6_150	150	1.80	25	21	5	2398
Sandy soil	Pmu1_T1_170	170	1.37	35	30	5	8732
Sandy soil	Pcl5_230	230	1.47	31	27	4	31603
Silty gravelly soil	Ptrab7_230	230	1.51	37	36	2	5
Silty soil	Pcl6_292Kv	292	1.90	28	27	1	45

* K -Hydraulic conductivity (mm/d), ρ-density (mg/cm^3), n-porosity, S_r – field capacity, S_y – specific yield

3.10. Differential GPS

The elevation and location coordinates of the piezometers and wells were obtained with differential Leica system GPS in which the accuracy is within few centimeters. Such accuracy was important to simulate the heads in the MODFLOW model and also the geometry of the model was corrected using these accurate elevation data. The locations of GPS survey are shown in *Figure 3:1*.

3.11. Inverse auger tests (slug tests)

In the dry season, the river bed is dried which precluded conventional slug test or pump testing. Instead, the inverse auger-hole method was employed as described by (Macaulay and Mullen, 2007). The initial water level was measured after known volume of water was injected. The water level drop was measured by "Keller" differential data logger/ transducers which configured to record for every one minute time interval. The time vs. water level were plotted and it is shown the curve gradually flattens out and become linear when soil becomes saturated. The vertical hydraulic conductivity was calculated using the relation

$$K_x = \frac{1.15r\{\log[h(t_i) + r/2] - \log[h(t_n) + r/2]\}}{t_n - t_i} \qquad (3\text{-}4)$$

Where K_x is vertical hydraulic conductivity (m/day), r the test borehole radius (m), $h\ (t_i)$ the initial wetting depth (m), $h\ (t_n)$ the final wetting depth (m) and t_i, t_n are initial time (s) and the final time (s) respectively. t_i and $h\ (t_i)$ were taken at the point where soil immediately surrounding the borehole become saturated. Saturation point was determined by the plot of $[\log (h\ (t_i) + 0.5\ r) - \log (h\ (t_n) + 0.5r)]$ against time (t) where the curve started to be linear due to saturation. The graphs of the two sites are shown in *Figure 3:5*.

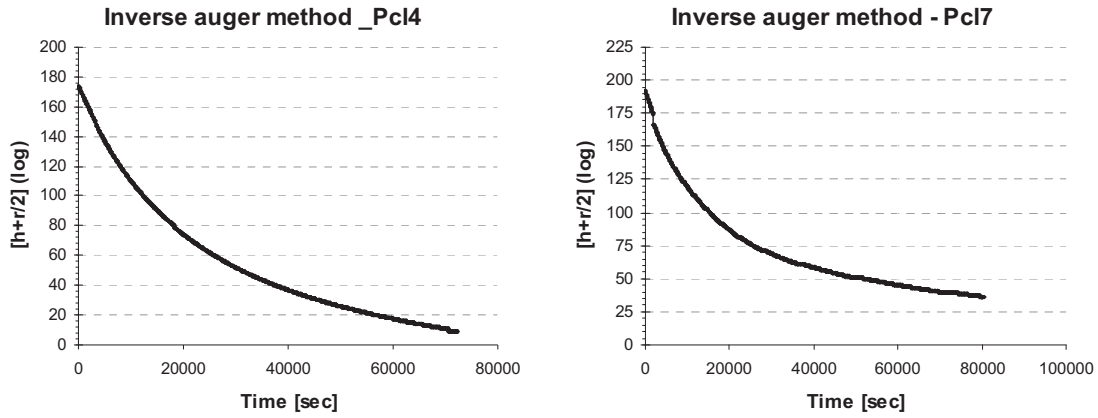

Figure 3:5 The time vs. water level in the two boreholes tested for drain conductance.

K_x assessed by this model (*Table 3-4*) were used to define the river conductance more reliably in the drain package of final MODFLOW model. Two tests were done at the Sardon river bed near to Pcl4 and Pcl7 piezometers (see *Figure 3:1*) and the test was repeated twice at each site as the dry river bed absorbs water more swiftly at the start and therefore the second test was more reliable to determine the river bed conductance.

Table 3-4: Inverse auger results at Sardon river bed near to Pcl3 and Pcl7 piezometers locations.

Location	Hole diameter (cm)	Test-hole depth (cm)	Initial water level (cmagl)	Sensor Depth (cmbgl)	K(cm/day)
Pcl4	14.1	60.0	128.6	50.0	14.01
Pcl7	14.1	60.0	110.2	50.0	3.50

*cmagl- cm above ground level; K – Hydraulic conductivity

3.12. Tracer tests

A forced gradient test was carried out at Muelledes site during field work September 2008 and the condition was simulated in the numerical model to determine the dispersivity. The details of this tracer test and the model setup are explained in Chapter 5.

4. Assessment of recharge and groundwater evapotranspiration

This chapter mainly deals with the pyEARTH-1D model assessment of spatio-temporal recharge and actual evapotranspiration fluxes further integrated with spatial maps by using remote sensing and GIS.

4.1. Recharge evaluation

The quantification of the recharge (R) and ET_g in an aquifer is a critical factor in semiarid regions. The reliability of the estimation of all the components of the groundwater budget largely depends on the accuracy of R and ET_g. There are different techniques available in the estimate of recharge and ET_g. The applicability of the techniques depends on its limitation and reliability, available data and the amount of data required. The application of EARTH and SWAP models are limited due to difficulty in finding necessary parameters readily available (Obakeng, 2007). However, these models are more reliable compared to widely used water balance models for recharge estimation (Obakeng, 2007). This is especially critical in semiarid areas where the groundwater recharge is relatively small in comparison to other components of rainfall or evapotranspiration, thus difficult to determine accurately (Bouwer, 1989; Brunner et al., 2004). The multiple recharge estimation techniques are required to compare and check the reliability of the applied techniques.

The overall understanding of the area and recharge influencing factors such as climatic condition, topography, landuse, soil and vegetation type, hydrogeologic data (Scanlon et al., 2002), should be assessed before applying any recharge technique. The available recharge estimation methods for semi-arid areas have their own limitations. Therefore, it is required to have a thorough understanding of the hydrogeogical processes of the study area and the measurement point of recharge should be well represented for the area, to obtain the recharge estimates reliably. The chloride mass balance, pyEARTH-1D model and well hydrograph analysis results were used to evaluate the recharge spatially and temporally, finally validated in MODFLOW / MT3D models.

4.1.1. Recharge by Chloride Mass Balance (CMB)

The CMB method is based on the assumption of conservation of mass between the inputs of atmospheric chloride and the chloride flux in the subsurface (Sharda et al., 2006). CMB is a better choice due to its simplicity, less data requirement but it gives lower recharge values compared to other techniques (Cook, 2003), hence it is required to compare with another method to check the reliability. The technique is based on the mass balance of chloride and therefore it can not be applied in areas underlain by evaporates or areas where mixing of saline groundwater occurs and in coastal or industrial areas where high variability of chloride in rainfall is occurred.

During the field work in September 2008, chloride concentrations of groundwater were analysed from 23 water samples collected at the existing boreholes and newly constructed piezometers (refer *Figure*

3:1). The average chloride content in the rainwater was 1.4 mg/l and average annual precipitation of the catchment is 574 mm/year. The quantitative point recharge is determined using the following equation.

$$R = \frac{PCl_p + D_{Cl}}{Cl_{gw}} \qquad (4\text{-}1)$$

Where R is mean recharge rate in mm, Cl_p is chloride concentration in precipitation (mgl^{-1}), Cl_{gw} is chloride concentration in groundwater (mgl^{-1}), D_{Cl} (mgl^{-1}) is dry deposition of chloride assumed negligible in this study and P is mean precipitation in mm/yr. The information of the location and the recharge calculated at different location by CMB method is shown in *Table 4-1*.

Table 4-1: Chloride concentration of the groundwater samples (September, 2008) used for point recharge calculation by CMB method and annual recharge as rainfall percentage.

ID	Place	Cl_{gw} (mg/l)	Recharge (mm/year)	Recharge % to annual rainfall
Fsdw	Sardon and Valdenora	8.10	99.2	17.3
Pcl1	Trabadillo; near the bridge	23.19	34.7	6.0
Pcl3	Trabadillo ; near flume	19.78	40.6	7.1
Pcl4	near Penalbo	13.52	59.4	10.4
Pcl5	Tremadal; penalbo	19.57	41.1	7.2
Pcl6	Tremadal	26.01	30.9	5.4
Pcl7	Tremadal(slug test2)	13.47	59.7	10.4
Pcl8	Adjoning Sardon river	20.83	38.6	6.7
Pgb0	Close to Gejuello del Barro	11.92	72.1	12.6
Pgj0	Close to Gejo	18.93	43.5	7.6
Pmu1	South to Muelledes ADAS station	16.37	49.8	8.7
Pmu1_T1	Near pmu1 well	14.26	56.4	9.8
Pmu1_T2	Near pmu1 well	15.04	53.4	9.3
Pmu1_T3	Near pmu1 well	14.50	55.4	9.7
Pmu2	North to Muelledes ADAS station	14.03	61.5	10.7
Pmu3	Muelledes ADAS station	29.01	32.8	5.7
Ppn0	Penalbo, close to river	16.67	49.8	8.7
Ppn1	App. 50 m from Ppn0 (pond)	15.84	50.7	8.8
Psd0	Sardon village	33.10	24.3	4.2
Psd2	Sardon and Valdenora	9.70	82.8	14.4
Ptb1	Trabadillo	7.23	111.1	19.4
Ptbgj0	Trabadillo and Gejo dos Reyes	10.74	78.2	13.6
Ptm1	In Tremedal village	55.38	16.3	2.8

The average chloride concentration in groundwater calculated from the analysed samples is 16.8 mg/l and the distribution is governed by amount of recharge, ET_g and natural groundwater flow regime. The higher recharge values of Sardon, Trabadillo and Gejo locations are due to geomorphologically higher locations thus higher potential recharge zones compared to Muelledes and Penalbo locations which are located in discharge zones. The annual average recharge of the entire catchment is 44.2 mm/yr (8 % rainfall) calculated by CMB method from the chloride harmonic mean of 18.17 mg/l. The recharge values from the CMB methods are in generally used as input for steady state numerical

models because it represents long term average recharge estimate due to slow and complex process of mixing (Lubczynski and Gurwin, 2005).

4.1.2. Recharge by well hydrograph analysis

The application of well hydrograph method can be considered as reliable in Sardon since the catchment is not affected by groundwater abstraction. Under such a condition, recharge can be deduced from the groundwater level fluctuation as an indirect method (Kruseman, 1997) by following formula.

$$R = \Delta h S_y + Q_{ab} + \Delta Q_{in-out} \qquad (4\text{-}2)$$

Where R, Δh, S_y, Q_{ab} and ΔQ_{in-out} are recharge, change in water level elevation, specific yield, groundwater abstraction and difference of lateral inflow-outflow respectively. The recession constant is required to calculate the amount of rise in a recharge event of the well hydrograph and it is given;

$$H_t = H_0 . e^{-\alpha t} \qquad (4\text{-}3)$$

Where H_t is groundwater level at time t, H_0 is initial groundwater level and α is recession constant. The recession constant was calculated by well hydrograph analysis (Dingman, 2002). The result of the analysis in piezometers and wells is summarised below. The analysis data processed from the hydraulic head data are in Appendix E.

Table 4-2: Recharge analysis results by well hydrograph method

Well	α (10^{-3} m/day)	S_y	RF %
Gejo	3.10	0.030	12.9
Gejuello	4.90	0.080	20.7
Muelledes1	9.59	0.025	04.7
Muelledes2	6.46	0.020	05.7
Sardon	19.4	0.022	05.2
Trabadillo	12.46	0.010	03.7

α - recession constant; S_y - specific yield; RF – recharge as rainfall %

The specific yields of the locations were used considering the soil sample results, available literature and parameter configuration of calibrated pyEARTH-1D model.

4.1.3. Temporal recharge by pyEARTH-1D model

The temporal variation of the recharge was assessed using the EARTH model theory, which is a 1-D lumped parameter hydrogeological model for simulation of soil moisture content, actual evapotranspiration, recharge and deep groundwater level fluctuations (Gehrels and Van der Lee, 1990). The model result provides daily recharge at discrete points. It is required unsaturated soil properties and aquifer parameters which can be obtained through laboratory testing and field work. The temporal input data required by the model is daily rainfall and potential or reference evapotranspiration. Model calibration was performed by the adjustment of soil moisture values and aquifer parameters until the calculated hydraulic head is matched with the measured hydraulic heads.

The advantage of EARTH model is its simplicity and insensitivity to the type of recharge mechanism, hence not restrained by preferential flow (Healy and Cook, 2002). On the other hand, the model does not account for lateral groundwater flow in recharge evaluation. The EARTH model consists of four sequential modules or reservoirs and each represent a specific zone in the process of recharge as illustrated in *Figure 4:1*. The first two modules, MAXIL and SOMOS represent the agro-hydro-meteorological zone while LINRES and SATFLOW modules stand for the hydro-geological zone of the modelled space. MAXIL simulates the canopy interception. SOMOS is a module which simulates water balance in the root zone where the precipitation is redistributed into actual evapotranspiration (Et_a), percolation and soil moisture storage. LINRES module controls the percolation from the SOMOS unsaturated zone into the SATFLOW module representing saturated zone of groundwater reservoir (The description of each module of the EARTH included in the Appendix F).

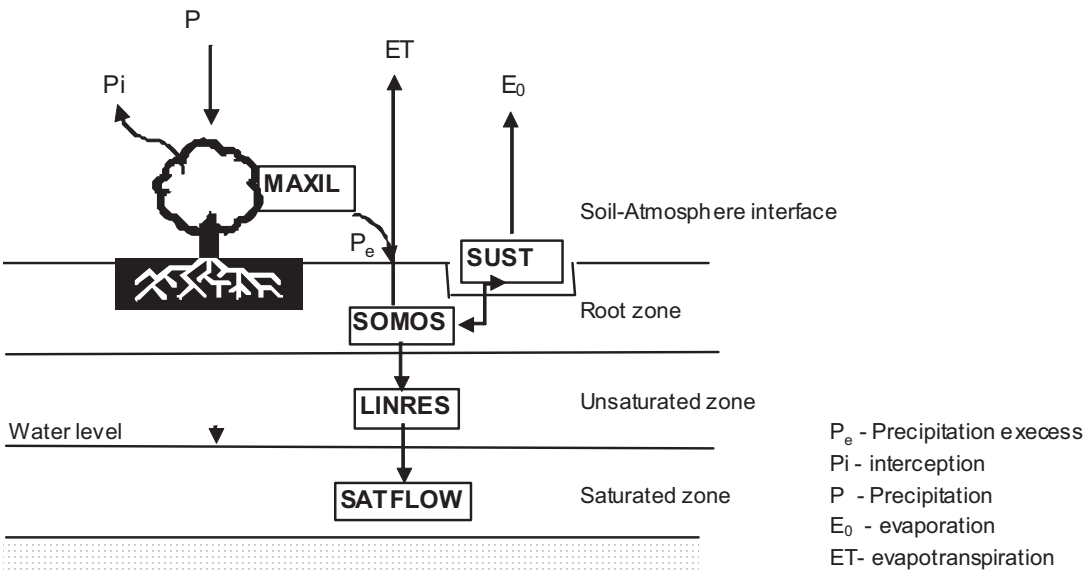

Figure 4:1 EARTH model represented by subsequent modules of subsoil, unsaturated zone followed the saturated zone (after Francés, 2008).

In this study, the computations were made using the modified EARTH version called pyEARTH-1D developed by Francés(2008b) in Python language. Besides the implementation of a graphical user interface (GUI), this new code introduced few modifications to improve the pre and post-processing and to implement new functions.

4.1.3.1. Model input data

In this study, the model parameters were estimated by combination of direct field work, laboratory test and available field data with the literature (*Table 4-3*). The processed daily rainfall and ET_o calculated from the ADAS monitoring data was used as temporal input data for the pyEARTH-1D model.

Soil moisture content at field capacity, saturated hydraulic conductivity, residual soil moisture and porosity were also determined through laboratory analysis on soil samples collected during field work

(Chapter 3.9) and the data were used in the model calibration of pyEARTH-1D at different piezometer locations.

Table 4-3: Soil and aquifer parameters for pyEARTH-1D model and their derivations for the study

Modules parameters	Derivation method
MAXIL(Interception) Maximum interception loss (mm)	Recommended by Pitman (1973) for different land cover types; (2-3mm range)
SOMOS (Soil moisture storage) Maximum soil moisture content (mm) Residual soil moisture content (mm) Initial soil moisture content (mm) Soil moisture at field capacity (mm) Saturated conductivity (mm/day)	Laboratory tests of collected soil samples
SUST (Surface storage) Maximum surface storage (mm)	Field observations
LINRES (Linear reservoir routing) Unsaturated recession constant (days) Number of reservoirs	Calibrations
SATFLOW (Saturated flow model) Saturated recession constant (days) Storage coefficient Initial groundwater level (m) Local base level (m)	Analysis of temporal hydraulic head data; available field data

The saturated recession constant and local base level of the locations was determined through well-hydrograph analysis (Dingman, 2002). The general recession equation of a well hydrograph is

$$h = h_o + (h_o - h_b).e^{-kt} \qquad (4\text{-}4)$$

Where h_b is local base level, h_0 is initial hydraulic head from local base level, k is recession constant (equivalent to saturated recession constant in pyEARTH-1D model) and t is time. In this procedure, the recessions of the hydraulic head were calculated for several dry periods and obtained the average for a representative recession constant using the procedure explained in Dingman (2002). Since SATFLOW is highly sensitive to aquifer specific yield and to recession constant parameters, accurate determination of recession constant and local base level is indispensible step in calibration of pyEARTH-1D. The calibrated result of the model provides the temporally variable recharge and ET_a.

4.1.3.2. Recharge and ET_a calculation

The hydraulic head data at six piezometers in the catchment were used for calibration with pyEARTH-1D model to determine the recharge for the period of 2003 - 2008. For calibration of pyEARTH-1D model the daily groundwater levels of Gejo and Gejuello wells from September 2003 to December 2008, Muelledes1 and Muelledes2 wells with data from September 2003 to mid of 2005 and Sardon and Trabadillo piezometers with data from 2004 to 2008 were used. The manual water level measurements obtained in the previous field works were also used to fill the data gaps (see appendix J).

The groundwater level data were used for calibration and various soil and aquifer parameters were applied for parameter configuration in pyEARTH-1D model. SOMOS parameters were obtained from the results of soil sample analysis for different soil types as explained in the Chapter 3.9. The recession constant/drainage resistance and local base level parameters of SATFLOW were assessed by recession curve determination method (Dingman, 2002). The obtained values are shown in the *Table 4-4* which was used in the calibration. The soil analysis results indicated the specific yield is 0.02 - 0.12 range and soil porosity changes between 0.31 to 0.42. The saturated hydraulic conductivity varies from 448 mm/d to 6122 mm/day and during optimization it was observed that the hydraulic conductivity did not significantly influence on the calculated recharge. The MAXIL and initial soil moisture were determined by the available information. LINRES values were applied on trial and error method for calibration. The sandy clayey top soil layer in the Sardon area is well compacted and therefore the infiltration capacity is not very high. Because of this reason, surface storage was given a small capacity to generate considerable runoff during the calibration process. The storage coefficient *(STO),* is one of the most sensitive parameters for the estimation of recharge from groundwater modelling (Gehrels and Van der Lee, 1990). The final parameter configurations for each of the piezometer are shown in *Table 4-4*.

Table 4-4: Input parameters used in final calibration of pyEARTH-1D

Location	S_{max}	S_r	S_I	θ_{fc}	MAXIL	K_s	URC	n	SRC	STO	h_0
Gejo	300	110	150	200	1.0	1300	5	1	70	0.030	805.49
Gejuello	300	100	100	200	2.0	1000	5	2	275	0.080	805.70
Muelledes1	300	100	150	240	1.0	1200	17.5	1	150	0.025	796.90
Muelledes2	310	60	60	225	1.0	1100	25	1	80	0.020	781.35
Sardon	300	100	100	200	2.0	200	15	1	125	0.022	804.40
Trabadillo	300	150	125	250	3.0	120	35	2	50	0.010	739.10

S_{max} - maximum soil moisture content (mm); S_r - residual soil moisture (mm); S_I - initial soil moisture (mm); θ_{fc} - field capacity (in mm); *MAXIL* - maximum interception loss; K_s - saturated conductivity (mm/d): *URC* - unsaturated recession constant (days): n - number of reservoirs; SRC - saturated recession constant (days); STO - storage; h_0 - local base level (m)

Muelledes1 and Muelledes2 wells are located in a same hydrogeological condition of the area. However except the storage coefficient, the other properties of the unsaturated zone determined in the final pyEARTH-1D model calibration are considerably different. The detail results of recharge and ET_a are presented in appendix D.

In unsaturated zone, many parameters are used for simulation of measurements and therefore use of general parameter estimation programmes is not a good choice (Gehrels, 1999). Therefore model calibration of pyEARTH-1D was performed manually. The high spatial variability of soil properties over depth and space in the Sardon area created difficulty in efficient calibration of head measurements. The simulation of the observed data was difficult in locations at the discharge areas where lateral groundwater fluxes are more pronounced compared to vertical downward recharge through percolation since the pyEARTH-1D model is a 1-D model and not accounted these lateral fluxes. Some of the piezometers were flooded in winter periods and still this is been calculated by the pyEARTH-1D model as recharge thus the calculated recharge was overestimated during these flooded periods. The simulated heads in the piezometers were therefore raised above the elevation level. This effect was corrected in the pyEARTH-1D model. In this model, the simulated excess recharge above the piezometric level is conveyed to SUST module and the unrealistic recharge effect is prevented.

The summary of the pyEARTH-1D result are shown in *Table 4-5* and the calibration curves of the piezometers are illustrated in *Figure 4:2* to *Figure 4:7*.

Table 4-5: Mean daily and mean annual recharge summarized by the pyEARTH-1D model results

Location	Recharge		
	MD	MA	RF %
Gejo	0.46	168.3	29.3
Gejuello	0.42	151.8	26.4
Muelledes1	0.31	111.6	19.4
Muelledes2	0.30	108.6	18.9
Sardon	0.30	109.6	19.1
Trabadillo	0.16	59.93	10.4

*all figures are in mm; RF% - recharge as a rainfall percentage; MD - mean daily; MA - mean annual;

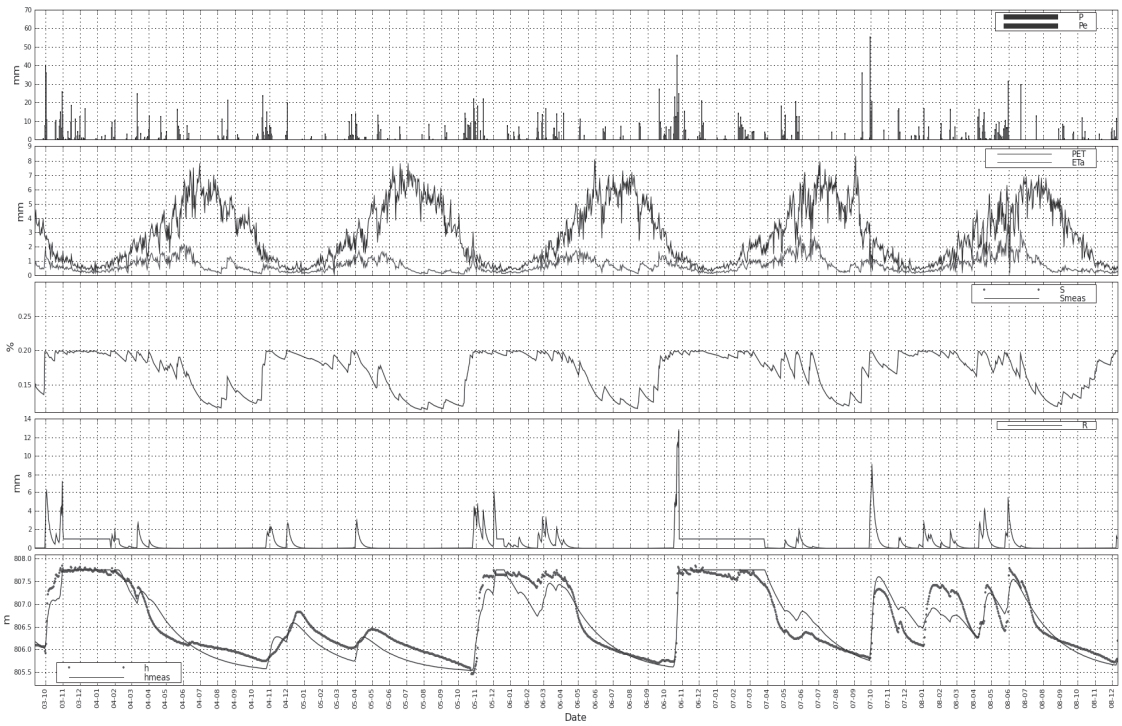

Figure 4:2 The results of pyEARTH-1D model calibration at piezometer Gejo.

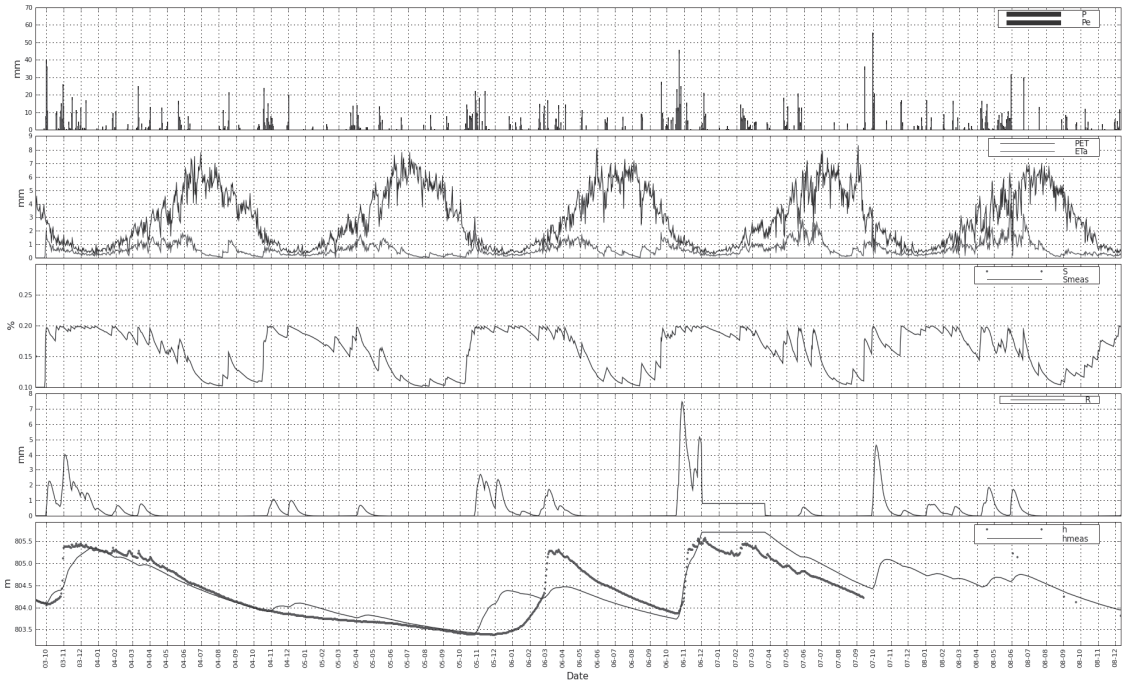

Figure 4:3 The results of pyEARTH-1D model calibration at piezometer Gejuello.

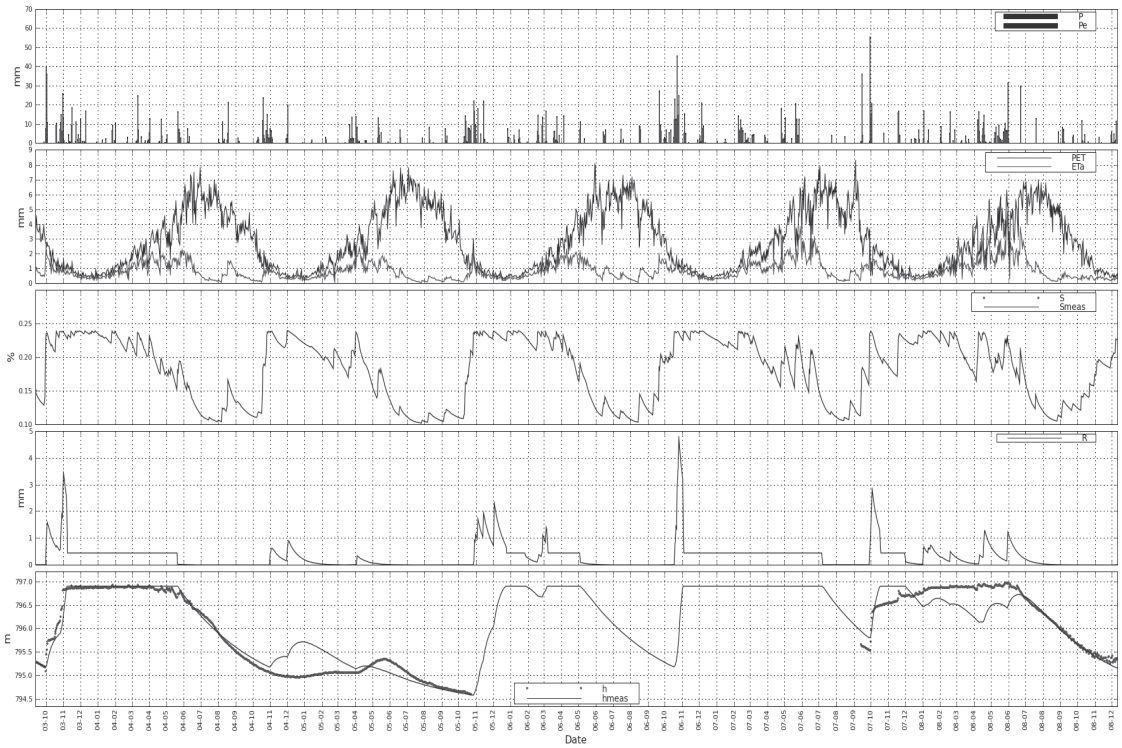

Figure 4:4 The results of pyEARTH-1D model calibration at piezometer Muelledes1.

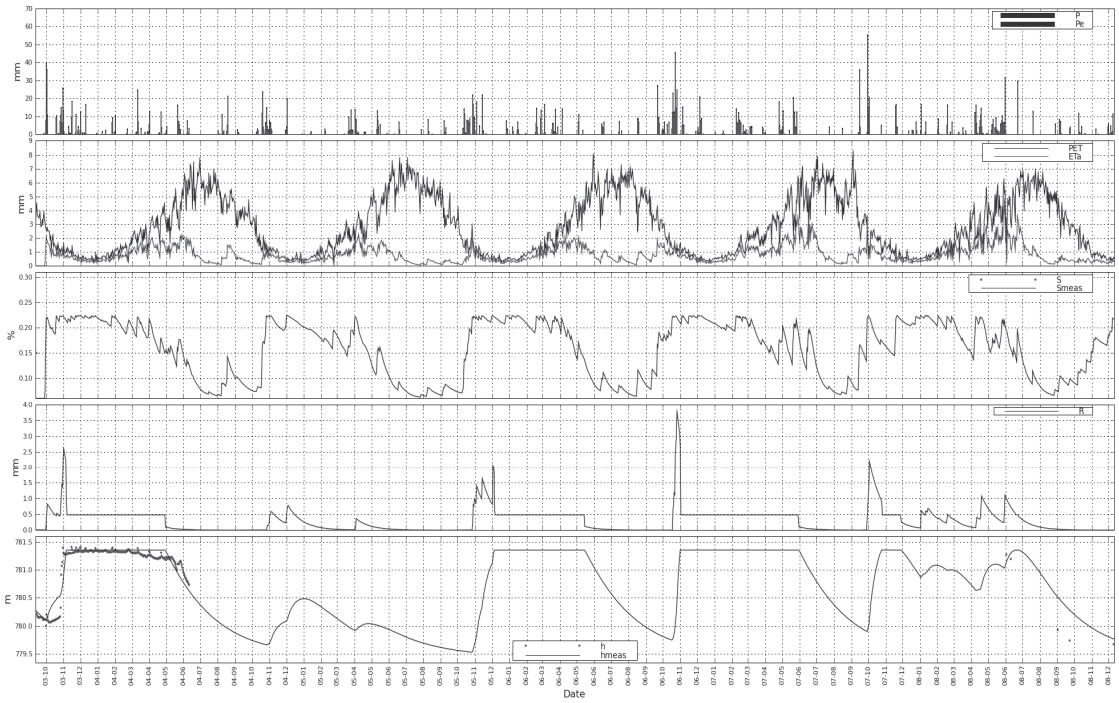

Figure 4:5 The results of pyEARTH-1D model calibration at piezometer Muelledes2.

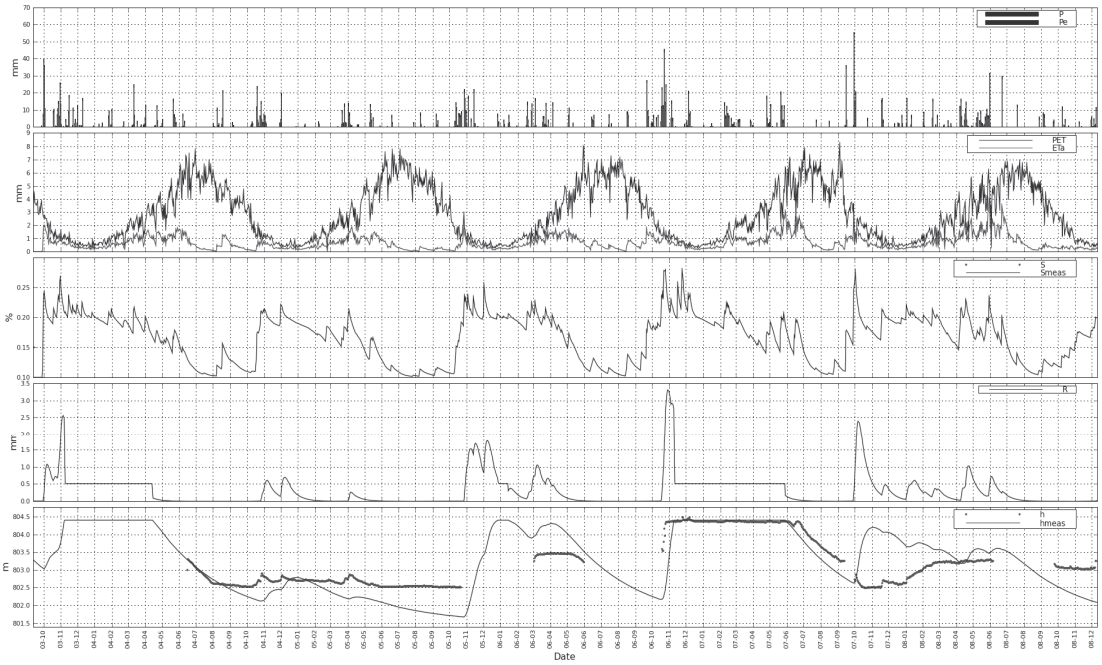

Figure 4:6 The results of pyEARTH-1D model calibration at piezometer Sardon.

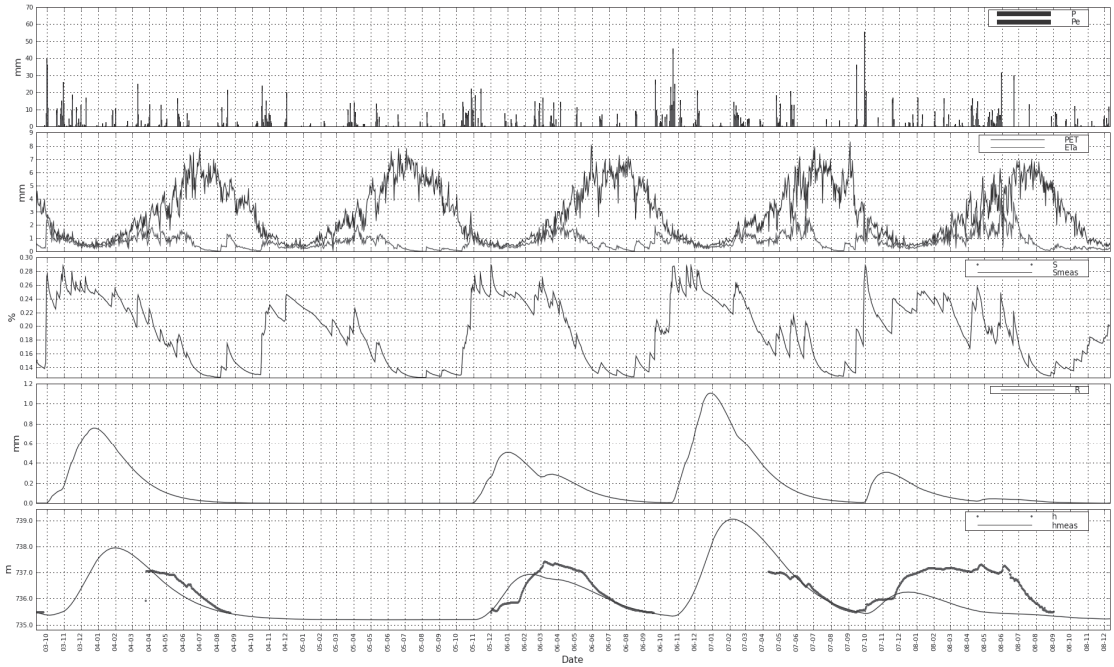

Figure 4:7 The results of pyEARTH-1D model calibration at piezometer Trabadillo.

In all of the graphs in Figure 4.2 to 4:7, from top to bottom indicated the daily rainfall, daily ET_0 (thick line) and model calculated Et_a (lighter line), soil moisture and recharge respectively. Finally calculated and measured daily hydraulic heads in the bottom.

4.1.4. GIS map modelling for spatial distribution of recharge

The model results of pyEARTH-1D and chloride mass balance method indicated a high spatially and temporarily varied recharge in the study area despite the uniform rainfall. This spatial variation is due to spatial heterogeneity originated from spatially varying topography, vegetation, soil characteristics etc. Therefore, interpolation of point recharge through a geostatistical analysis is not always realistic and accurate procedure to obtain spatial recharge distribution particularly in data scarce environments such as Sardon study area (Lubczynski and Gurwin, 2005). Instead, GIS cross-overlay procedure (Shakya, 2001) can be used to obtain the recharge spatial distribution maps for each defined stress period.

The maps of vegetation cover, vegetation type, landuse, drainage density, fracture density, lithology, outcrop and soil type, recharge and discharge area, slope, groundwater depth and soil thickness were considered as influential factors on the groundwater recharge. These maps were classified into zones and different weighted scores within 1 to 10 were given for each zone in a map considering the amount influence on recharge. Each individual map was then assigned a map weight and merged together in GIS platform using ILWIS map calculation procedure. Finally, a single map was produced with showing relative susceptibility for recharge on pixel basis. This is classified into different relative recharge distribution zones with slicing procedure in ILWIS. The resulted qualitative map was cross checked with point recharge data obtained from CMB and pyEARTH-1D model to verify and or adjust the validity of the zoned map. The assigning of weights for different attribute maps were

changed until the relative recharge zones and point recharge data distribution of the piezometer locations were in satisfactorily agreed.

Spatial recharge maps which are required for each defined stress period in the transient model were constructed using this relative recharge zoned map and the average recharge flux determined for each stress period from the result of pyEARTH-1D model at six piezometer locations. These spatio-temporal recharge maps were applied as recharge input to the transient model simulations.

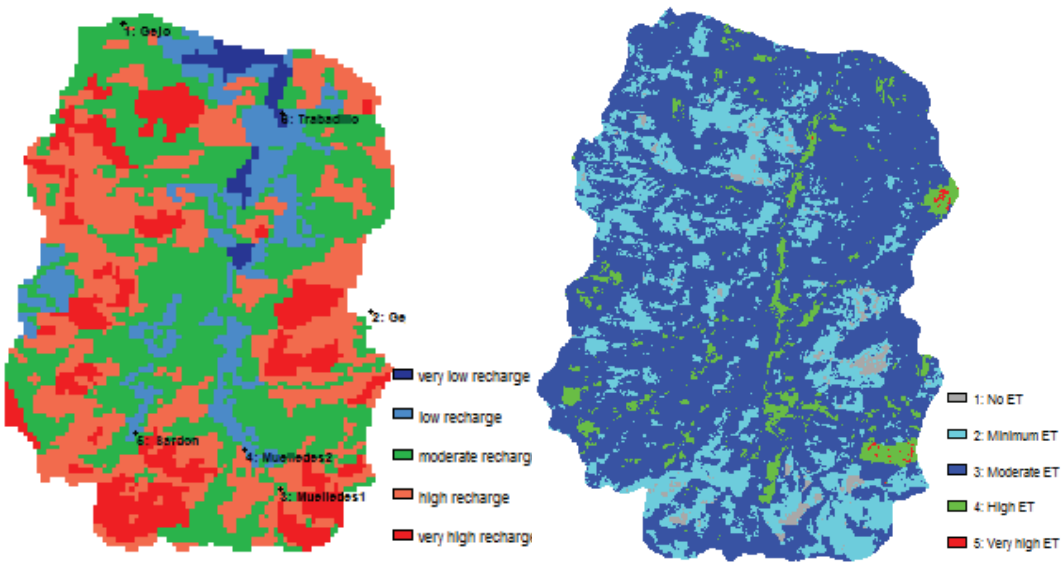

Figure 4:8 Recharge zonation map by index-overlay procedure and evapotranspiration zonation map by SEBAL algorithm (After Worku, 2000)

4.2. Evapotranspiration - groundwater interaction

The evapotranspiration is generally referred as the evaporation from bare soil, water surface and transpiration from vegetation covers. Even in case of unsaturated zone was completely depleted, the evapotranspiration could exist due to direct water loss from groundwater table as groundwater evaporation (E_g) and/or tree groundwater transpiration (T_g) due to the action of tree roots taping groundwater (Lubczynski and Gurwin, 2005). These tree species (phreatophytes) can play an important role in groundwater balance studies of arid and semi-arid regions due to the interaction between phreatophytes and groundwater (Batelaan, 2006). The groundwater loss due to T_g and E_g is collectively referred as groundwater evapotranspiration (ET_g) and plays an important role in overall groundwater balance studies specially semi arid regions.

The hard rock terrain of Sardon area is covered by thin overburden soil layer and it is totally depleted during dry period. Therefore it can be assumed that the evapotranspiration in dry season taken place almost entirely from saturated zone. However evapotranspiration in the unsaturated zone may exist even during dry season, depending on the soil moisture availability (Lubczynski, 2000). For the convenience of groundwater modelling, it could be regarded as ET_g in dry season. This has been

confirmed by the sapflow measurements of trees combined with tracer tests by previous studies (Shakya, 2001) during dry seasons.

4.2.1. Temporal ET_g assessment

The temporal variation of actual evapotranspiration (ET_a) was calculated by pyEARTH-1D model calibration on piezometric head data applied in the previous section 4.1.3. The average flux of ET_g for each stress period defined in the fully-transient model was calculated using daily ET_a at these six locations. This point fluxes are used for the spatial map preparation for each stress period with the assumption that actual ET_a in dry season is equal to ET_g. The mean daily and annual ET_a is summarised in the Appendix D.

4.2.2. Spatio-temporal ET_g map preparation

The spatial distribution map of ET_a processed by Worku (2000) was used to construct the spatial ET_g maps for each stress period. This base map has been constructed using Landsat image with the SEBAL algorithm (Bastiansen, 1998) by energy balance methods in the dry season. The ET_a result obtained by pyEARTH-1D model was scaled with spatial variability ET map to produce spatio-temporal maps of ET_g for different stress periods in the dry seasons of 2003-2008. These spatially distributed zones of ET_g were used as input maps for the groundwater transient model.

5. Dispersivity assessment by tracer tests

In addition to flow model parameters, effective porosity and dispersivity are required to simulate solute transport modelling. This chapter is focused on deriving solute and hydraulic parameters by local scale model with the use of tracer test results which provide the input data required to simulate in the numerical model. The numerically derived dispersivity was upscaled to apply in the regional solute transport model.

Movement of contaminant dissolved in groundwater is governed by advection and diffusion while the spread and dilution is controlled by dispersion (Fetter, 2001). Advection is due to the flow of water in which contaminant is dissolved. The direction and rate of transport coincides with the groundwater flow. Hence the advection is completely governed by the flow velocity. Dispersion occurs by diffusion and mixing processes. Diffusion is governed by Fick's law and mixing process referred as mechanical dispersion is due to velocity variations (Vandenbohede and Lebbe, 2003). Dispersivity is considered as characteristic property of a porous medium and in practice, it is quantified in longitudinal and transverse to the flow direction. The advection-dispersion equation is based on the law of mass conservation presented by Freeze and Cherry (1979) and as follows.

$$\frac{\partial C}{\partial t} = D_x \frac{\partial^2 C}{\partial x^2} + D_y \frac{\partial^2 C}{\partial y^2} + D_z \frac{\partial^2 C}{\partial z^2} - \bar{u}_x \frac{\partial C}{\partial x} - \bar{u}_y \frac{\partial C}{\partial y} - \bar{u}_z \frac{\partial C}{\partial z} \qquad (5\text{-}1)$$

Where, C = C(x,y,z,t) is the solute concentration, $\bar{u}$ = average linear velocity and D_x, D_y, D_z are dispersivities in x, y, z directions respectively.

5.1. Tracer tests

Tracer testing can provide insights into groundwater flow characteristics and contaminant transport processes that are not provided by conventional aquifer testing methods (Paul and Bruce, 2004; Vandenbohede and Lebbe, 2003). In a tracer test, the chemical component of groundwater is monitored to deduce the advection and dispersion. The main objective of this trace test was to derive the solute transport properties for simulating the regional solute transport model. Different types of tracer tests have been designed in field applications to derive the dispersivity such as natural gradient, forced gradient tracer test etc. In the multiple wells forced gradient test (MWFGT), a known concentration and volume of tracer-mixed water is injected to the injection well and pumping is continued at the nearby observation borehole. This way the plume movement is monitored and determined the dispersivity by analytical solutions or numerical modelling.

In multiple wells natural gradient test, except the pumping, the procedure is identical as described in multiple forced gradient tests. Natural-gradient tracer tests are difficult to implement since long tracer transport times are involved. Natural-gradient tracer tests are desirable because of flow regimes are

not distorted. However, the forced-gradient tests minimise the density effect due to higher induced horizontal advection and consequent result of dispersion by pumping (Vandenbohede and Lebbe, 2003). Therefore, multiple wells forced gradient test (Vandenbohede and Lebbe, 2006) was performed at Muelledes, Pmu1 location (see *Figure 3:1*) during the field work to derive hydraulic and solute transport parameters. The approach is discussed in the following sections 5.2 before the starting of tracer test and section 5.3 discussed the methodologies used during the test.

5.2. Tracer test setup preparation

The subsurface stratigraphy of Sardon catchment area is two layered structure and the top soil is followed by weathered fractured granite at varying thickness, composition and texture which are controlled by geology and structure. Muelledes area was selected since the stratigraphy represents the general stratigraphy of the Sardon catchment. Before the tracer test, the following procedures were followed,

- Site selection
- Piezometer constructions
- Geophysics

5.2.1. Site selection

Two pumping tests were initially carried out at Muelledes1 and Muelledes2 wells to select a suitable site for the tracer test (see *Figure 3:1* indicated as Pmu1 and Pmu2). The pumping test Muelledes2 lasted for 0.5 hours at discharge rate of 15 lpm (litres per minute) due to low well-yield. 80% recovery was observed after 27 hours. Muelledes well was pumped at 5 lpm for 4.5 hours and stopped due to dewatering of the well. The 80% recovery of this well was obtained within 0.5 hours. These tests were carried out as single well constant discharge test and the aquifer condition seemed to be leaky unconfined. As short pumping time, the analysis of pumping result was not accurate due to high influence of well storage. Therefore recovery data was also analysed through Theis's recovery method (Kruseman and de Ridder, 1992), addition to Jacob's straight-line method applied for pumping data. The recovery data is considered more reliable in pumping test analysis because recovery occurs at a constant rate, whereas a constant discharge and equilibrium flow condition during the pumping is often difficult to achieve in the field (Kruseman, 1997). The final result obtained from the Theis's recovery is summarized in *Table 5-1*. The Muelledes2 recovery test data was not recorded due to an error in the monitoring logger. The analysed results of the muelledes1 well are shown in the table 6.1 and pumping test analysis curves are in Appendix G.

Table 5-1: Pumping test results for site selection

Location	Depth(mbgl)	Initial GWL (mbgl)	Discharge (lpm)	Pump time (min.)	T(m_2/day)	K (m/day)
Muelledes1	7.90	1.30	5.00	278.0	2.60	0.39
Muelledes2	17.95	1.59	15.00	20.0	not analysed	

*mbgl - meters below ground level; lpm - litres per minute

Muelledes, Pmu1 well site was selected for tracer test from the result of pumping test analysis. The safe well yield of Pmu1 was also very low (5 lpm), despite the rapid well recovery.

5.2.2. Piezometer constructions

Three piezometers were constructed at different distances from the pumping well (Pmu1) considering the natural groundwater flow as shown in the *Figure 5:1*. The top most soil and alluvium layer is 1.5 m thick while the weathered fractured granite layer is 10-12 m thick. T2 and T3 piezometers are penetrated and screened only in top layer. T1 was screened only in second layer and blank casing was installed on top layer. The existing well (Pmu1) was used as pumping and observation well which is 6.5 m below the top soil alluvium layer. The distance of these piezometers from Pmu1 were decided based on the result of pumping test analysis. T1was selected for injection of tracer considering flow direction, borehole depths and other piezometers were used as observation wells. The technical details of the all piezometers and Muelledes1 well is summarised in *Table 5-2*.

5.2.3. Geophysics

Before the tracer test, one deep Schlumberger vertical electrical sounding (VES) was carried out at the injection well (T1) to delineate the subsurface condition which required to construct the conceptual model of the site. Electrical resistivity tomography (ERT) was also performed at the T1 along two transect directions N-S and E-W to a probing depth of 15 m before the test. These ERT survey was performed under supervision of Michel Groen, Free University of Amsterdam.

5.3. Forced Gradient Tracer test with pumping test

After the completion of the setup described above, the forced gradient tracer test were carried out at the site and the following steps were involved during the test,

- Pumping test
- Tracer injection
- Geophysics
- Plume monitoring in piezometers

5.3.1. Pumping test

The safe well yield of the Pmu1 was very low and it was estimated as 5 lpm from the initial pumping tests done before the tracer test. Therefore pumping was carried out several times with a recovery in between. During the tracer test, the pumping well (Pmu1) was pumped seven times at a rate of 5.0 lpm. The total pumping time was 590 minutes within 2 days longer tracer test.

5.3.2. Tracer injection

Salt (NaCl) was selected as the tracer, because chloride is considered as a conservative element due to low sorption and radioactive decay (Serrano, 2001). At low concentration levels (approximately electrical conductivity less than 20 mS/m), the groundwater flow regimes are unaltered (Anderson and Woessner, 1992). Therefore, the density effect on the plume distribution was assumed negligible.

The tracer injection was started at piezometer, T1 after 1.5 hours of pumping at the well (Pmu1) since no immediate response in three piezometers (T1, T2 and T3) was observed due to pumping in Pmu1.

Tracer volume of 250 litres with electrical conductivity (EC) 21 mS/cm was injected into the piezometer, T1 for 7.5 hours at 0.5 lpm. The piezometer (T1) is located at 4.60 m away from the pumping well. The tracer injected piezometer is screened only in the second weathered granitic layer (*Figure 5:1*).

5.3.3. Geophysics

The geophysical ERT was carried out at 2.0 m from the injection well (T1) towards the pumping well, Pmu1 (see *Figure 5:2*). Twenty-two ERT surveys were carried out along the groundwater flow and transverse directions (N-S and E-W) during the test to detect the spreading of the plume. ABEM-4000 terrameter with switching unit was used and Schlumberger short normal array was selected due to limited electrodes availability. Schlumberger is better compared to Wenner array since more data point can be obtained and also the lateral resolution in shallower depth (around 10 m) is reasonably better in Schlumberger. 30 m long-normal Schlumberger ERT array (64 electrodes) was carried out with inner electrode spacing of 0.5 m and outer electrode spacing of 1.0 m considering higher resolution data requirement for better interpretation at shallower depth 0.0-5.0 m. The initial inversion ERT section obtained before the tracer test (section 5.2.3) were used to identify the relative variation of resistivity with the ERT surveys performed during the trace test. This reveals the plume migration. The interpretation of these ERT inversions enables to estimate the magnitude of migration along longitudinal, transverse and vertical direction approximately.

From the S-N and E-W inverse ERT sections, it was observed that the plume movement has drifted towards the groundwater flow direction and vertical spreading is noticeable until the middle of the second layer. Further, the longitudinal dispersion is appeared more dominant compared to transverse dispersion obviously due to groundwater flow.

5.3.4. Plume monitoring in piezometers

During the tracer test, drawdown and EC was measured in the pumping well (Pmu1) and other piezometers (T1, T2 and T3) by the EC loggers to detect the tracer movements with time. The logger installed depth were determined considering the groundwater level, borehole depths, tracer injected depth in injection well and stratigraphy of the site. The logger installation depths in piezometers are shown in *Table 5-2*.

Table 5-2: Technical details of the piezometers and depth of installed loggers

Piezometer /well	Depth (mbgl)	Diameter (cm)	Sreen depth range (m)	ISWL(mbgl)	Logger depth (mbgl)
T1	2.00	5.0	1.60-2.00	1.27	1.80
T2	1.57	5.0	0.67- 1.57	1.28	1.55
T3	1.68	5.0	0.78 - 1.68	1.33	none
Pmu1	7.90	22.5	open hole	1.25	3.50 (Top)
Pmu1	7.90	22.5	open hole	1.25	6.00 (Bottom)

ISWL – Initial static water level

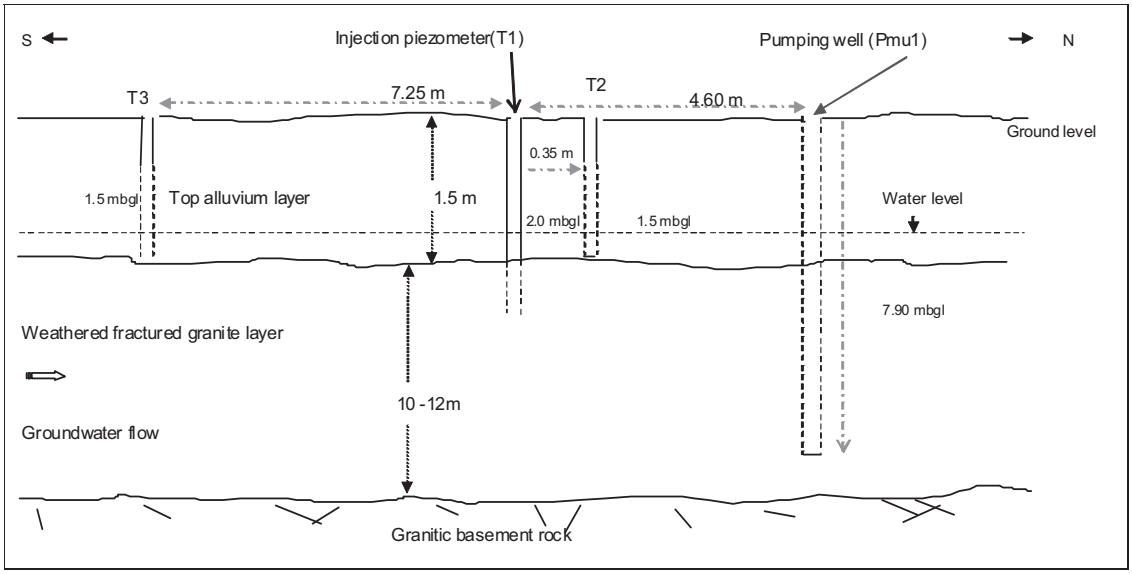

Figure 5:1 The cross section of tracer test design

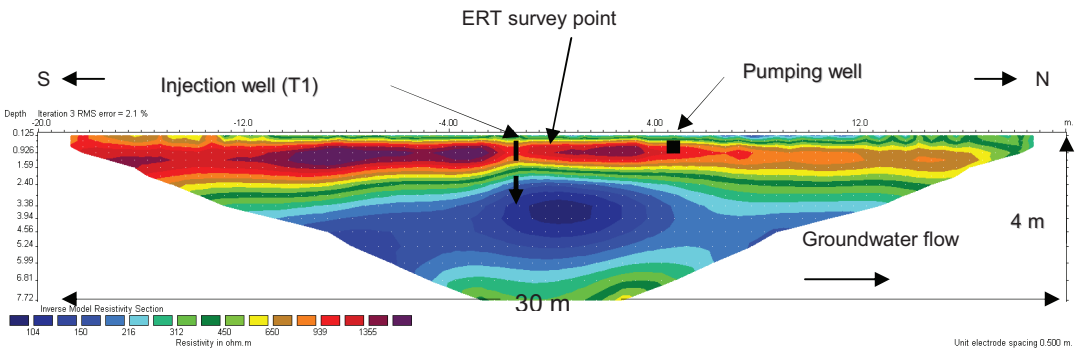

Figure 5:2 A conversion section processed by the 2-D ERT data obtained during the test in N-S longitudinal direction

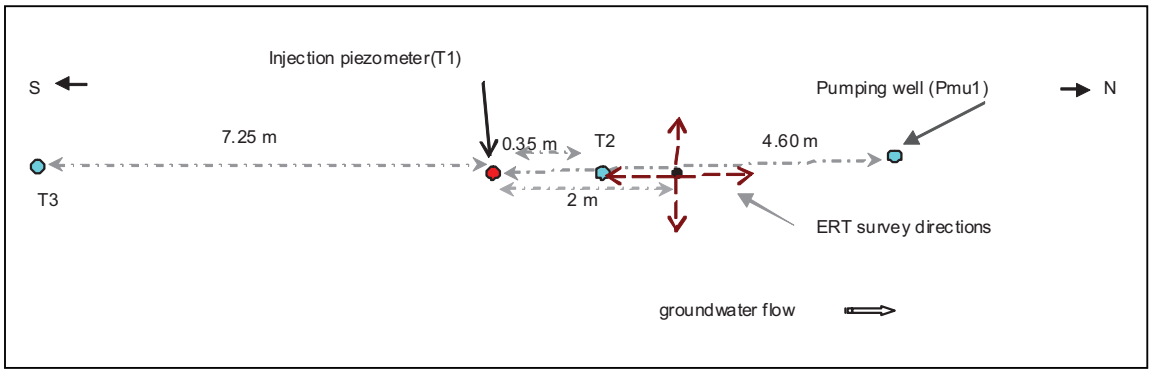

Figure 5:3 The overview of the tracer test design

The depth of the pumping well, Pmu1 was well below the top layer thus the forced gradient created by pumping is influenced on the both layers. However, the injection at T1 was carried out into the second layer therefore the dispersion of tracer is propagated mainly along the second layer. The water column in the first layer was only 20 cm and during pumping, for most of the time was dry. Therefore the tracer test simulated in the numerical modeling represents dispersivity of second layer.

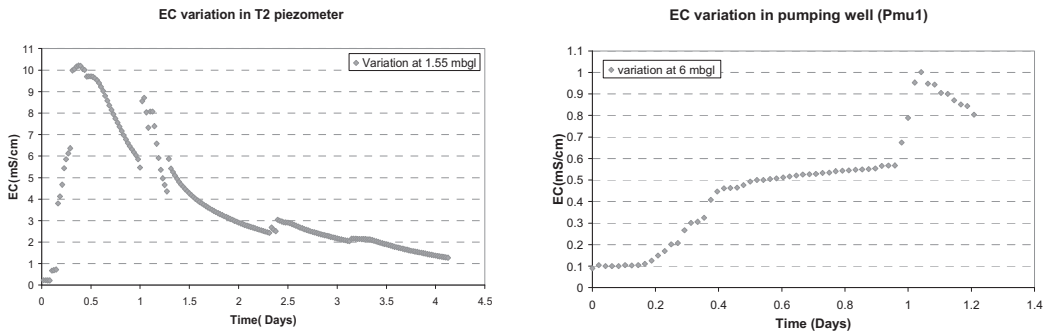

Figure 5:4 The EC variation with time at T2 piezometer and Pmu1 pumping well (bottom) respectively.

The *Figure 5:4* shows the variation of EC of groundwater with time after the injection of the tracer. The piezometer T2 is located 0.35 m away from the injection well and the depth of this well is 0.5 m above the bottom of the injection well. However it indicates EC increases up to a maximum of 10.0 mS/cm at 0.4 days after the injection and gradually diminishes to around 1.02 mS/cm. Therefore, it shows some upcorning of the fresh-saltwater transition zone in addition to the tracer movement. In the pumping well (pmu1), maximum tracer breakthrough was occurred after approximately 25 hours from the injection. Thereafter, the EC was decreased up to 0.8 mS/cm from the peak value of 1.0 mS/cm.

This repetitive pumping-recovery procedure precludes any analytical solutions to determine the dispersivity. Further, maximum break through curve cannot be used to estimate the seepage velocity and thereby the effective porosity because of this non-equilibrium condition. Therefore, the tracer test site was conceptualized and modelled in MODFLOW and MT3D sub-package for the calibration of groundwater level fluctuation due to pumping and electrical conductivity variation as a result of the tracer movement. The obtained dispersivity through the model was extrapolated to regional solute model calibration as explained in Chapter 6.4.2.

5.4. Numerical modeling

5.4.1. Conceptual model

Before the numerical modelling, the constructed conceptualized model of the tracer test is shown in *Figure 5:1* and it envisages the site stratigraphy, piezometer setup and the distances, groundwater flow direction.

5.4.2. Model setup and model boundaries

A fine grid local scale numerical model was developed to simulate the tracer transport and groundwater flow of the tracer test to determine the dispersivity. The conceptual model (*Figure 2:1*) was used to construct the numerical model in MODFLOW and MT3D sub-package. The site was simulated as two layered structure with upper layer unconfined and lower layer varies between unconfined /confined depending on the first layer condition. This model covers 50 by 50 m area with cell size of 0.1 m. The upstream and downstream boundaries were assigned as general head boundary condition and left and right side of the model were assigned no flow boundary considering the groundwater flow, pumping test results and hydrogeology of the site.

5.4.3. Calibration of flow model and solute model

The hydraulic conductivity obtained from the analysis of pumping test was initially used in the calibration process of steady state model and the initial hydraulic head values of piezometers were taken as the calibration targets. Initial calibration was done in manual trial and error method and the hydraulic conductance at the general head boundaries were adjusted later by PEST programme for better optimization. The specific yield and specific storage values were applied in the transient model from the result of soil sample analysis of the piezometer constructions. The final parameter configuration is illustrated in *Table 5-4*. The transient flow model was calibrated using the hydraulic heads monitored by the loggers in piezometers during the tracer test.

Table 5-3: The stress periods defined in the transient flow model

Stress period	Time(min.)	Time step	Remark
1	130	26	Pumping
2	40	8	Recovery
3	160	32	Pumping
4	50	10	Recovery
5	55	11	Pumping
6	60	12	Recovery
7	55	11	Pumping
8	840	168	Recovery
9	125	25	Pumping
10	55	11	Recovery
11	80	16	Pumping
12	55	11	Recovery
13	15	3	Pumping
14	1720	344	Recovery

Pumping test carried out before the tracer test was not indicated any variation of EC of the groundwater in pumping well and observation piezometers. Therefore, EC variation of groundwater monitored by the loggers during the test was directly used in the calibration of the solute model without any conversion into chloride concentration. Additional input parameters of effective porosity and dispersivity of the solute model was calibrated manually. The pumping and recovery periods used in the tracer test were simulated as different stress periods and it is summarized in the *Table 5-3*.

Table 5-4 The parameter configuration applied in the model

Layer	K (m/d)	Kv (m/d)	S_s (m^{-1})	n_e	S_y	D_L	D_v	D_T
1	2.70	0.11	0.0005	0.15	0.15	0.010	0.0010	0.0005
2	0.17	0.05	0.00003	0.05	0.05	0.015	0.0015	0.00015

* where K – hydraulic conductivity, K_v – vertical hydraulic conductivity, S_s – specific storage, n_e – effective porosity, S_y – specific yield, D_L - longitudinal dispersivity, D_v – vertical dispersivity, D_T – Transverse dispersivity

5.4.4. Model results

The steady state model calibration is shown in the *Figure 5:5* and transient flow model was used in the calibration of solute model. The optimised effective porosity was 0.15 and 0.05 for the two layers by the model calibration. The solute model indicates a longitudinal dispersivity of 0.01 m and 0.015 m for the first and second layers respectively. The calibrated longitudinal dispersivity in the first layer is approximately an order of one tenth of the transport distance (0.1 m) selected in the numerical model. The proper selection of grid size is critical in simulating the solute transport in porous media since the dispersivity is scale dependant and larger the grid size the micro-scale dispersion within the cell distance of the model is ignored (Vandenbohede and Lebbe, 2003).

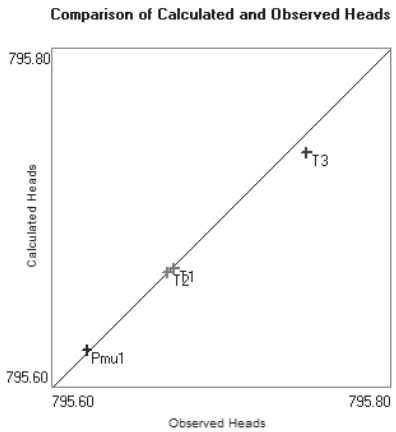

Figure 5:5 The calibrated hydraulic heads in steady state model.

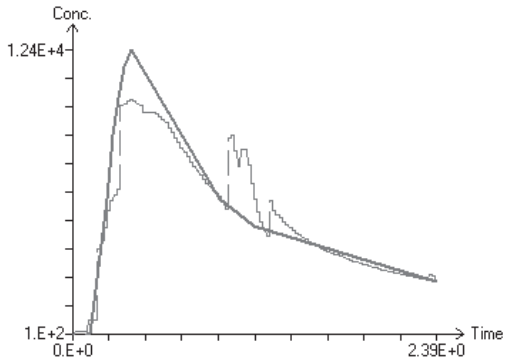

(Time - days and concentration - mS/cm)

Figure 5:6 Simulated solute model for EC variation in T2 (thick line-simulated)

The simulation of the piezometer T2 is shown in Fig. 6.7 and the EC observed in the pumping well (Pmu1) was difficult to simulate in the numerical model. This response of higher EC observed in the pumping well (Fig. 6.5 (b)) may be resulted by preferential groundwater flow through the boundary of the two layers which was observed during the tracer test. The derived dispersivity from the local scale model was used to regionalise the dispersivity as explained in the section 6.4.2.

6. Groundwater model development

6.1. Conceptual groundwater model

Once the input data is assessed, conceptual model is developed to represent the field groundwater flow system in a simplified version for better understanding of the site conditions. The conceptual model is schematised as a cross section or block diagram which reflects the system behaviours and it leads to determine numerical model characteristics. This helps to select and build a suitable numerical model for simulate the system behaviour for evaluations or predictions. The closer the conceptual model to reality, the numerical model will be more accurate (Anderson and Woessner, 1992). In process of conceptualization, primarily hydrostratigraphic units, flow system and water budget should be considered.

6.1.1. Hydrostratigraphic units and groundwater flow network

The area is composed of two layers underlain by the massif granite basement. The fractured network in granitic hard rock layer is covered by the uppermost weathered granitic layer and alluvial deposits. This constitutes the main hydrostratigraphic units in the area (*Figure 2:3*). The spatial variation of the hydrogeological properties and depth of these two layers are highly heterogeneous. The scattered massif granite outcrops indicates the exposure of basement rock and the absence of these two strata at certain areas. The thickness of the topmost layer is varied from 0.0 to 4.0 m and geophysical analysis shows wide range of depth variation in the lower hydro-stratigraphic strata which is developed up to 80.0 to 90.0 m in some places along the major fault zone (Attanayake, 1999).

Hydraulic heads are used to identify the groundwater movement, discharge-recharge areas and inter-connection of the aquifers and relation with surface water bodies (Anderson and Woessner, 1992). The hydraulic head measurements have shown that the spatial variation of local flow system controls by topography and subsurface structure in the area. The piezometric map is shown a concentric pattern in groundwater table of the area largely controlled by the Sardon fault-river drainage line (Lubczynski and Gurwin, 2005). The major groundwater flow direction is generally in S-N direction except in places where the flow movements are temporarily altered by the two NNE-SSW and NNW-SSE trending lineament systems. The regional groundwater flow is determined by the interconnected fracture systems at regional scale which directed the flow into Sardon fault-river drainage.

The main influx to the groundwater is recharge from rainfall and lateral flow exchange at catchment boundaries is considered non-existent. Groundwater outflow is occurred as discharge at the catchment outlet and ET_g. Precipitation and evapotranspiration are considered the major responsible for the temporal variation of the flow system and the groundwater abstraction is negligible.

6.2. Numerical groundwater model

The numerical flow model was simulated based on the conceptual model and utilised code of MODFLOW (Harbaugh and Mc Donald, 1988) software of USGS. This numerical modelling was performed using the interface of PMWIN processing MODFLOW, Version 5.3 (Chiang and Kinzelbach, 2001) as code environments for data input and output management. The governing equation for groundwater flow in two dimensionally in this numerical modeling code is based on the law of mass balance and Darcy's law.

$$\frac{\partial}{\partial x}\left(K_x \frac{\partial h}{\partial x}\right) + \frac{\partial}{\partial y}\left(K_y \frac{\partial h}{\partial y}\right) = W + S_s \frac{\partial h}{\partial t} \qquad (6\text{-}1)$$

Where K_x and K_y are hydraulic conductivity components along x and y directions respectively; W is source or sink; S_s is specific storage; h and t are head and time respectively.

The numerical groundwater modeling can be performed in steady state or transient state conditions. In steady state, the long term average fluxes or parameters were used as constants over the period of simulation. The results of this steady state were used as inputs in fully transient modeling where the fluxes are changed spatio-temporarily (Lubczynski and Gurwin, 2005).

6.3. Steady state flow model

During the past studies, the steady state model of the Sardon catchment was developed by Lubczynski and Gurwin (2005). The model has spatially discretized into 100 m cell size, covering the total area of Sardon catchment. The extent of the model is 80 square kilometers with 10 km in length and 8 km width. The cells outside the no flow boundary in the domain were defined as inactive cells. The area is located in 4,547,394-4,557,080 m of UTM X-coordinates and 736,378-739,552 m of Y-coordinates.

The numerical model comprised of two layered structure with upper and lower boundaries defined using the DEM and interpolated layer thickness maps of the two layers. The geophysical analysis at 59 different locations (Tesfai, 2000), borehole data, lithological maps and available hydrogeological maps were used to obtain the interpolated layer thickness maps. The bottom of the second layer is impervious hard massif granite simulated by very low vertical hydraulic conductivity in the model.

In the previous study, digital elevation map (DEM) was prepared using the surveyed contour maps and SRTM image of the Sardon area. The error of this map was checked in this study with the differential GPS precision data. This assessment showed 4-18 m error in the DEM processed map at different locations. Therefore the surface and the two layers were corrected using the interpolated map processed in GIS using 64 differential GPS points obtained during the field work. The model was recalibrated after these corrections.

6.3.1. Boundary conditions

Boundary conditions are mathematical statements which specify the head or fluxes at the boundaries of the model domain. The correct assign of boundary condition is important since it controls the flow regime of the numerical model.

No flow boundary conditions have assigned along the all external boundaries of the catchment, considering the topography, geology and structure of the area which indicated well defined water divides. Sardon river which flows along the major fault zone was simulated by drain boundary condition in which the drain elevation was selected bottom of the river. The applied boundary conditions and model grid of the numerical model is shown in *Figure 6:1*. The white zones in the first layer is illustrated the inactive cells where the rock outcrops are existed in the catchment.

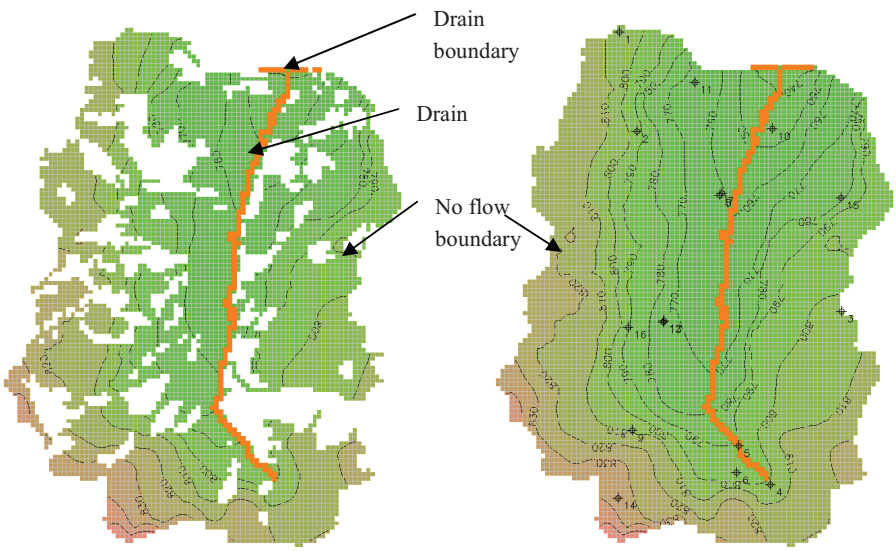

Figure 6:1 The boundary condition applied in the numerical model in the layer 1 and 2 respectively.

6.3.2. Hydraulic heads

In the steady state model, 23 field measured hydraulic head values were used for the interpolation of point heads to obtain initial head distributed map. Since there are no artificial groundwater abstractions, the hydraulic heads represent the natural groundwater piezometric surface. These individual point heads were used in the final steady state calibration.

The hydraulic head data were available at 23 locations and there were some data scarce areas which are important in steady state model calibration. Therefore regression equations were developed using differential GPS points and water level elevations obtained during three different time intervals (see *Figure 6:2*). These equations were applied to predict the groundwater level at data scarce locations using DEM elevations. This method is suitable for catchments where the groundwater level is shallow (Eve L. Kuniansky et al., 2009) and readily applicable to the Sardon catchment since the shallow groundwater levels are observed. The fictitious groundwater levels derived by this method and existing heads of piezometers were used as calibration targets in the steady state model (see the

Figure 7:2 for locations of fictitious points denoted as v1, v2 etc.). The steady state model result and the fictitious point details are in Appendix H.

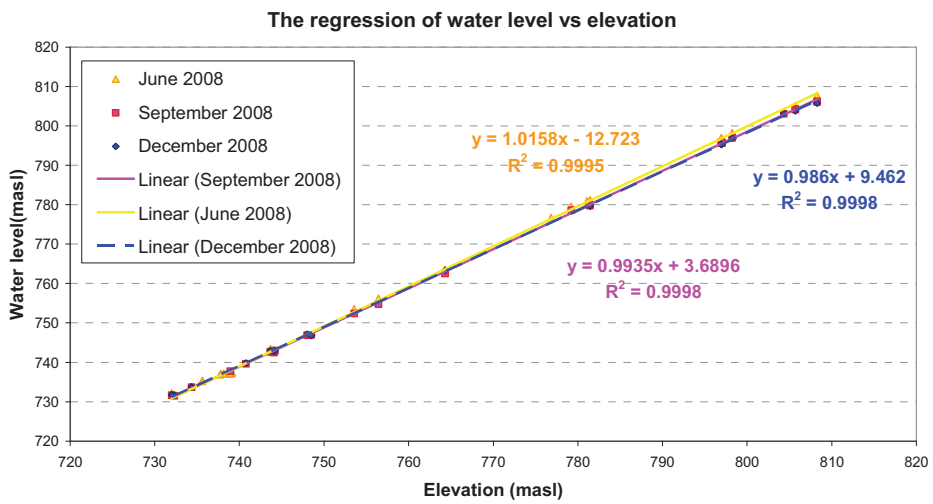

Figure 6:2 The regressions developed for elevation and water level of the Sardon catchment

6.3.3. Groundwater fluxes

Natural groundwater fluxes comprise: recharge, *ETg* and groundwater outflow.

Recharge

Recharge in the study area depends entirely on the precipitation of the area and it varies from place to place despite the precipitation shows uniform distribution. The different recharge zones were used as classified according to influential factors as explained in the chapter 4.1.4. The recharge applied in the highest active cell in the model depending on the condition of the vertical column of the cell.

Groundwater evapotranspiration (ETg)

The ET_g occurs either as E_g when the water level is close to the land surface or as T_g through phreatophytes characterized by deep roots tapping groundwater. The ET_g was simulated in the model by evapotranspiration package of MODFLOW and the different zones were defined based on the results of the SEBAL solution, explained in chapter 4.2.2. The elevation of the ET surface in the MODFLOW was assumed as the topographical surface and the extinction depth was set 5.0 m considering the maximum rooting depth of the area. In the steady state model calibration, the recharge calculated by CMB method was used because it represented the long term average recharge.

Groundwater outflow

The groundwater outflow from the aquifer in the model was simulated by drain package representing main Sardon river course matching regional fault system zone. Groundwater flow occurs when aquifer hydraulic head head was higher that the defined drain elevation and ceases when aquifer hydraulic head falls below the defined drain elevation. The groundwater outflow to the drain (Q_d) was calculated by;

$$Q_d = C_d.(h - d) \qquad (6\text{-}2)$$

Where $C_d = KL$ and K is equivalent hydraulic conductivity, L is length of the drain within a cell, h aquifer hydraulic head and d elevation of the drain. The value of C_d was adjusted during the calibration process.

6.3.4. Model parameterisation

Hydraulic conductivity

The hydraulic conductivity varied spatially and the zones were defined in the first layer based on the geophysical analysis, slug tests and borehole investigations with soil sample analysis performed in the previous fieldworks. These zoned maps prepared in ILWIS were imported into MODFLOW as an ASCI file and finally adjusted during steady state model calibration (Lubczynski and Gurwin, 2005).

The second weathered fractured granite layer was zoned using GIS cross overlay procedure which is similar to the recharge zoned map preparation explained in the Chapter 4.1.4. The groundwater head gradient map, lineament density map through Landsat-TM5 images, geophysical data were used in the weighting process to identify the different hydraulic conductivity zones (Lubczynski and Gurwin, 2005). These hydraulic conductivity zones were optimized in the steady state model calibration.

6.4. Steady state solute transport model

Advection, dispersion, adsorption, biodegradation and chemical reactions are the main transport processes considered in groundwater (Domenico and Schwartz, 1998). In this study, advection and dispersion processes are only considered since the chloride is conservative elements and biodegradation and retardation are negligible. Advection is being the far most dominant transport process compared to dispersion in solute transport modelling. The solute transport is simulated in numerical modelling by advection-dispersion equation (see equation 5.1).

The steady state solute transport model was calibrated using chloride concentrations of groundwater to validate and constrain the steady state flow model. In addition to the input parameters defined in the flow model, the effective porosity and dispersivity are required in the solute transport model. The local scale dispersivity was regionalised as explained in the Chapter 6.4.2 and effective porosity was initially estimated by the porosity of the soil sample analysis described in Chapter 3.9 for the solute transport calibration.

The solute model was simulated in MT3D which is a comprehensive 3-D numerical model linked with the MODFLOW in PMWIN environment, designed specifically to handle advection-dominated transport conditions without the need to construct refined models for solute transport in complex hydrogeological settings (Lautz and Siegel, 2006). The following setup and criteria was considered in the simulation of solute transport:

- Defined stratigraphy, grid size, layer type, computed heads and cell-by-cell fluxes in MODFLOW flow model were used by MT3D transport model without a change.

- MODFLOW boundary conditions were converted to MT3D conditions: the active cells were assigned as active concentration cells while inactive and dry cells were considered as no-transport boundaries i.e. not taken into account for transport simulation.
- Initial concentration was applied by geo-statistical interpolation of point chloride measurements obtained in June, 2008.
- Regionalised dispersivity and effective porosity were initially assigned in the solute model calibration.

6.4.1. Effective porosity and dispersivity

The seepage velocity is a function of hydraulic conductivity and effective porosity, which is important in solute transport models since advection is completely determined on it. The dispersion is partly influenced by seepage velocity because dispersion occurs in porous media due to diffusion and mechanical dispersion i.e. mixing due to velocity variations.

$$v = -\frac{K}{n_e}\frac{\partial h}{\partial l} \qquad (6\text{-}3)$$

Where v is seepage velocity (m/d), K is hydraulic conductivity (m/d), effective porosity is n_e and $\partial h / \partial l$ represent the hydraulic gradient.

Dispersivity is considered a characteristic property of a medium and it is proportional to the aquifer heterogeneity while it increases with decreasing porosity (Xu & Eckstein, 1997). The dispersion in porous media is mainly measured along longitudinal, transverse and vertical direction. Longitudinal dispersivity is approximately a ten times larger than transverse dispersivity at a given scale under same velocity filed. This is applicable at microscopic or larger scale (Vandenbohede and Lebbe, 2003). The vertical dispersivity is negligible unless the concentration of the transport tracer does not alter the groundwater flow regime by density effect.

$$D_L = \alpha_L v \qquad (6\text{-}4)$$

and

$$D_T = \alpha_T v \qquad (6\text{-}5)$$

Where D is dispersion, α is dispersivity, v is seepage velocity and L, T represent the longitudinal and transverse directions respectively.

6.4.2. Regionalisation of the dispersivity

The implementation of derived parameters from field applications in the regional groundwater flow model is always a problem as the limited knowledge of aquifer heterogeneity (Vandenbohede and Lebbe, 2003). In addition, transport models can not afford to describe the necessary small scale dispersive, diffusive and chemical processes (Fernandez-Garcia and Gomez-Hernandez, 2007). As a result, upscaled aquifer transport properties were transferred to numerical transport models. However, the dispersivity is scale dependant and upscaling trend is not universal and difficult to establish a one relation for all modelling applications due to uniqueness of every aquifer dealing with (Gelhar et al.,

1992). Gelhar has presented some relations of dispersivity with scale from the field tests data as shown in *Figure **6:3***. The dispersivity obtained through the local model was plotted and compared with the Gelhar's relations as shown in *Figure 6:3*. The dispersivity estimated for the regional scale grid size of 100 m is in the range of 8-15 m considering Gelhar's plot and literature (ASTM, 1995 ; Gelhar et al., 1992). This was initially used for the solute transport model calibration.

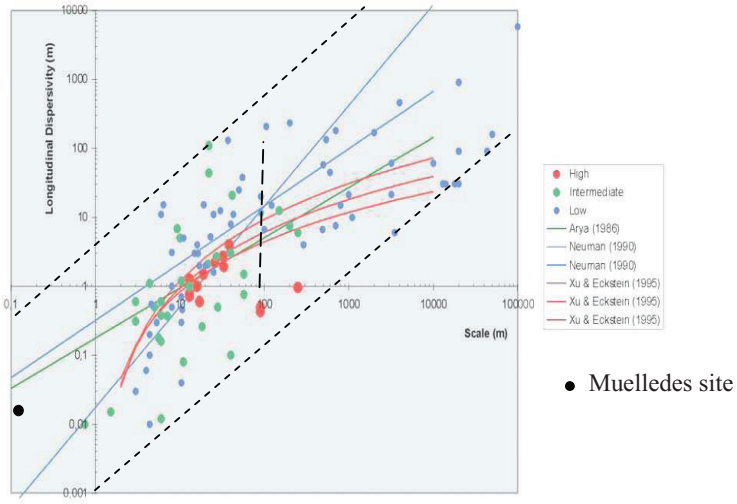

Figure 6:3 Some relationships of longitudinal dispersivity in function of scale compared with the dataset of Gelhar et al. (1992) and plot of Muelledes site.

6.4.3. Chloride concentrations

The chloride concentrations were obtained through water sample analysis as explained in chapter 3.8 at four time intervals during June to December 2008 and no data was available prior to this period. Further, temporal variability of chloride concentration in groundwater in this period was negligible. A steady state solute model was developed to validate the steady state flow model using these chloride concentrations. The chloride influx was considered entirely from the recharge of precipitation and uniform over the study area. The influx chloride concentration was 1.4 mg/l.

6.5. Transient flow model

Transient models are more reliable compared to steady state model solutions, since they are constrained by temporal fluxes and the scenario prediction is more accurate. The steady state model solutions are used as initial conditions in transient mode calibration. In standard transient model calibration, the temporal head variation is due to human interferences (e.g. pumping wells) resulting in temporal change in aquifer storage. These transient solutions are referred as partially or quasi-transient (Lubczynski, 2000). They are particularly efficient in case of large stress responses, substantially greater compared to natural system responses. In contrast to the partially transient models, the fully transient models require high temporal resolution of fluxes. This is critical in arid and semi-arid areas where the fluxes vary substantially affecting aquifer storage. In this study, the required spatio-temporal data was obtained and processed for fully transient model calibration.

6.5.1. Hydraulic head data

Transient model was calibrated using measured hydraulic heads at six locations from September 2003 to December 2008 and five additional wells with the data from June to December 2008. In some periods data was not available due to shifting of the loggers to another location or due to other reasons. The information of the head data is explained in Chapter 3.6.

6.5.2. Storage coefficient (S)

In the numerical model, the top (first) layer was assigned as unconfined and specific yield was used to calculate the rate of change in storage. The second layer was selected as unconfined/confined option (MODFLOW layer option 3) since it varies from unconfined to confined depending upon the position of hydraulic head of the second layer as compared to its top elevation. Therefore confined storage coefficient is used to calculate the rate of change in storage if the layer was fully saturated , otherwise specific yield is used (Harbaugh and Mc Donald, 1988).

The specific yield (S_y) of the first layer was defined using shallow borehole samples..The second layer storage coefficient (S) zones were defined using the GIS cross overlay procedure similar to the one explained in the section 4.1.4. The weighted score fracture density map and apparent resistivity map were summed and zones have been constructed with the comparison of S data points received from the 1D-EARTH model results (Lubczynski and Gurwin, 2005). These defined zones were adjusted in the fully transient model calibration.

6.5.3. Time discretization

The stress periods were identified based on the temporal variability of the rainfall and recharge evaluated from pyEARTH-1D model and measured groundwater level fluctuation which reflected aquifer responses of the simulated period, September 2003 to December 2008.

Table 6-1: Stress periods defined for simulation in the transient model

Stress period	Start	End	Days	Weeks
1	12-Sep-2003	3-Nov-2003	56	8
2	4-Nov-2003	9-Feb-2004	98	14
3	10-Feb-2004	14-May-2004	91	13
4	15-May-2004	12-Oct-2004	154	22
5	13-Oct-2004	22-Mar-2005	161	23
6	23-Mar-2005	24-May-2005	63	9
7	25-May-2005	21-Oct-2005	147	21
8	22-Oct-2005	20-Mar-2006	147	21
9	21-Mar-2006	19-May-2006	63	9
10	20-May-2006	16-Oct-2006	147	21
11	17-Oct-2006	16-Feb-2007	126	18
12	17-Feb-2007	16-Jun-2007	119	17
13	17-Jun-2007	13-Sep-2007	91	13
14	14-Sep-2007	4-Jan-2008	112	16
15	5-Jan-2008	26-Feb-2008	56	8
16	27-Feb-2008	4-Jun-2008	98	14
17	5-Jun-2008	07-Dec-2008	182	26
	Total		1911	273

Stress periods are defined within the individual simulation periods of groundwater model in MODFLOW which represent a one uniform groundwater flow regime. Such uniform period is referred as stress period.

The length of the 17 irregular stress periods varied from 8 to 26 weeks (*Table 6-1*). The stress period were divided into time steps of one week each. The selected stress periods can be divided primarily into two classes; (i) of dry summer season where groundwater recessed continuously and (ii) wet season of the winter season where the groundwater was replenished by recharge. The winter periods are characterized by the different magnitudes of recharge events as shown by head variation in the figure *Figure 6:4*. Therefore number of stress periods could be defined within this period which shows the changes in hydraulic heads and other fluxes as well due to change in recharge. The transient model solution is better when the more stress periods are defined in time descritization, however the calibration is then more complicated and demands higher temporal data resolutions as well as computation time.

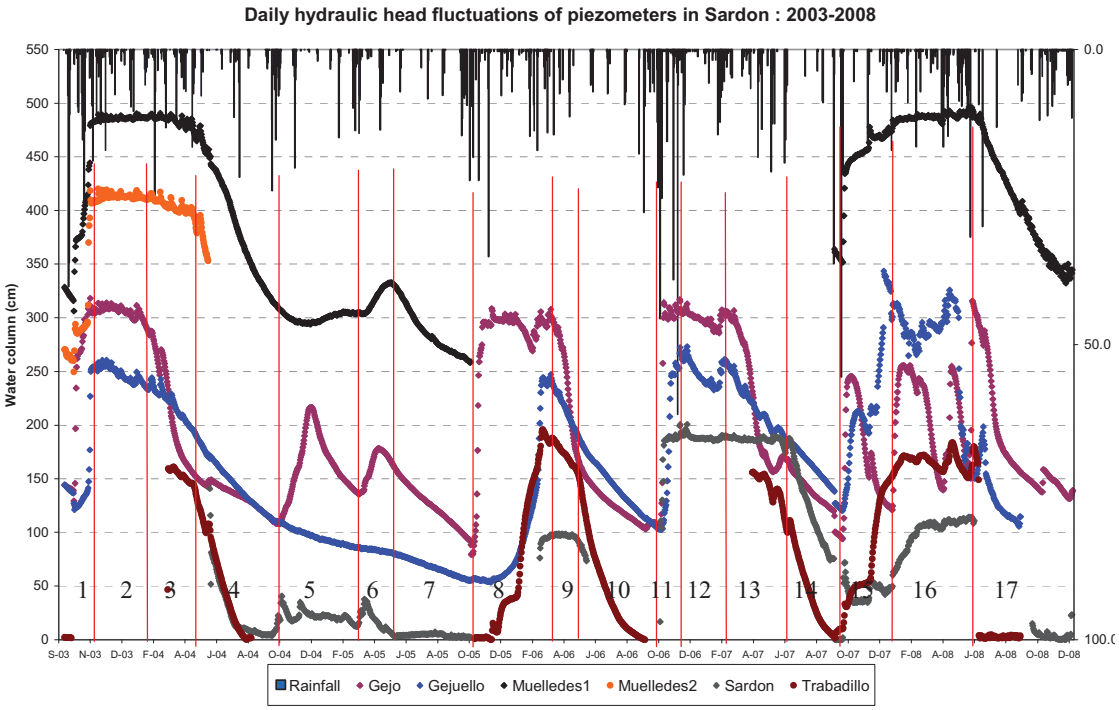

Figure 6:4 The defined stress periods for fully transient modelling.

6.5.4. Recharge and groundwater evapotranspiration (ET_g)

The spatio-temporal zoned recharge and ET_g maps for each stress period were prepared as explained in the chapter 4.1.4 and 4.2.2 respectively. These maps were imported as ASCI files in MODFLOW recharge and evapotranspiration packages to simulate each stress condition of the fully transient model.

7. Model calibration

The model calibration is achieved by optimizing the set of parameters and conditions in the simulated model which reproduce the calibration target, i.e. field observed values (Anderson and Woessner, 1992). If the calibration target is not achieved as defined by the objective function or not matched with the acceptable range of simulated and measured values, the numerical model or even conceptual model is to be revised. The calibration target can also be achieved by automated parameter estimation or manual adjustment by trial and error procedure.

The Sardon model calibration was carried out in: (i) steady state flow model; (ii) steady-state flow and solute transport model; (iii) transient flow and solute transport model. The transient flow and solute transport model calibration was not performed since the spatio-temporal chloride data was available only for six months (June 2008 - December 2008) and their variability was negligible. For transient solute calibration, longer temporal data is required because the concentration changes occur on a much larger time-scale than head changes (Leif, 1993).

7.1. Steady state flow model calibration

The steady state model was recalibrated using 37 new hydraulic head data at different locations; drain conductance data obtained by slug tests, recharge values obtained from chloride mass balance method which representative of long term flux and other information for better optimization. The hydraulic conductivity zones defined in the previous model calibration by Lubczynski and Gurwin (2005) were only slightly altered in general, although some zones were considerably changed due to new layer and water table elevations corrected by high-precision differential GPS as explained in Chapter 6.3.

The steady state model was calibrated initially by readjusting the hydraulic conductivity with manual trial and error method and later by automated parameters estimation programme, PEST (Doherty, 2000) was applied. The PEST execution was not efficient in some instances due to the drying of some observation wells during the internal iterative process that caused the programme to terminate before the solution was not converged. The manually adjusted hydraulic conductivity values were used in the PEST optimization.

7.1.1. Head calibration target

The model calibration error can be expressed qualitatively by mean error (ME), mean absolute error (MAE) and root mean square error (RMSE). The mean error is the mean differences between simulated hydraulic head (h_c) and observed hydraulic head (h_o):

$$ME = \frac{1}{n}\sum_{i=1}^{n}(h_c - h_o)_i \qquad (7\text{-}1)$$

The mean absolute error (MAE) is the mean of the absolute value of the differences in simulated hydraulic head (h_c) and observed hydraulic head (h_o):

$$MAE = \frac{1}{n}\sum_{i=1}^{n} |(h_c - h_o)_i| \qquad (7\text{-}2)$$

The root mean squared error (RMSE) is the average of the squared differences in simulated hydraulic head (h_c) and observed hydraulic head (h_o):

$$RMSE = \left[\frac{1}{n}\sum_{i=1}^{n}(h_c - h_o)_i^{\,2}\right]^{0.5} \qquad (7\text{-}3)$$

Where n is the number of observations.

During inverse modelling, PEST checks the hydraulic head solution and adjusts the parameters selected in the PEST parameter optimization list until the convergence criterion or objective function is satisfied.The differences in simulated and observed heads at 37 locations are tabulated in the appendix H. The summary of the error analysis in calibration is shown in the *Table 7-1*.

Table 7-1: The evaluated calibration statistics

ME	1.04 m
MAE	2.29 m
RMSE	3.24 m

7.1.2. Hydraulic conductivity

In the calibration process, the hydraulic conductivity values used in the previous model of Lubczynski and Gurwin (2005) were slightly adjusted to optimize hydraulic heads. The hydraulic conductivity in upper layer showed higher values compared to lower weathered fractured granite layer. The hydraulic conductivity varied from 0.2 to 25.0 m/day in first layer with highest conductivity along the Sardon river course towards the upper catchment. In the second layer, hydraulic conductivity varied from 0.05 to 1.5 m/day and the hydraulic conductivity zones were clustered into smaller areas compared to the first layer, possibly due to local fracture networks.

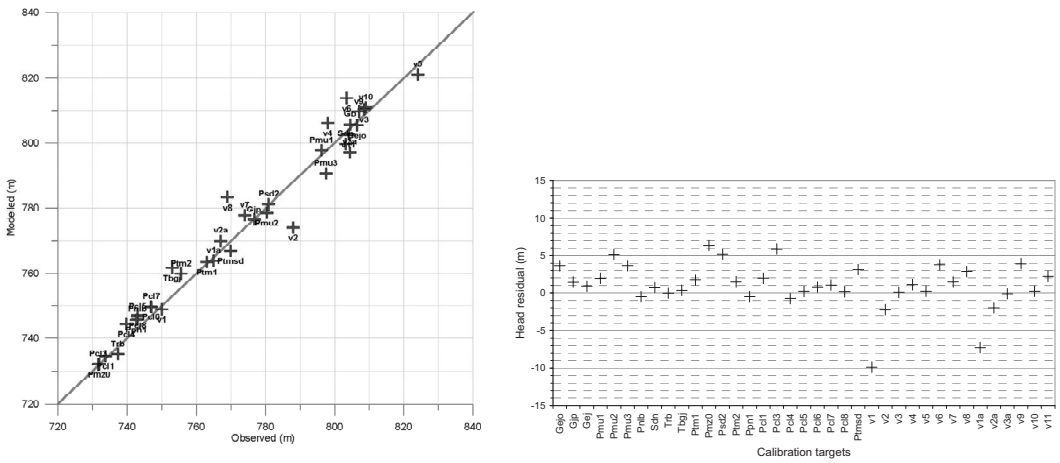

Figure 7:1 (a) Scatter plot of steady state simulated vs. observed hydraulic heads and (b) Head residuals at calibration targets.

The final steady state model scatter plot of goodness of fit between measured and simulated is illustrated in the *Figure 7:1*(a) and the residual of calibration targets are shown in *Figure 7:1*(b).

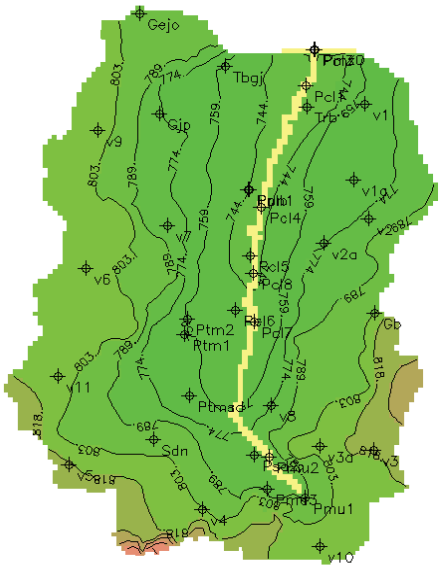

Figure 7:2 Steady state hydraulic head distribution in the calibrated model

7.1.3. Recharge and ET_g

The long term average of recharge and groundwater evapotranspiration values at different locations in the catchment were used in the preparation of spatially distributed zoned map with the use of ILWIS as explained in chapter 4.1.4 and 4.2.2. The calibrated recharge varies spatially within 0.0-153 mm/yr range in the catchment. Mainly two recharge zones could be identified from the spatial recharge map; one, which shows approximately 0 to 30 mm/yr recharge in the lowland surrounding the river valley areas and the upland areas having 30 to 153 mm/yr of recharge. The categorized values used in the different zones for recharge and ET_g are summarised in the *Table 7-2*.

Table 7-2: Recharge and ET_g used in steady state model

	Recharge(10^{-2} mm/day)	ET_g(10^{-2} mm/day)
Very low	5.0	0.0
Low	9.0	8.0
Moderate	13.0	14.0
High	25.0	19.0
Very high	42.0	34.0

7.1.4. Water budget

The components of the water budget in the calibrated model domain indicate the influx and outflux of groundwater within the aquifer system. The precipitation is the only source of recharge while the outflux from the system is ET_g and river discharge at catchment outlet. The entire budget could be simply formulated as following equation.

$$R_{pptn} = ET_g + G_{of} \pm \Delta S \qquad (7\text{-}4)$$

Where R_{pptn} , ET_g , G_{of} and ΔS are the recharge from precipitation, ET_g, groundwater outflow to the drain and change in the storage (in steady state equal to zero) respectively.

Table 7-3: Steady state water balance of the model

Flow term	In	Out	In-out
Drains (G_{of})	0.00	10,608.40	-10,608.40
ET_g	0.00	4,843.50	- 4,843.50
Recharge (R)	15,502.10	0.00	15,502.10
Total	15,502.10	15,451.90	50.10
Percent discrepancy (%)			0.32

*all figures are in m^3/day

The long term average of fluxes is represented in the water balance calculated by the steady state model. The recharge(R) is 70.7 mm/yr, approximately 12.3% of annual rainfall; ET_g is 22.0 mm/yr and groundwater outflow (G_{of}) is 48.7 mm/yr. One third of the water budget component is approximately the ET_g and the remaining is the groundwater outflow through drain. The illustrative diagram of the steady state water balance is shown in the *Figure 7:3*.

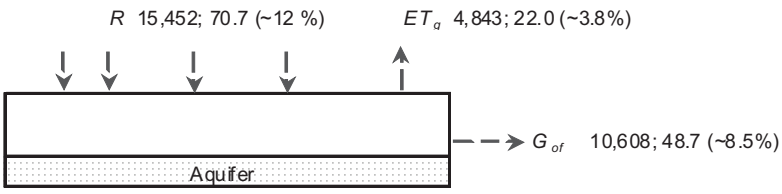

(units are in m^3/d, mm/yr and as rainfall % respectively)

Figure 7:3 The steady state water budget components

7.2. Steady state solute transport model

The calibration of steady state solute transport model was focused on the reproducing steady state chloride concentration distribution of groundwater in the Sardon catchment. This approach helped to validate and constrain the calibrated steady state flow model before the fully-transient modelling. The introduction of chloride concentrations as an additional constrain reduces the number of degree of freedom in the flow model solution thus increasing the reliability of the model.

The calibration of the solute transport model was carried out by tedious trial and error methods. This was because the PMWIN environment used in this study was not adapted to PEST optimization of the MT3D solute transport model.

During the steady state solute model calibration, the dispersivity value range was selected based on the literature of dispersivity following Gelhar (1992) as explained in 6.4.2. As a result the longitudinal dispersivity was approximately an order of magnitude smaller than the transport distance between 100 to 1000 m. Therefore the initial longitudinal dispersivity of 10 m was assigned to the entire catchment

assuming uniform porous media. The transverse dispersivity and vertical dispersivity were taken as 1 m and 0.5 m respectively (ASTM, 1995 ; Gelhar et al., 1992). The effective porosity zones were constructed based on the soil sampling analysis.

7.2.1. Calibration result

The final parameters of the calibrated solute transport model are shown in *Table 7-4*. The calculated chloride concentrations compared to the observed data (*Figure 7:4*) in the solute model calibration indicated that the flow model calibration was satisfactory. However, the solute transport model was optimized at unrealistically high effective porosity (n_e) compared to the estimated values from soil sample analysis work (see *Table 7-4*). This reveals that the hydraulic conductivity defined in the calibrated flow model was too high considering the relation expressed by the equation 6.4. This concludes also that the flow model still requires further improvement by changing hydraulic conductivity and eventually fluxes (recharge and ET_g). The calibration of steady state solute model was performed by trial and error method and therefore the back-calibration of flow model was not performed due to time constrain of this research work. The result of the calibrated solute model of this study is included in the Appendix I.

Table 7-4 The parameter configuration applied in the solute model

Layer	n_e (range)	D_L	D_T	D_v
1	0.03 - 0.65	10	1	0.5
2	0.02 - 0.70	10	1	0.5

* Where n_e – effective porosity, D_L - longitudinal dispersivity, D_v – vertical dispersivity, D_T – Transverse dispersivity

Table 7-5 The error analysis statistics of the solute mode calibration

ME	0.00 mg/l
MAE	1.09 mg/l
RMSE	1.67 mg/l

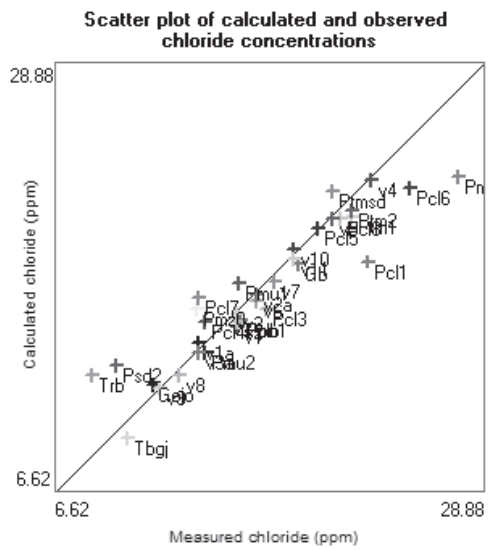

Figure 7:4 Scatter plot of observed chloride concentrations (in the second layer) compared to calculated values after 20 years simulation time.

7.2.2. Sensitivity analysis

A sensitivity analysis is the process of varying model input parameters systematically over a reasonable range and observing the relative change in model response. This helps to identify the uncertainty of input parameters. If model was highly sensitive to an input parameter, further characterization is required on that specific parameter. This is performed in the calibration stage to identify the higher sensitive parameters on the calibration results. The results of the model calibration could be evaluated either qualitatively or quantitatively. The RMSE (root mean square error) was used to evaluate the calibration quantitatively, which yield the average of the squared difference between measured and computed chloride concentrations of groundwater in piezometers.

In this study, sensitivity analysis was performed on transport parameters of longitudinal dispersivity (D_l), transverse dispersivity (D_t) and vertical dispersivity (D_v) with respect to the chloride concentrations in groundwater.

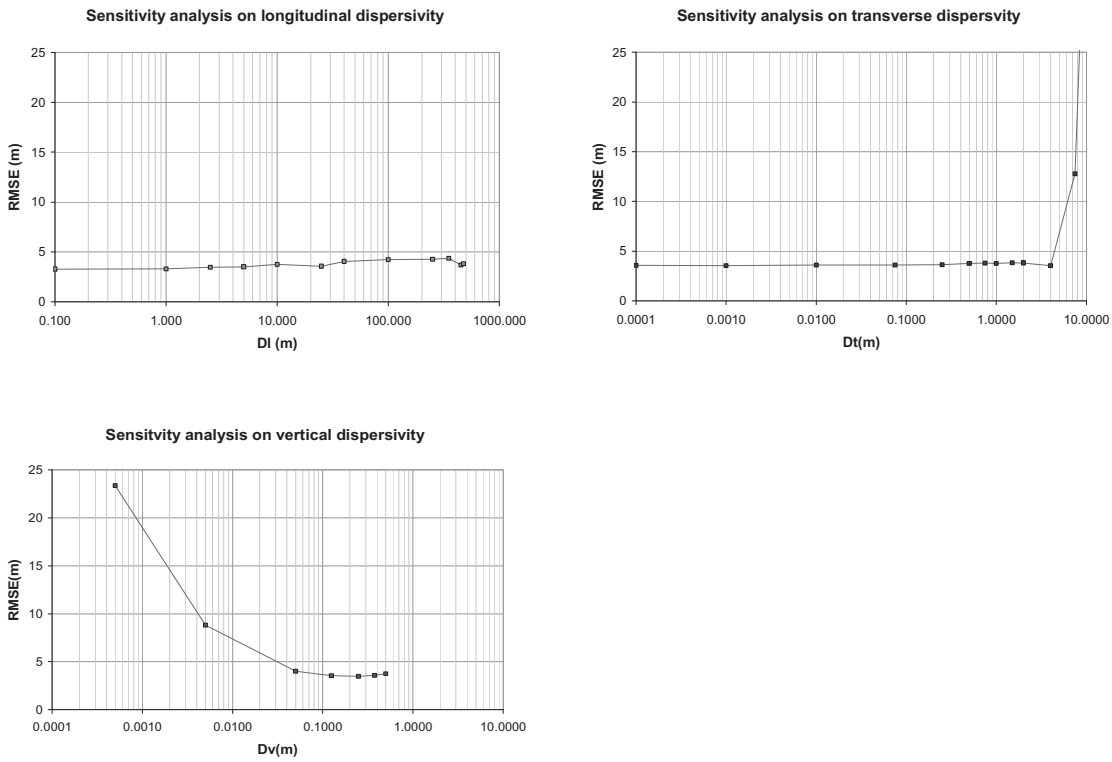

Figure 7:5 The sensitivity analysis result on dispersivity parameters of the second layer

The sensitivity analysis was carried out keeping other parameters constant while the tested parameter was changed fractionally to identify the model response by means of RMSE. The results in *Figure 7:5* indicated that the solute transport model is insensitive to the changes of D_l and D_t while there is a moderate sensitivity of D_v. Therefore further calibration of dispersivity was not critical.

7.3. Transient model calibration

During the transient model calibration, the values of uncertain parameters such as specific yield and specific storage were adjusted. In this study, the calibrated steady state model was used as initial condition of the transient flow model. The transient model was calibrated for hydraulic head data of 2003-2008 period. The storage parameters defined in the model calibrated by Lubczynski and Gurwin (2005) were used and later adjusted to match with hydraulic heads.

The transient model was calibrated using temporal hydraulic head data at six locations. Heads at other locations were also used but for very short time period as explained in chapter 3.6. During the initial calibration steps, PEST programme was used to optimize the main storage parameters, specific yield and storage coefficient within the variability range applied in the previous model (Lubczynski and Gurwin, 2004) and suggested by standard modeling literature. The PEST calibration was performed only at initial stages since the PEST model calibration was not found time efficient particularly when using large number of variables. Therefore after the initial PEST model runs, the fine tuning of the model was further carried out with minor adjustment of recharge and ET_g by manual trial and error method.

7.3.1. Hydraulic heads

Although the evaluated water budget components by steady state model indicated a average condition, the temporal behaviour of these components are highly fluctuated depending on the climatic period prevail in the region (winter or summer). This is more pronounced in the catchment since the recharge flux in the water balance is entirely dependant on the precipitation.

The comparison between the simulated and observed hydraulic heads at the six calibrated wells/piezometers is shown in *Figure 7:6 and Figure 7:7.*

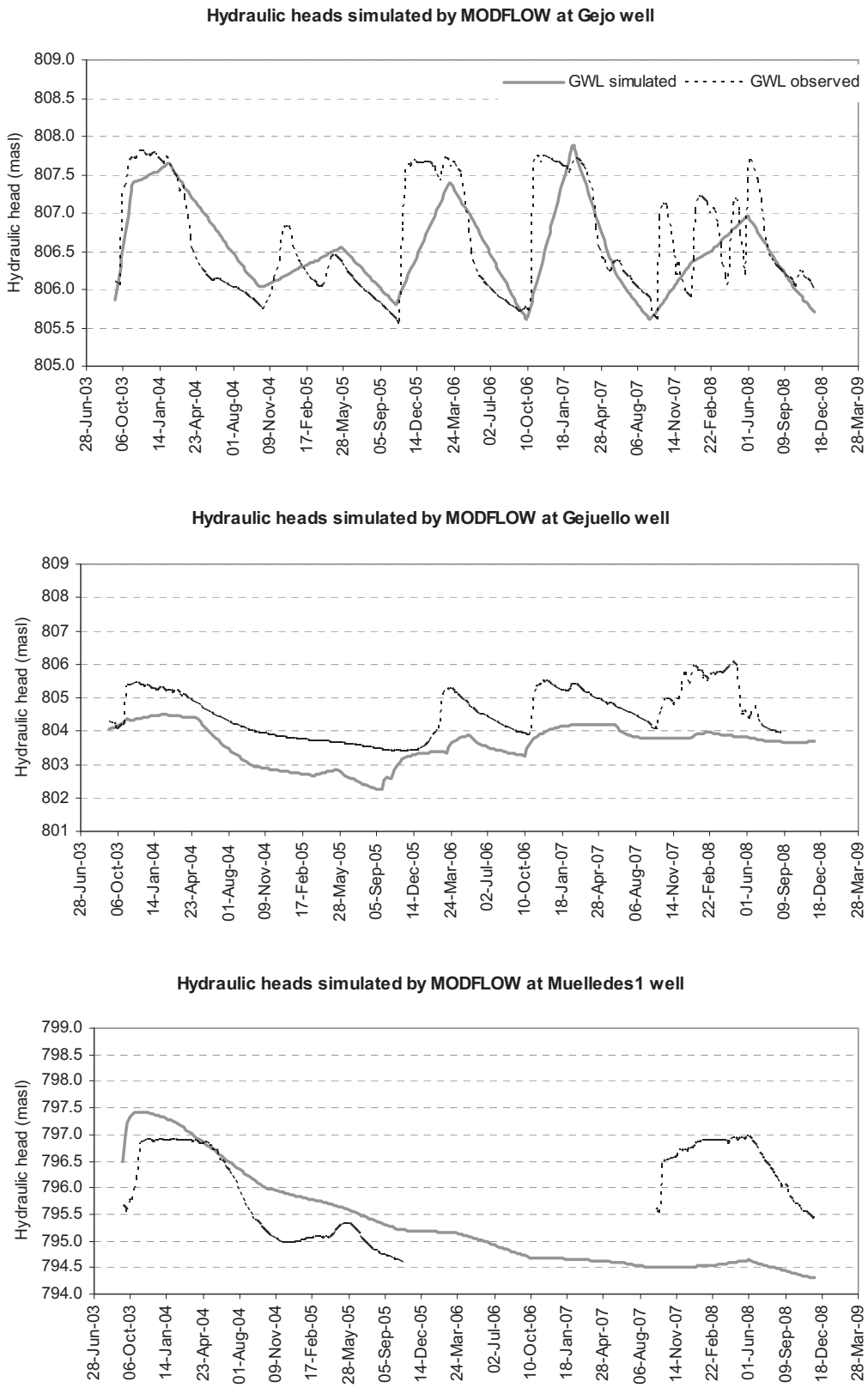

Figure 7:6 Simulated hydraulic heads of Gejo, Gejuello and Muelledes1 wells

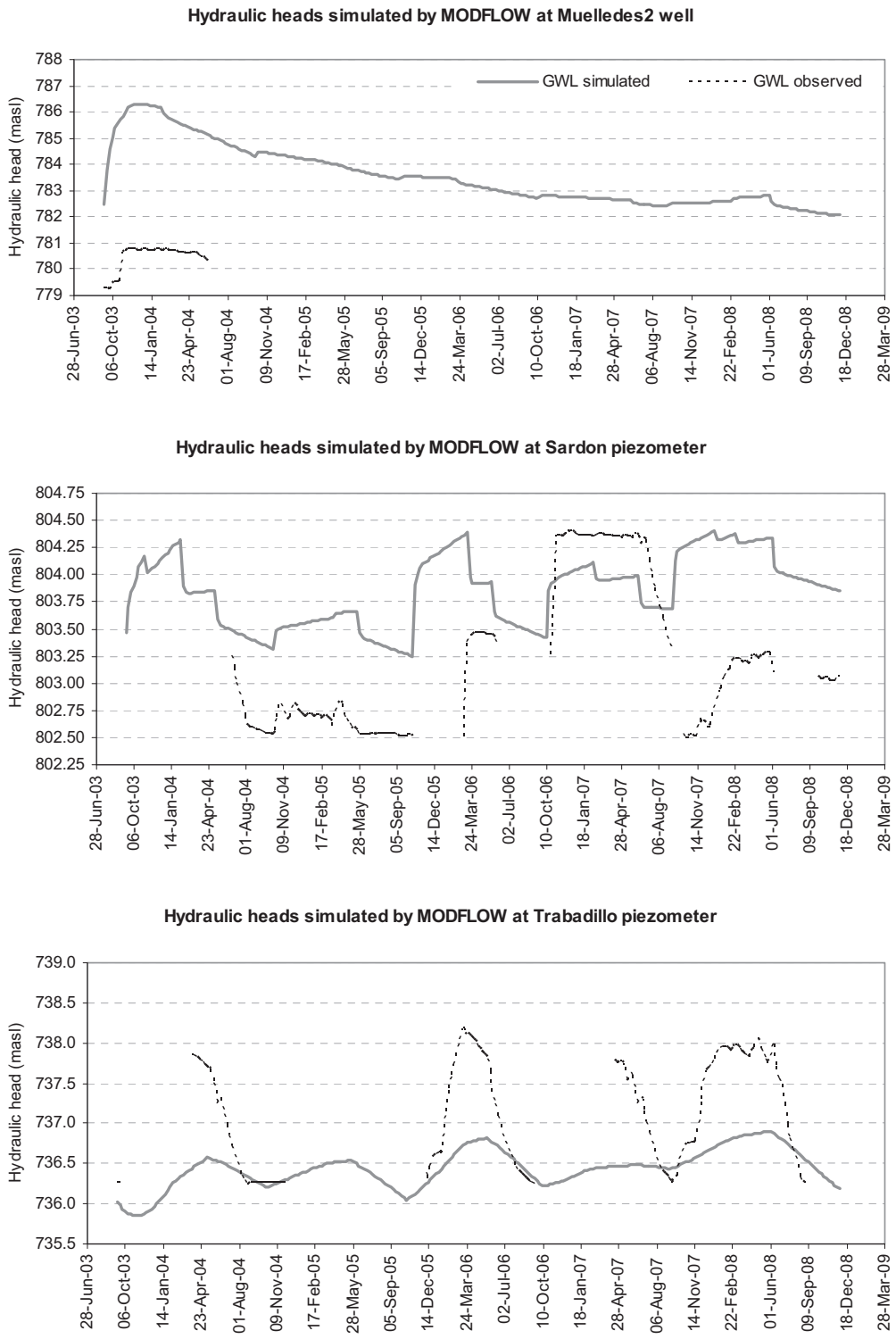

Figure 7:7 Simulated hydraulic heads of Muelledes2 well and piezometers Sardon, Trabadillo

7.3.2. Hydraulic conductivity and specific yield

The adjusted hydraulic conductivity values from the recalibrated steady state model with new initial hydraulic head data was kept unchanged in the initial transient model calibration. The other inputs were calibrated by PEST programme at the start and later performed in manually. The hydraulic conductivity was partially adjusted during later model calibration steps.

In the calibration process, the highest specific yield (0.35) of the first layer was used along the central valley region where as the alluvium and colluvium soils are existed. The zone surrounding the Gejuello was calibrated with the specific yield of 0.19 and the lowest 0.03 was observed at zone surrounding the Gejo located in a higher elevated area. The distribution of specific yield in the first layer is governed by the soil characteristics. However, in the second layer it is controlled by several factors such as weathering stage, fracture density and their openings due to structural influences. The specific yield varies between 0.01 and 0.05 in the second layer revealed the lower porosity of the weathered granite. A satisfactory model result was obtained for the specific yield ranging from 0.03 to 0.35 for the first layer and 0.01 to 0.05 for the second layer.

7.3.2.1. Water balance

The recharge, ET_g, groundwater storage and outflow through drain package are the major components of the groundwater water balance in the study area. All these components were calculated by the model for each defined stress period.

Table 7-6 : Water balance of the stress periods (September 2003 - December 2008)

Stress period	Start	End	Days	Weeks	Rainfall	Recharge	ET_g	Storage	Drain
						m^3/day			
1	12/09/2003	03/11/2003	56	8	320000	74689	6978	41283	26421
2	04/11/2003	09/02/2004	98	14	120000	59040	4560	27202	27283
3	10/02/2004	14/05/2004	91	13	112000	24591	2751	-2165	23988
4	15/05/2004	12/10/2004	154	22	64000	5409	15286	-30811	20934
5	13/10/2004	22/03/2005	161	23	89344	18709	3481	-3535	18762
6	23/03/2005	24/05/2005	63	9	128820	22081	14317	-9150	16939
7	25/05/2005	21/10/2005	147	21	56000	7295	29811	-36697	14192
8	22/10/2005	20/03/2006	147	21	152000	58389	2714	36427	19153
9	21/03/2006	19/05/2006	63	9	104000	26260	16325	-8988	18936
10	20/05/2006	16/10/2006	147	21	83680	7013	24735	-34010	16270
11	17/10/2006	16/02/2007	126	18	275122	42412	1768	25468	15225
12	17/02/2007	16/06/2007	119	17	136000	28974	15621	-5165	18544
13	17/06/2007	13/09/2007	91	13	40000	8796	9160	-18444	18114
14	14/09/2007	04/01/2008	112	16	163540	43938	3071	22066	18764
15	05/01/2008	26/02/2008	56	8	104000	37655	7048	12324	18260
16	27/02/2008	04/06/2008	98	14	194182	34463	17264	-1140	18314
17	05/06/2008	10/12/2008	182	26	72000	10379	23108	-26777	14010
	Total		1911	273					

The 5 year (2003-2008) average flux components of the fully transient model are illustrated below in the *Figure 7:8*. They indicate that average recharge(R) of 0.38 mm/d represents ~24 % of annual rainfall and the average ET_g of 0.14 mm/d represents ~9% of rainfall). The groundwater outflow (G_{of}) through the drain along Sardon fault zone is 0.24 mm/d (~15 % of annual rainfall).

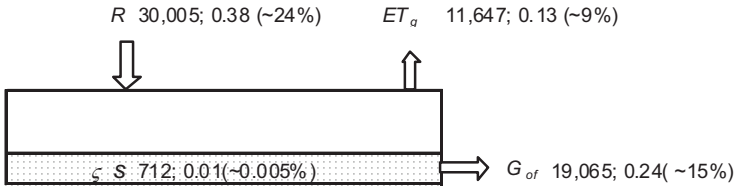

(units are in m^3/d, mm/d and as rainfall % respectively)

Figure 7:8 The average groundwater balance components of the transient model solution

The temporal variability of recharge is closely related with the rainfall pattern. The lowest recharge of ~0.07-0.10 mm/d is observed during the summer stress periods while the highest in winters in order of 0.5 to 0.92 mm/d (Figure 7:7).

The ET_g of each stress period varies with the saturated water level and the other climatological factors such as humidity, solar radiation etc. The minimum ET_g observed by the calibrated model result shows 0.02 mm/d in the stress period 11 in which the recharge is higher compared to average recharge of the other stress periods. The highest calculated ET_g is 0.37 mm/d in the stress period 7, around the peak of summer period. The detail of the water budget components for each stress period generated by the model is shown in *Table 7-6*.

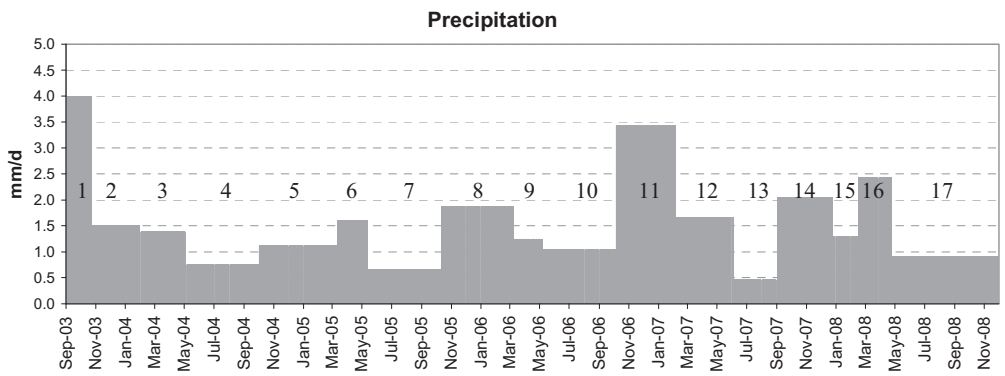

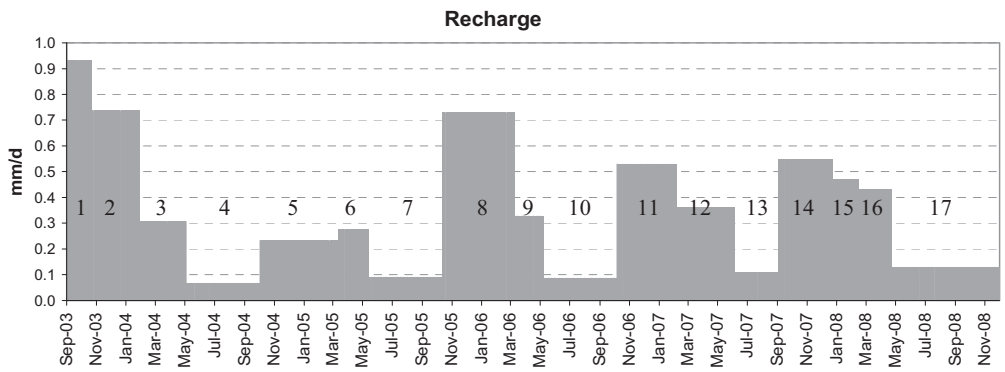

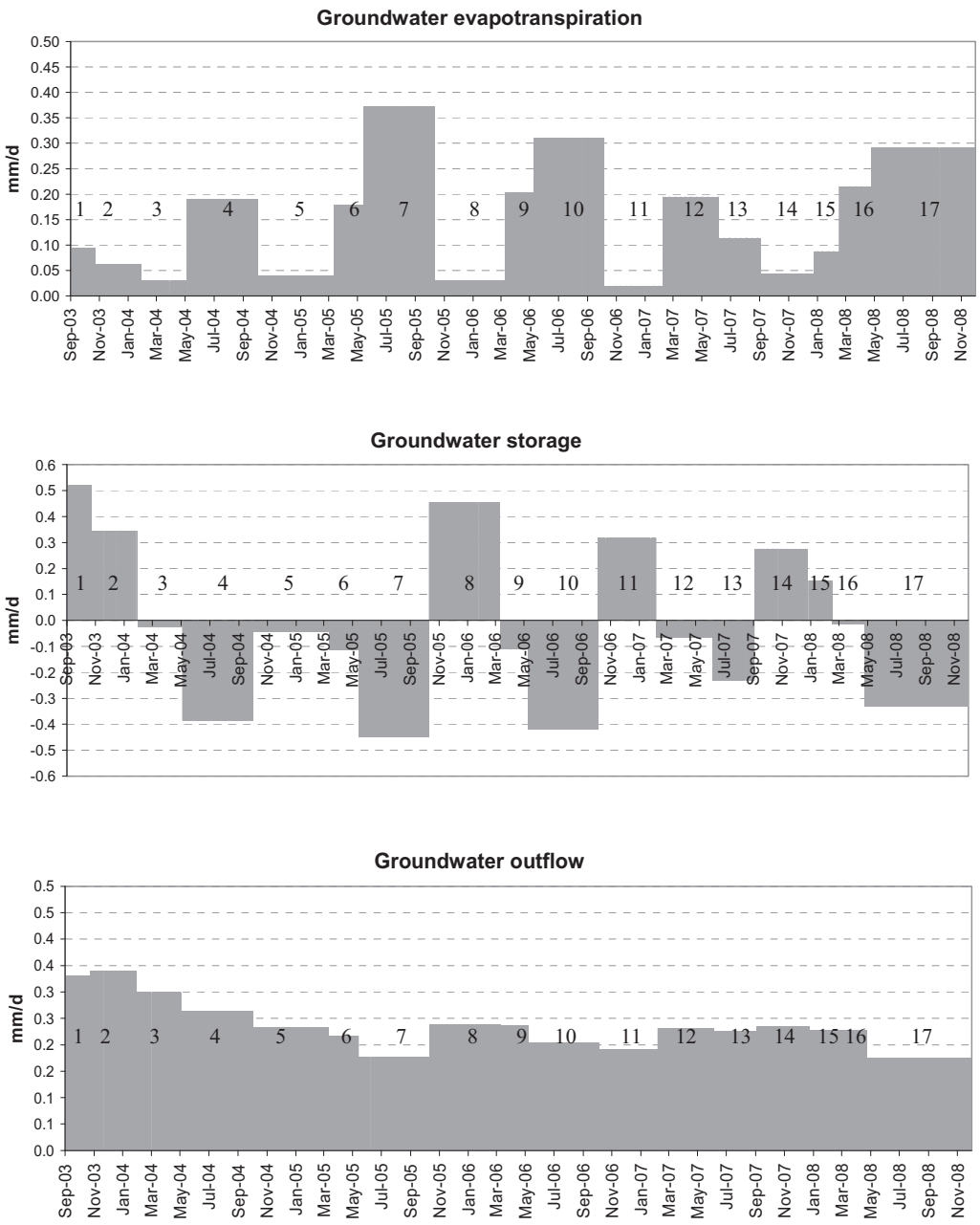

Figure 7:9 The temporal variability of fluxes for the period of September 2003 -2008 December.

The average rainfall and fluxes of each stress period calibrated by the fully-transient model result is illustrated in Figure *7:8 and Figure 7:9*. The stress periods 4, 7, 10 and 13 indicated a lower rainfall and recharge compared to other periods with higher ET_g (approximately 0.26 mm/d) representing the dry seasons.

8. Discussion, conclusions and recommendations

8.1. Discussion

8.1.1. Field tests and spatio-temporal data acquisition

The field tests and data acquisition were carried out to achieve the objectives mentioned in the Chapter 1.4. This included utilising maximum field data coverage for (i) integration of spatio-temporal parameters and fluxes; (ii) deriving the solute parameters through tracer test.

The ADAS monitoring network and head monitoring water level recorders installed in piezometers were critical for the assessment of spatio-temporal variability of recharge, ET_g and state variables to characterise the Sardon catchment aquifer. The field study allowed to obtain: (i) the ADAS climatic data; (ii) hydraulic head monitoring data from water level recorders installed in piezometers and wells; (iii) maximum coverage of spatio-temporal chloride concentration in groundwater from sampling existing piezometers/wells and the new piezometers drilled in this study that improved the number of observations thus reducing the number of degree of freedom in the flow and solute transport model; (iv) soil properties of unsaturated and saturated zones through sampling and analysis; (v) high-precision GPS survey to correct hydraulic heads and geometry of groundwater model and to provide good initial hydraulic head condition and fictitious hydraulic head points in data scarce areas for steady state flow model calibration as explained in Chapter 6.3.2; (vi) river bed conductance by slug tests to reduce the uncertainty in the model calibration; (vii) solute transport parameters at local scale by numerical modelling using forced gradient tracer test with ERT survey.

8.1.2. Spatio-temporal recharge and ET_g

The groundwater fluxes (recharge and ET_g) are spatially and temporally dependent so they involve time dimension which creates additional complexity and difficulty in their assessment. Therefore compared to the geostatistic interpolation, consideration of different influential factors such as soil type, geology and land cover on these fluxes were important in the spatio-temporal assessment. The recharge and ET_g zoned maps produced by the remote sensing and GIS application tools in the previous model (Lubczynski and Gurwin, 2005) were also used in this study for the spatio-temporal flux assessment. Such approach requires however the reference quantitative data.

Combination of recharge estimate techniques i.e. chloride mass balance, well hydrograph and pyEARTH-1D model were used as reference data for the spatially distributed GIS approach. As usually happens, different methods produced different results (*Table 8-1*). The long term (steady state) recharge is best represented by CMB in this semi-arid catchment since the chloride in groundwater is only naturally replenished by rainfall because of no any human or industrial activities in this area. The point recharge obtained form this study varies in the range of 16.3 - 162.0 mm/yr.

However, it was 10 to 342.6 mm/yr in a previous study done by Uria (2000). The large upper range of the recharge in the former study was likely due to possible error resulted by assumption of pretty high chloride concentration in rainfall of 7.0 mg/l based on only one sample. In this study the concentration of rainfall was 1.4 mg/l and was based on the analysis of two rainfall samples at two different times. This was confirmed by a previous study (Kagaba, 1997). The point recharge varies within 22.0- 208.0 mm/yr determined by CMB in the study done by Lubczynski and Gurwin (2005) and it is more comparable with this study result.

The well hydrograph method indicated a lower recharge values as compared to CMB and pyEARTH-1D model. It is due to the difficulty in graphical determination of recession curve since the hydraulic head data in dry seasons are not complete in some of the piezometers such as Trabadillo and Sardon (see *Table 8-1*) missing the driest part due the limited depth of piezometers. The well hydrograph and pyEARTH-1D model used in this study are both 1-D modelling technique which ignored the lateral flow in the assessment of recharge. This problem affected mainly the recharge calculations in discharge areas such as Trabadillo. The high recharge indicated at Trabadillo was due to the negligence of this lateral flow by these recharge techniques and it has confirmed by Cornejo (2000).

Table 8-1 The recharge assessed by pyEARTH-1D, CMB and well hydrograph and ET_a by pyEARTH-1D

Location	ET_a			Recharge						
				pyEARTH-1D			WH		CMB	
	MD	MA	RF%	MD	MA	RF %	MA	RF %	MA	RF %
Gejo	0.69	252.4	44.0	0.46	168.3	29.3	74.2	12.9	43.5	7.6
Gejuello	0.62	227.3	39.6	0.42	151.8	26.4	119	20.7	72.1	12.5
Muelledes1	0.83	303.1	52.8	0.31	111.6	19.4	26.8	4.7	49.8	8.7
Muelledes2	0.80	290.9	50.7	0.30	108.6	18.9	32.8	5.7	61.5	10.7
Sardon	0.67	245.2	42.7	0.30	109.6	19.1	29.8	5.2	24.3	4.2
Trabadillo	0.70	257.2	44.8	0.16	59.93	10.4	20.91	3.6	111.1	19.3

*All values are in mm except RF% - values as rainfall percentage; MD - mean daily; MA - mean annual; WH -well hydrograph; CMB - chloride mass balance

The highest recharge is in Gejo and Gejuello locations which represent recharge areas. Muelledes1 and Muelledes2 wells located in close proximity, also in recharge areas indicated similar recharge values. The CMB recharge represent average condition on longer time scale compared to temporal recharge received by pyEARTH-1D. The discrepancy of recharge in these methods may be influenced due to this reason. As an overall, the recharge calculated by pyEARTH-1D is higher as compared to other methods.

The temporal variability of ET_a that gives a clue about the ET_g, at least in dry season when ET_a can be roughly assumed as equal to ET_g was modelled in pyEARTH-1D. In pyEARTH-1D, the ET_a is calculated as a fraction of ET_0 dependant on the current soil moisture even though the ET_a is not a linear function of ET_0. In addition, the simulation of observed hydraulic head was difficult mainly due to depth-wise heterogeneity which can not be modelled in pyEARTH-1D because it has only one reservoir (SOMOS) that simulate the soil reservoir.

8.1.3. Steady state flow and solute transport models

The previously developed steady state model (Lubczynski and Gurwin, 2005) was based on DEM that involved survey discrepancy of 4-18 m. Therefore in this study the geometry of the model (model layers) was corrected using high-precision differential GPS data. This minimised the error in the numerical model. The recalibration of steady state model was performed with the measured hydraulic heads and fictitious steady hydraulic heads calculated using the regression analysis between elevation and hydraulic head explained by Kuniansky et al.(2009) for data scarce areas. This approach increased the reliability of the steady state model and consequently the fully transient model as well. The flux components of the water budget in this recalibrated model is comparable with the previous steady state model (Lubczynski and Gurwin, 2005) as shown in the *Table 8-2*.

Table 8-2 The water balance of the previous model and recalibrated steady state model

	Previous model(2005)	Recalibrated model
Recharge	56.0 (11.0%)	70.7 (12.3%)
ET_g	20.0 (4.0 %)	22.0 (3.8%)
G_{of}	36.0 (7.0%)	48.7 (8.5%)

The values are in mm/yr and within bracket indicated as a percentage to rainfall

The approach of validating flow model by solute transport model using groundwater chloride tracer introduced valuable additional constrain to the model that reduced the number of degrees of freedom in the flow model solution. The approach was effective since it enabled to identify the uncertainties associated with the parameters and fluxes in the flow model. For example, the optimized effective porosity during the solute model calibration was unrealistically high as compared to the field estimates which showed uncertainty in hydraulic conductivity as indicated by the equation 6.4. This observation emphasized the need of further improvement in the flow model by changing hydraulic conductivity and eventually other fluxes (recharge and ET_g) for which however, there was no sufficient time in this study.

The sensitivity analysis of the solute transport model based on the steady state flow model, indicated that D_l and D_t are insensitive to chloride concentration changes whereas, the vertical dispersivity showed some sensitivity. This is because the tracer was provided in the model with the constant (steady-state) rate and concentration. For example this would not happen in the fully transient flow and solute transport model because then the chloride input would be temporally variable following the temporal variability of recharge. As mentioned transient solute transport model was not carried out because the spatio-temporal chloride data was available only for six months (June 2008 - December 2008) and the variability was negligible. For such model solution much longer temporal data is required because the concentration changes occur on a much larger time-scale than head changes (Leif, 1993).

PMWIN (5.3) environment used in this study is not adapted to PEST optimization of the MT3D solute transport model. Therefore calibration was carried out by trial and error. This was a very tedious work.

8.1.4. Fully-transient model

Transient model was initially calibrated by adjusting storage parameters with PEST and later by adjusting recharge and ET_g by manual fitting. In this calibration the temporal pattern between simulated and observed heads was assessed. The best match was observed in the Gejo location while the simulated heads in rest of the piezometers follow the trend of observed general head fluctuation but there were misfits in some periods. The differences between simulated and measured head data of these locations may be attributed to several factors. The simulating of minor and sharp head variations observed in the wells such as Trabadillo and Sardon was resticted in the transient model due to the limitation of space and time. The model-simulated hydraulic heads represent relatively long term conditions over large areas, however very often the field-measured heads indicate short term, local influence from recharge and ET_g etc. Therefore within a stress period defined in the transient model, the spatio-temporal fluxes vary in reality, but keep constant in the numerical model thus restricting the simulation of the measured hydraulic heads.

Flooding conditions was observed in most of the piezometers during the winter period starting from November to May of each year due to high rainfall in the area. The hydraulic head variation of all piezometers in the catchment shows high fluctuation of rise and recession. This rapid groundwater rise reflects two reasons: first one is the quick response of rainfall recharge through the shallower and thin upper most layer which allows percolation in short time period to the saturated zone during wet period. Second, is the low storage coefficient 0.001-0.03 implying quick water table rise and recession. The differences in the water table rises and recessions are attributed to heterogeneity in aquifer parameters (hydraulic conductivity and storage) and fluxes (*R* and *ETg*).

The temporal variability of recharge is closely related with the temporal variability of rainfall. The wet season is prolonged from the beginning of November up to May. It starts with characteristic heavy short rains indicated by the rain gauges during this period. The response of high recharge in this wet period around November of ever year can be observed in *Figure 7:9*. This recharge response is abrupt due to low retention capacity and thin unsaturated zone enabling percolation in a short time period. This can be observed from the head fluctuations of the piezometers during this period (*Figure 6:4*).

The water balance of the fully transient model developed in this study shows the result is almost similar to previous model (Lubczynski and Gurwin, 2005) result as shown in the table *Table 8-3*, except the groundwater outflow flux in this study was higher compared to the previous study. The groundwater outflow was approximately constant in both dry and wet season (see *Table 7-6*). This can be explained by the low hydraulic conductivity of fractured granitic layer which conveyed and controlled the groundwater flow towards the outlet flow along the Sardon fault zone (Lubczynski and Gurwin, 2005).

The average recharge for the period 2003 to 2008 (24.1% of rainfall) is higher recharge compared to the steady state recharge (12.3% of rainfall). This may be influenced due to: (i) higher recharge calculated by 1-D EARTH model which was applied in both of these studies (ii) preparation of spatio-temporal maps for each stress period through the use of qualitative zoned maps was difficult since the recharge assessment was restricted to six locations with considerable data gaps.

Table 8-3 The comparison of average water balance of the previous and this work

	Transient model (1996-2000)	Transient model (2003-2008)
Recharge	0.37 (24.5 %)	0.38 (24.1%)
ET_g	0.12 (8.0 %)	0.14 (8.2 %)
G_{of}	0.15 (9.8 %)	0.24 (15.2 %)

The values are in mm/d and within bracket indicated as a percentage to rainfall

The highest recharge estimated by the calibration indicates 0.92 mm/d in stress period 1 and the lowest is 0.07 mm/d occurred during 2004-2005 period since a long drought was prevailed.

The ET_g of each stress period was assigned on the base of the pyEARTH-1D *ETa* results. During the wet season, the uptake of groundwater by plant root and groundwater evaporation is at minimum since the unsaturated zone possesses sufficient water moisture content. This is resulted by lower ET_g compared to the dry season and it is approximately an average of 0.09 mm/d for the wet periods. The highest calculated ET_g is 0.37 mm/d in the stress period 7, around the peak of summer dry period (*Figure 7:9*). The transient model results of the previous study (Lubczynski and Gurwin, 2005) indicated the dry season ET_g is 0.55 - 0.8 mm/d that was larger than this study and the wet season < 0.05 mm/d in wet season that was lower than the in this study.

8.2. Conclusions

The main objective of this work was to improve the reliability of the Sardon model. This was achieved through different aspects. The spatio-temporal data acquisition, field tests and methods were effectively and successfully integrated as input for spatio-temporal parameters and fluxes assessment. The spatio-temporal fluxes were assessed through different combination of methods and integrated in GIS derived maps further used in steady state and fully transient model. The following conclusions were drawn from the discussion and model result of this study.

- The recharge calculated by pyEARTH-1D model resulted in higher values than determined by CMB and well hydrograph method. The average recharge from the transient model was higher as compared to steady state model that used recharge calculated by CMB method.

- The limited amount of piezometers restricted the accurate map processing for the transient flux input of recharge and ET_g.

- The high fluctuation (sharp rises and recessions) of groundwater level in the Sardon catchment are due to low aquifer storage coefficient (0.001 - 0.03) and low unsaturated zone retention capacity resulting in the rapid recharge through the thin unsaturated layer.

- The calibration of steady state model using additional high precision GPS survey data and additional fictitious hydraulic head point method for data scarce areas, was very effective and successful in improving the reliability of the flow model.

- The approach of validating the flow model by solute transport model is highly effective since the flow model is constrained by the additional data providing additional constrain.

- The integration of all the spatio-temporal fluxes and spatial parameters were satisfactory in the assessment of groundwater fluxes through fully transient model. The simulated model results for period 2003-2008, indicated average recharge is 0.38 mm/d (24.1 % of annual rainfall) and the ET_g is 0.14 mm/d (8.2 of annual rainfall). The average groundwater outflow is 0.24 mm/d (15.2 % of annual rainfall).

- Fully transient flow models are heavily constrained by the temporal data however still involved uncertainty particularly when the temporal input is limited; coupling such model with solute transport model will provide additional value, still improving the reliability of the overall model calibration.

8.3. Recommendations

- More and deeper monitoring piezometers in the study catchment are needed to improve model reliability.

- More parameter data such as storage parameters and hydraulic conductivity is requirred to improve the reliability of the model.

- Longer period of spatio-temporal groundwater chloride concentration data is required to perform the solute transport model in transient condition and to test the dispersivity further.

- Better link e.g. by using PEST between MODFLOW and MT3D is needed to improve the calibration these flow and solute transport models.

- The dispersivity should be assessed by an analytical method and compared with the numerical model solution to improve the reliability.

References

Anderson, M.P. and Woessner, W.W., 1992. Applied groundwater modeling : simulation of flow and advective transport.

Appiah Duah, A., 1999. Groundwater recharge modeling in hard rocks using remote sensing and GIS applications: a case study in the Rio Tormes basin Salamanca province, Spain, ITC, Enschede, 76 pp.

ASTM, 1995 Standard Guide for Risk-Based Corrective Action Applied at Petroleum Release Sites. American society for Testing and materials ASTM Designation E17390095.

Attanayake, A.N.B., 1999. Analysis of fractures in a granitic terrain and their tectonic and hydrogeological implications: A study from Sardon catchment area, Salamanca province, Spain, ITC, Enschede.

Bastiansen, W., 1998. A remote sensing surface energy balance algorithm for land (SEBAL). Journal of Hydrology.

Batelaan, O., 2006. Characterizing groundwater recharge and discharge using remote sensing, GIS, ecology, hydrochemistry and groundwater modelling. Phd Thesis(Department of Hydrology and Hydraulic Engineering,Faculty of Engineering,Vrije Universiteit Brussel,Pleinlaan 2,1050 Brussels): pp. 332.

Bouwer, H., 1989. Estimating and enhancing groundwater recharge. In: Sharma, M.L., (Ed.), Groundwater Recharge(Balkema, Rotterdam, Netherlands,): p. 1.

Brunner, P., Bauer, P., Eugster, M. and Kinzelbach, W., 2004. Using remote sensing to regionalize local precipitation recharge rates obtained from the Chloride Method. Journal of Hydrology, 294(4): 241-250.

Chiang, W.H. and Kinzelbach, W., 2001. Processing MODFLOW (version 5.3), A simulation system for modeling groundwater flow and pollution.

Cook, P.G., 2003. A guide to regional groundwater flow in fractured rock aquifers. CSIRO-Sea view Press, South Australia, ISBN 1740082338 pp. 108.

Craig, E.D. and Jeffrey, J.M., 2005. The future of applied tracers in hydrogeology. Journal of Hydrogeology, (2005) 13:255-258 : DOI 10.1007/s10040-004-0416-3(J. J. McDonnell, Department of Forest Engineering, Oregon State University, Corvallis, OR, USA).

Dingman, S.L., 2002. Physical Hydrology. Second Edition(Prentice Hall, Upper Saddle River, New Jersey 07458): 646.

Doherty, J., 2000. PEST-Model-Independant Parameter Estimation, User's Manual. Water Mark Computing(Australia).

Domenico, P.A. and Schwartz, F.W., 1998 Physical and chemical hydrogeology. Second Edition(John Wiley & Sons, New York).

Eve L. Kuniansky, Mark A. Lowery and Campbell, B.G., 2009. How Processing Digital Elevation Models Can Affect Simulated Water Budgets. Groundwater Journal, National Groundwater Association (NGWA), , 47(No. 01): 99 -107.

FAO, 1998. Crop evapotranspiration - Guidelines for computing crop water requirements. FAO Irrigation and drainage paper, 56(Rome: Food and Agriculture Organization of the United Nations).

Fernandez-Garcia, D. and Gomez-Hernandez, J.J., 2007. Impact of upscaling on solute transport: Travel times, scale dependence of dispersivity, and propagation of uncertainty. Water Resources Research, 43(2).

Fetter, C.W., 2001. Applied Hydrogeology. Fourth edition(Upper Saddle River,Prentice Hall): 598.

Francés, A.P., 2008a. Sardon field work and data processing. ITC, Internal report.

Francés, A.P., 2008b. Spatio - temporal groundwater recharge assessment : a data - integration and modelling approach, ITC, Enschede, 57 pp.

Freeze, R.A. and Cherry, J.A., 1979 Groundwater. Prentice Hall(Englewood Cliffs, New York).

Gehrels, J.C., 1999. Separation of natural from anthropogenic influences and determination of groundwater recharge in the Veluwe area, the Netherlands.

Gehrels, J.C. and Van der Lee, J., 1990. Modeling Aquifer recharge. Journal of Hydrology, 157(1-4): 105-138.

Gelhar, L.W., Welty, C. and Rehfeldt, K.R., 1992. A critical review of data on field-scale dispersion in aquifers. Water Resources Research, 28(7): 1955-1974.

Harbaugh, A.W. and Mc Donald, M.G., 1988. A modular three-dimensional finite difference groundwater flow model MODFLOW.

Healy, R.W. and Cook, P.G., 2002. Using groundwater levels to estimate recharge. Hydrogeology Journal, 10: 91-109.

Kagaba, S., 1997. Evaluation of groundwater resources in hard rocks by numerical flow modelling combined with GIS : lower Rio Tormes basin, Salamanca province, Spain, ITC, Enschede, 100 pp.

Kruseman, G.P., 1997. Recharge from Intermittent flow : Recharge from phreatic aquifers in (semi-)arid areas. IAH, 19: pp. 145-184.

Kruseman, G.P. and de Ridder, N.A., 1992. Analysis and Evaluation of Pumping Test Data. ILRI, Netherlands.

Lautz, L.K. and Siegel, D.I., 2006. Modeling surface and ground water mixing in the hyporheic zone using MODFLOW and MT3D. Advances in water resources, 29(11): 1618-1633.

Leif, C., 1993. Palla road and Khurutshe groundwater resources investigation Phase 2, Appendix 5, Groundwater modelling(Republic of Botswana, Department of Water Affairs).

Lopez, P. and Carnicero, A., 1987. Hercynian plutonism of the Salamanca-Zamora peneplain (Central western Spain). In Geologia de los granitoids y rocas asociadas del macizo(Hesperico, University of Salamanca, E. D. S. Libro Homenaje A. L. C. Garcia de Figuerola.).

Lubczynski, M.W., 2000. Groundwater evapotranspiration - underestimated component of groundwater balance in a semi-arid environment -Serowe case Botswana. Past Achievement and Future Challenges(Balkema, Rotterdam): pp. 199-204.

Lubczynski, M.W. and Gurwin, J., 2004. Modeling of complex multi-aquifer systems for groundwater resources evaluation - Swidnica study case (Poland). Journal of Hydrogeology, 13:627-639(Speringer-Verlag).

Lubczynski, M.W. and Gurwin, J., 2005. Integration of various data sources for transient groundwater modeling with spatio-temporally variable fluxes-Sardon study case, Spain. Journal of Hydrology, 306(1-4): 71-96.

Macaulay, S. and Mullen, I., 2007. Predicting salinity impacts of land-use change: Groundwater modeling with airborne electromagnetic and field data,SE Queensland, Australia. International Journal of Applied Earth Observation and Geoinformation, 9: 124-129.

Mattle, N., Kinzelbach, W., Beyerle, U., Huggenberger, P. and Loosli, H.H., 2001. Exploring an aquifer system by integrating hydraulic, hydrogeologic and environmental tracer data in a three-dimensional hydrodynamic transport model. Journal of Hydrology, 242(3-4): 183-196.

Obakeng, O.T., 2007. Soil moisture dynamics and evapotranspiration at the fringe of the Botswana Kalahari, with emphasis on deep rooting vegetation. Vrije Universiteit Amsterdam, Amsterdam 225 pp.

Onnis, O. et al., 2007. Use of environmental tracer data for groundwater mdeling. Geophysical Research Abstracts, Vol. 9, 09120,2007(European Geosciences Union).

Paul, W.R. and Bruce, A.R., 2004. Characterization of groundwater using nonreacting and reacting tracers. (Identifying Technologies to Improve Regional Water Stewardship: North-Middle Rio Grande Corridor): 150 - 161.

Scanlon, B.R., Healy, R.W. and Cook, P.G., 2002. Choosing appropriate techniques for quantifying groundwater recharge. Hydrogeology Journal, 10(1): 18-39.

Serrano, S.E., 2001. Solute transport under non-linear sorption and decay. Water Research, 35(6): 1525-1533.

Shakya, D.R., 2001. Spatial and temporal groundwater modeling integrated with remote sensing and GIS: hard rock experimental catchment, Sardon, Spain, ITC, Enschede, 125 pp.

Sharda, V.N., Kurothe, R.S., Sena, D.R., Pande, V.C. and Tiwari, S.P., 2006. Estimation of groundwater recharge from water storage structures in a semi-arid climate of India. Journal of Hydrology, 329(1-2): 224-243.

Tesfai, B.H., 2000. Subsurface characterization of granitic basement from structural and resistivity data MSc. Thesis(ITC, Enschede, The Netherlands).

Uria Cornejo, S.P., 2000. Groundwater recharge modelling in hard rocks area : Sardon case study, Spain, ITC, Enschede, 89 pp.

Vandenbohede, A. and Lebbe, L., 2003. Solute transport in heterogeneous aquifers, parameter identification and its use in groundwater pollution and salt water intrusion problems. Universiteit Gent, Faculteit geologie en Bodemkunde: p.238.

Vandenbohede, A. and Lebbe, L., 2006. Double forced gradient tracer test: Performance and interpretation of a field test using a new solute transport model. Journal of Hydrology, 317(1-2): 155-170.

Appendices

Appendix A: Rainfall analysis data and statistics

Monthly rainfall of Trabadillo station and surrounding stations (2003-2008)

Date	Berrocol	Ledesma	Fresno	Villar	Iruel	Trabadillo
31/01/2003	112.0	137.7	121.2	153.3	141.5	137.7
28/02/2003	39.7	60.3	55.9	71.5	64.9	60.3
31/03/2003	31.5	53.4	40.0	59.9	77.0	53.4
30/04/2003	70.0	67.5	72.2	89.6	101.0	87.2
31/05/2003	7.5	0.0	7.7	2.8	2.5	4.4
30/06/2003	11.0	0.0	27.6	20.3	17.3	16.1
31/07/2003	6.5	15.0	10.9	19.3	11.9	14.1
31/08/2003	23.9	28.4	21.0	31.2	33.3	28.4
30/09/2003	51.0	51.2	59.7	69.9	10.0	51.2
31/10/2003	156.5	159.6	104.3	140.9	215.5	159.6
30/11/2003	63.5	73.6	65.9	66.7	86.8	73.6
31/12/2003	31.0	48.0	36.7	34.6	18.2	38.5
31/01/2004	31.0	29.0	34.8	31.7	37.5	36.0
29/02/2004	21.7	21.7	25.8	19.1	17.7	21.7
31/03/2004	51.5	40.0	54.9	45.5	50.4	53.3
30/04/2004	25.0	35.0	35.9	35.2	32.0	36.2
31/05/2004	79.0	39.0	80.3	26.5	22.2	55.6
30/06/2004	4.5	19.0	5.5	22.1	7.8	13.3
31/07/2004	15.0	0.0	3.4	0.8	0.0	4.3
31/08/2004	25.5	23.0	67.8	45.0	59.7	47.5
30/09/2004	2.0	4.8	4.8	8.5	3.7	4.8
31/10/2004	76.5	71.5	93.6	105.1	110.9	99.6
30/11/2004	15.5	20.2	20.2	22.7	0.0	20.2
31/12/2004	28.0	29.3	28.8	16.6	39.0	29.3
31/01/2005	0.0	2.9	8.3	2.4	0.0	2.9
28/02/2005	27.0	14.0	25.7	13.4	31.0	24.1
31/03/2005	30.0	36.0	35.6	30.2	39.2	37.9
30/04/2005	46.0	40.9	36.0	35.4	38.0	40.9
31/05/2005	54.5	36.1	28.8	25.0	27.5	36.1
30/06/2005	14.5	10.9	4.9	1.7	21.6	10.9
31/07/2005	0.0	3.6	2.8	3.8	7.7	3.6
31/08/2005	11.0	10.6	12.5	10.0	6.3	10.6
30/09/2005	14.5	13.5	5.5	17.3	14.8	13.5
31/10/2005	106.5	119.9	119.9	128.6	133.9	119.9
30/11/2005	61.0	51.9	73.1	62.8	68.0	51.9
31/12/2005	43.5	55.5	38.0	54.7	64.5	55.5
31/01/2006	22.5	19.5	20.9	25.5	17.2	21.9
28/02/2006	40.0	45.8	59.7	56.4	56.1	54.6
31/03/2006	63.5	51.5	59.1	65.7	64.4	60.9
30/04/2006	47.5	21.0	41.8	35.8	27.6	30.3
31/05/2006	15.0	21.5	14.0	30.8	37.2	21.6
30/06/2006	54.0	60.5	49.0	16.5	28.0	23.4
31/07/2006	18.0	0.0	2.8	20.4	4.6	11.7
31/08/2006	21.2	15.0	24.2	37.5	26.5	25.8

30/09/2006	48.0	17.1	66.4	46.6	54.1	69.0
31/10/2006	110.5	33.1	149.5	197.8	192.8	178.5
30/11/2006	93.5	160.0	149.1	162.1	170.3	150.3
31/12/2006	42.5	47.4	41.8	65.7	31.3	47.4
31/01/2007	13.5	17.5	11.5	9.4	9.5	15.0
28/02/2007	79.5	76.6	88.6	92.4	56.6	73.2
31/03/2007	17.0	8.3	28.5	26.4	31.2	24.0
30/04/2007	87.0	55.0	44.6	59.9	38.0	46.2
31/05/2007	81.0	117.5	118.1	64.4	57.0	81.0
30/06/2007	41.0	53.5	55.0	65.2	75.6	48.0
31/07/2007	2.5	2.3	2.5	2.2	4.5	4.5
31/08/2007	16.6	11.3	21.5	21.5	11.3	21.6
30/09/2007	134.5	92.0	54.9	40.7	50.7	113.1
31/10/2007	51.5	49.0	40.3	49.6	16.0	42.9
30/11/2007	38.1	40.5	38.0	33.2	44.0	38.1
31/12/2007	14.5	14.2	10.9	20.3	17.2	18.3
31/01/2008	41.3	30.0	45.8	51.0	43.2	43.2
29/02/2008	45.5	62.0	45.6	15.0	59.1	45.9
31/03/2008	19.5	10.3	16.7	108.7	11.6	15.9
30/04/2008	106.3	85.6	87.5	72.3	125.6	102.3
31/05/2008	131.0	141.5	70.7	12.9	122.8	121.5
30/06/2008	15.0	32.5	31.0	2.1	7.7	40.2
31/07/2008	1.5	0.6	1.2	11.7	12.4	13.2
31/08/2008	3.0	3.3	6.0	19.2	5.0	6.0
30/09/2008	28.5	30.0	25.8	25.8	26.9	25.8
31/10/2008	57.0	35.8	35.8	35.8	45.7	37.4

Appendix B: Correlation of rainfall at Trabadillo with surrounding stations for 2005-2008

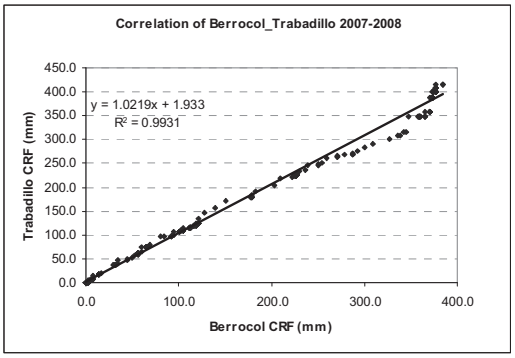

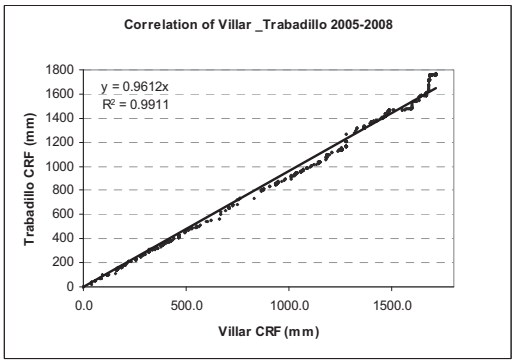

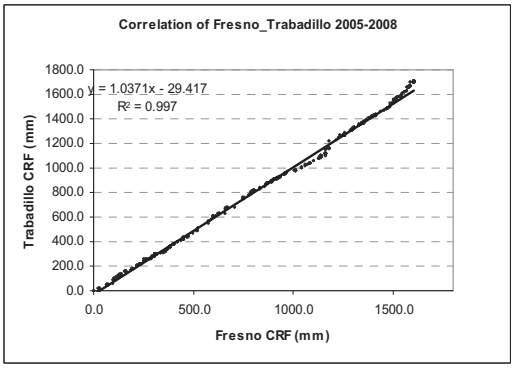

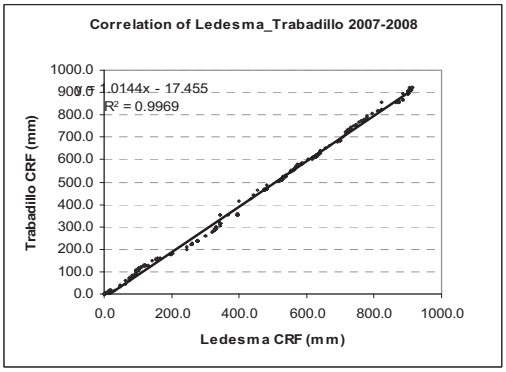

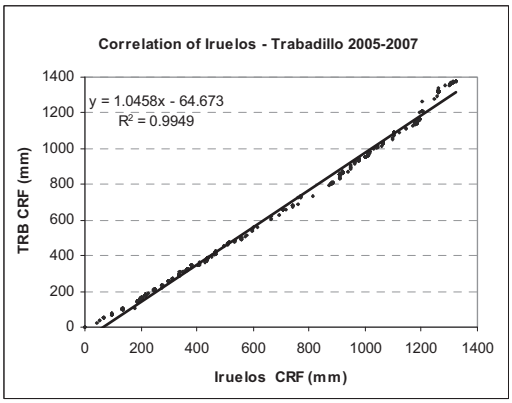

The location of surrounding rain gauges used for filling gaps of rainfall in Trabadillo station

ID-Station	Station	Elevation(masl)	Longitude	Latitude
2879E	Berrocol	821.0	6 00 072 W	40 57 00 N
2883O	Ledesma	816.0	6 03 552 W	41 12 42 N
2885I	Fresno	815.0	6 00 522 W	41 18 30 N
2893	Villar	767.0	6 21 472 W	41 03 20 N
2894	Iruelos	781.0	6 19 422 W	41 03 30 N

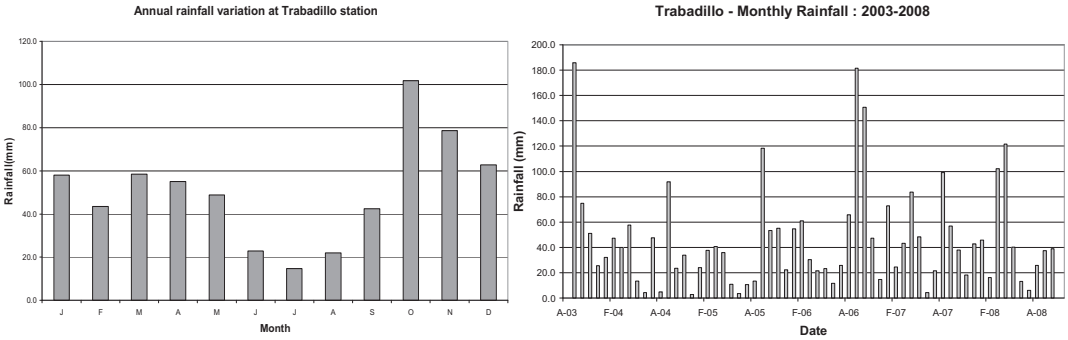

Average monthly rainfall variation in a year and monthly rainfall over the period 2003-2008.

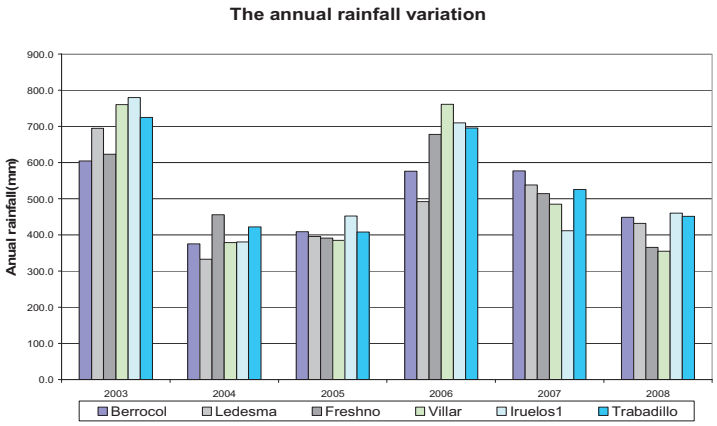

Annual rainfall of the surrounding rain gauges and Trabadillo station for the period of 2003-2008

Appendix C: The coordinates and technical details of the piezometers

ID	Place	UTMx	UTMy	ORTOz	Depth(mbgl)	Di-int(cm)	GWL(mbgl)
Ptb1	Trabadillo	739512.331463431	4555882.69232565	739.139	3.21	4.8	
Ptb2	Trabadillo	739508.008066763	4555882.4518	738.998	3.38	4.8	
Ptb3	Trabadillo	739468.082038619	4555866.0245872	738.151	2.56	4.8	
Ptb4	Trabadillo	739469.368362825	4555936.76105924	737.774	1.88	5.0	
Ptb5	Trabadillo	739379.935889012	4555957.70888752	735.616	1.39	4.8	
Ptb6	Trabadillo	739504.979932072	4555885.72378437	738.847	2.87		
Ptb7	Trabadillo	739509.297715727	4555885.85075211	738.94	2.64		1.16
Ptbgj0	Between Trabadillo and Gejo dos Reyes	737841.691320665	4556718.88104351	753.561	1.45	5.0	1.19
Ppn0	Penalbo, close to river	738315.870765932	4554145.86555891	743.665	1.20	5.0	1.00
Pgj0	Close to Gejo	736096.015364344	4557825.28975361	808.267	3.65		2.08
Pgjtm0	Between Gejo and Tremedal, path finish in the field	736502.82899869	4555730.8770458	776.829	1.08	4.5	
Pmu1	South to Muelledes ADAS station	739472.505509595	4547705.73117279	796.984	7.90		1.06
Pmu3	Muelledes ADAS station	738702.78101355	4547894.82577963	798.246	1.86	4.8	1.19
Pmu2	North to Muelledes ADAS station	738731.092242403	4548562.9137656	781.426	17.70		1.50
FsdW	Junction Sardon and Valdenora streams	738511.672809318	4548650.11515277	779.262			
Psd2	Junction Sardon and Valdenora streams	738435.923735244	4548595.55388508	781.066	1.19	5.0	
Pgb0	Close to Gejuello del Barro	741435.096902441	4551574.32061525	805.691	3.36		1.45
Ptm1	In Tremedal village	737006.234413911	4551115.94691752	764.323	3.13		1.68
Psdw	Junction Sardon and Valdenora streams	738511.842684891	4548651.21658793	779.228	0.71		0.60
Pmz0	Outlet catchment	739681.995190584	4557080.03347559	732.014	0.57	5.0	0.34
Ptm2	Outside Tremedal, close to Manantial de los Canos	737067.19210786	4551353.31416184	756.461	2.30		1.68
Psd0	Sardon village	736378.105629067	4548919.24249685	804.367	1.47	5.0	1.25
Ppn1	App. 50 m from Ppn0 (pond)	738330.29533036	4554144.61483559	744.069	2.75		1.50
Pcl1*	Trabadillo; near bridge(adjoining to Sardo river)	739491.268650334	4556314.54061316	734.346	1.80	5.0	0.65
Pcl3*	Trabadillo ; near flume	739659.625849881	4557062.37081636	732.318	0.96	5.0	0.76
Pcl4*	near existing aband. slug test transp.pipe	738584.778629854	4553782.92817684	740.804	1.76	5.0	1.13
Pcl5*	Tremadal; penalbo(completed at first work)	738355.135846686	4552765.77659189	744.184	2.51	5.0	1.19
Pcl6*	Tremadal	738057.118047429	4551633.83385684	748.507	2.14	5.0	1.57
Pcl7*	Tremadal(slug test2)	738426.54079049	4551375.18181061	747.996	1.11	5.0	1.11

Pcl8*	Adjoning Sardon river;(gauge stucked location)	738413.965274253	4552392.36296473	744.181	1.59	5.0	1.18
ID	**Place**	**UTMx**	**UTMy**	**ORTOz**	**Depth(mbgl)**	**Di-int(cm)**	**GWL(mbgl)**
Pmu1_T1*	Near pmu1 well	739474.308798254	4547701.1185369	796.957	1.99	5.0	1.32
Pmu1_T2*	Near pmu1 well	739474.241535348	4547701.46200914	797.009	1.68	5.0	1.33
Pmu1_T3*	Near pmu1 well	739473.982329027	4547693.86771441	797.056	1.57	5.0	1.36

Appendix D : The average recharge and actual evapotranspiration estimated from the pyEARTH-1D model for each stress period of the transient model

					Average recharge(mm/day)						Average Eta (mm/day)						Trabadillo
Stress period	Start	End	Days	Weeks	Gejo	Gejuello	Pmu 1	Pmu 2	Sardon	Trabadillo	Gejo	Gejuello	Pmu 1	Pmu 2	Sardon	Trabadillo	Rainfall
1	9/12/2003	11/3/2003	56	8	1.397	0.998	0.804	0.549	0.608	0.061	0.715	0.531	0.951	0.682	0.608	0.061	4.0
2	11/4/2003	2/9/2004	98	14	0.956	1.071	0.518	0.516	0.599	0.601	0.338	0.350	0.491	0.464	0.599	0.601	1.5
3	2/10/2004	5/14/2004	91	13	0.274	0.165	0.433	0.411	0.362	0.237	0.950	0.898	1.234	1.184	0.362	0.237	1.4
4	5/15/2004	10/12/2004	154	22	0.000	0.000	0.019	0.008	0.001	0.022	0.780	0.602	0.752	0.747	0.001	0.022	0.8
5	10/13/2004	3/22/2005	161	23	0.293	0.205	0.178	0.209	0.178	0.001	0.401	0.383	0.530	0.506	0.178	0.001	1.1
6	3/23/2005	5/24/2005	63	9	0.342	0.161	0.093	0.130	0.076	0.000	1.116	0.995	1.379	1.321	0.076	0.000	1.6
7	5/25/2005	10/21/2005	147	21	0.000	0.000	0.002	0.008	0.001	0.000	0.418	0.297	0.388	0.384	0.001	0.000	0.7
8	10/22/2005	3/20/2006	147	21	1.052	0.873	0.727	0.637	0.756	0.304	0.426	0.442	0.609	0.578	0.756	0.304	1.9
9	3/21/2006	5/19/2006	63	9	0.298	0.202	0.339	0.444	0.269	0.221	1.262	1.178	1.589	1.529	0.269	0.221	1.3
10	5/20/2006	10/16/2006	147	21	0.000	0.000	0.004	0.016	0.003	0.044	0.693	0.575	0.698	0.694	0.003	0.044	1.0
11	10/17/2006	2/16/2007	126	18	1.436	1.949	0.755	0.700	0.859	0.699	0.386	0.401	0.552	0.524	0.859	0.699	3.4
12	2/17/2007	6/16/2007	119	17	0.480	0.297	0.433	0.417	0.445	0.321	1.195	1.106	1.494	1.450	0.445	0.321	1.7
13	6/17/2007	9/13/2007	91	13	0.013	0.008	0.102	0.013	0.009	0.035	0.881	0.722	0.863	0.855	0.009	0.035	0.5
14	9/14/2007	1/4/2008	112	16	0.759	0.680	0.498	0.525	0.554	0.196	0.519	0.531	0.686	0.662	0.554	0.196	2.0
15	1/5/2008	2/26/2008	56	8	0.632	0.400	0.400	0.435	0.355	0.102	0.459	0.475	0.665	0.627	0.355	0.102	1.3
16	2/27/2008	6/4/2008	98	14	0.757	0.451	0.362	0.400	0.330	0.037	1.252	1.195	1.656	1.584	0.330	0.037	2.4
17	6/5/2008	12/7/2008	182	26	0.090	0.101	0.089	0.124	0.065	0.014	0.684	0.600	0.741	0.723	0.065	0.014	1.0
	Total		1910	273													

Appendix E: Well hydrograph analysis used in the recharge assessment using head data

Location - Gejo		Specific yield (S_y)	0.025
Recharge event	GWL peak(maximum)/ cm	Recession(minimum)/cm	Groundwater rise (cm)
1	280.0	110.0	170.0
2	330.0	85.0	245.0
3	310.0	120.0	190.0
4	225.0	65.0	160.0
5	300.0	65.0	235.0
6	300.0	65.0	235.0
7	245.0	110.0	135.0
8	250.0	105.0	145.0
9	250.0	130.0	120.0
10	310.0	150.0	160.0
		Total	1795.0
Recharge	61.83	mm/year	

Location - Gejuello		Specific yield (S_y)	0.025
Recharge event	GWL peak(maximum)/ cm	Recession(minimum)/cm	Groundwater rise (cm)
1	130.0	100.0	30.0
2	270.0	60.0	210.0
3	245.0	95.0	150.0
4	240.0	50.0	190.0
5	250.0	60.0	190.0
6	240.0	40.0	200.0
		Total	970.0
Recharge	37.17	mm/year	

Location - Muelledes1		Specific yield (S_y)	0.05
Recharge event	GWL peak(maximum)/ cm	Recession(minimum)/cm	Groundwater rise (cm)
1	795.60	794.61	99.0
2	796.73	794.34	239.0
3	795.50	794.75	75.0
4	794.94	794.37	57.0
		Total	470.0
Recharge	53.54	mm/year	

Location – Muelledes2		Specific yield (S_y)	0.03
Recharge event	GWL peak(maximum)/ cm	Recession(minimum)/cm	Groundwater rise (cm)
1	779.83	778.78	105.0
2	780.94	778.92	202.0
3	780.72	778.77	195.0
		Total	502.0
Recharge	49.26	mm/year	

Location – Trabadillo		Specific yield (S_y)	0.03
Recharge event	GWL peak(maximum)/ cm	Recession(minimum)/cm	Groundwater rise (cm)
1	737.02	735.47	155.0
2	737.38	735.47	191.0
3	737.12	735.48	164.0
4	737.15	735.39	176
5	737.21	735.42	179
6	737.23	735.44	179
		Total	1044.0
Recharge	20.91	mm/year	

Location – Sardon		Specific yield (S_y)	0.02
Recharge event	GWL peak(maximum)/ cm	Recession(minimum)/cm	Groundwater rise (cm)
1	802.87	802.50	37
2	803.95	802.49	146
3	802.78	802.54	24
4	802.73	802.50	23
5	803.64	802.50	114
6	803.61	802.50	111
		Total	455
Recharge	44.64	mm/year	

Appendix F : The description of modules in the EARTH model

MAXIL module

This module calculates the amount of precipitation retained after vegetation losses/ interception or surface depression storage and another fraction looses by surface storage evapotranspiration. The precipitation remained after these losses is transferred to subsequent SOMOS reservoir referred as precipitation excess (P_e) given by

$$P_e = p - MAXIL - E_0 \qquad \text{(A)}$$

Where p is precipitation (mm) and $MAXIL$ is the interception fraction (mm) and E_0 is evaporation from surface storage.

SOMOS module

In the SOMOS reservoir, a part of precipitation excess is percolated into deeper saturated zone of SATFLOW module. The remains after actual evapotranspiration and runoff losses; represent the change of soil moisture storage given by

$$\frac{dS}{dt} = P_e - ET_a - R_p - (SUST + Q_s) \qquad \text{(B)}$$

Where S soil moisture (mm) is, ET_a is actual evapotranspiration, R_p is the percolation (mm), $SUST$ is the ponding water (mm) and Q_s is the runoff (mm). The soil moisture storage in this unsaturated zone is defined as the volumetric soil moisture content multiplied by layer thickness in which the soil moisture changes occur.

ET_a is a function of potential evapotranspiration (*PET*), existing soil moisture (θ), maximum soil storage capacity in the root zone or porosity (ϕ) and finally the soil retention capacity or permanent wilting point (θpwp).

$$ET_a = PET \frac{(\theta - \theta_{pwp})}{(\phi - \theta_{pwp})} \qquad \text{(D)}$$

The percolation (Rp) or downward flux after root zone is described by Darc's law;

$$R_p = K\left(\frac{dh_p}{dz} + 1\right) \approx K_s \frac{(\theta - \theta_{fc})}{(\phi - \theta_{fc})}$$

Where K is the unsaturated hydraulic conductivity, dh_p/dz is the hydraulic head gradient, Ks is saturated hydraulic conductivity (mm/day). Below the root zone, soil water movement in unsaturated zone is mainly determined by gravity and capillary gradient is less influenced i.e. term $K.dh_p/dz$ is negligible compared to gravitational component. Therefore it is assumed the pressure head is constant with depth. The percolation in equation (D) reduces and equal to unsaturated hydraulic conductivity. Ks is saturated hydraulic conductivity, θ_{fc} is soil moisture at field capacity and other

terms are defined as above. The water fraction leaves from SOMOS is assumed to equal of recharge amount. But this groundwater recharge is delayed due to transfer through VADOS zone.

If infiltration rate exceeds the percolation when soil in SOMOS is at saturation, the surface ponding is appears. Surface runoff occurs when ponding water increases beyond the threshold of $SUST_{max}$. The equations for these conditions are

$$\frac{d(SUST)}{dt} = P_e - ET_p - R_p - E_o \qquad \text{(E)}$$

$$Qs = SUST - SUST_{\max} \qquad \text{(F)}$$

Where E_0 is open water evaporation (mm), $SUST_{max}$ is maximum surface storage capacity and Qs is runoff.

LINRES module

LINRES controls the time that percolation of water to reach the water table at variable depths. This control is governed by a numerical transfer function

$$R = Y_n = \frac{f}{(1+f)} \sum_{i=0}^{n} (1+f)^{-i} \, Y^*_{n-i} \qquad \text{(G)}$$

$$Y_o = \frac{(1+f)}{f} R_p \qquad \text{(H)}$$

Where R is the recharge (mm/day), f is unsaturated recession constant; n is the number of reservoirs, Y^* is the result from previous time step, R_p is percolation and Y_0 is upper boundary condition.

SATFLOW module

Saturated flow module is determined the groundwater level rise or recession based on the availability or absence of recharge. This is calculated by a simple 1-D parametric groundwater model.

$$\frac{dh}{dt} = \frac{R}{STO} - \frac{h}{RC} \qquad \text{(I)}$$

Where RC is saturated recession constant (days), STO is storage coefficient, R is recharge and h is groundwater level above local base level.

Appendix G: The pumping test curves and VES, ERT survey of the Muelledes1 tracer test site

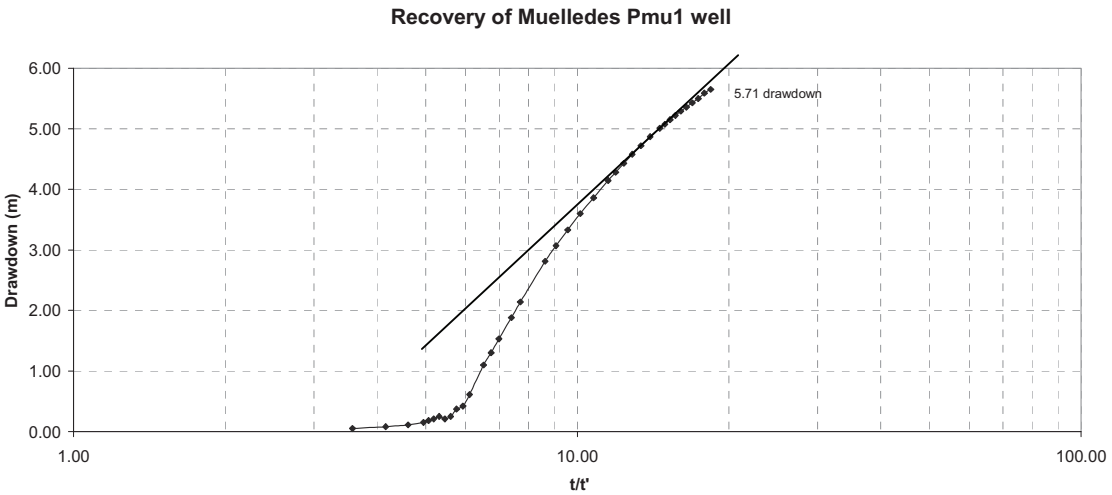

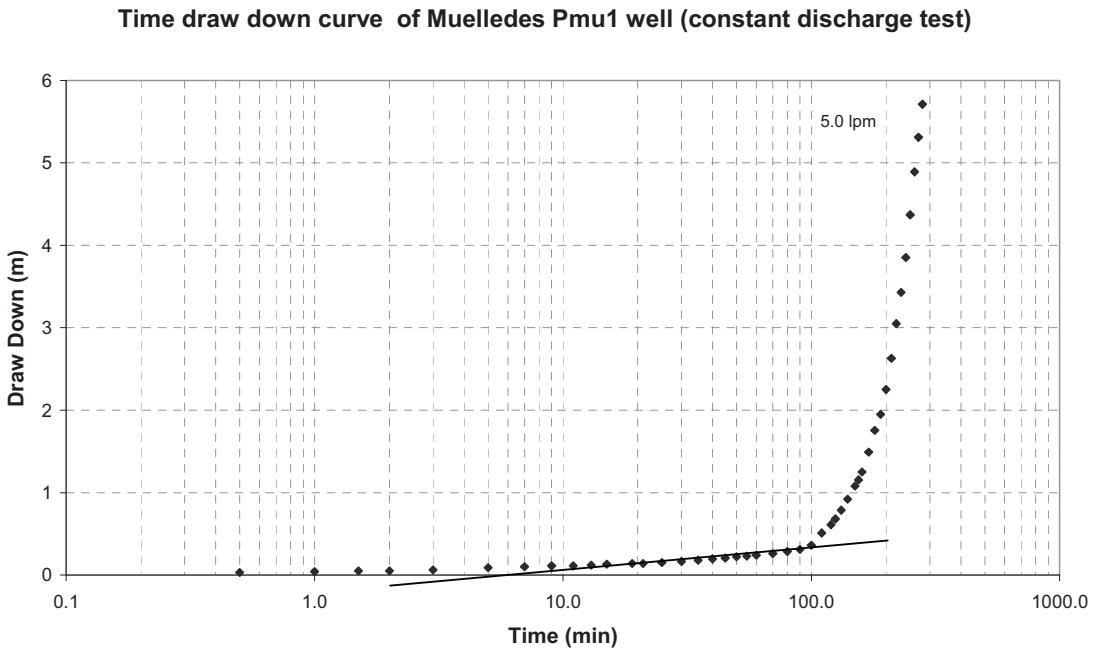

The resistivity curve of vertical electrical sounding (VES) survey at the Muelledes site

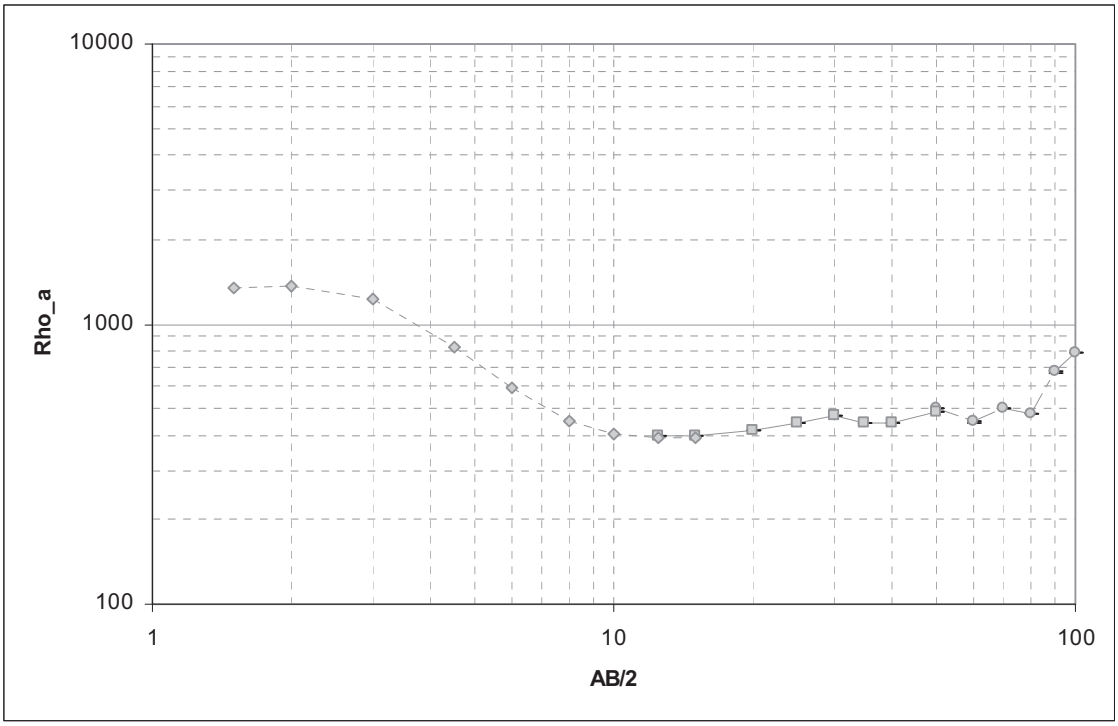

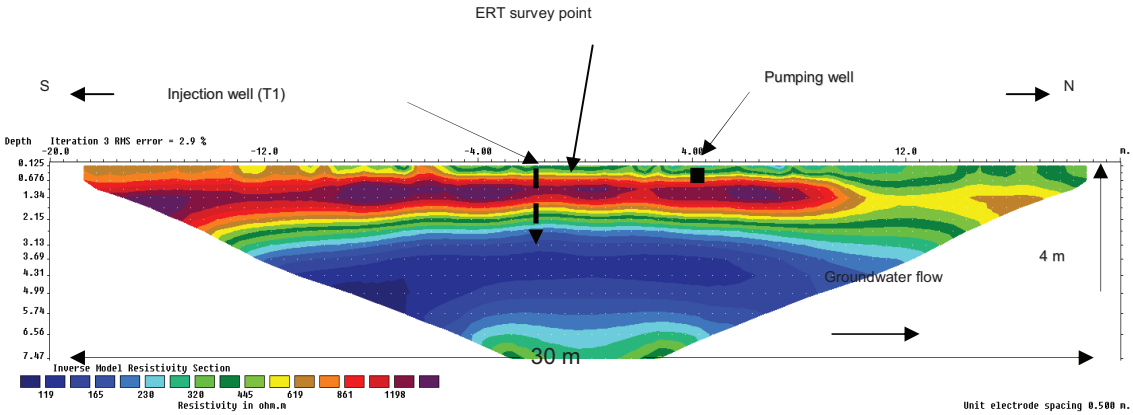

The ETR survey carried out before the tracer injection at Muelledes site

Appendix H: Simulated heads at the observed locations by the steady state model

No.	Location	UTM_X	UTM_Y	Sim. head(m)	Obs. head(m)	Residual (m)
1	Gejo	736096	4557825	799.87	807.69	7.82
2	Gjp	736503	4555731	775.08	776.15	1.07
3	Gej	741035	4551574	804.10	804.90	0.80
4	Pmu1	739472	4547705	788.58	796.87	8.29
5	Pmu2	738731	4548563	779.18	780.13	0.95
6	Pmu3	738703	4547895	783.65	798.00	14.35
7	Pnlb	738315	4554146	744.35	743.28	-1.07
8	Sdn	736378	4548919	795.39	803.59	8.20
9	Trb	739508	4555882	734.33	737.14	2.81
10	Tbgj	737842	4556719	758.76	753.40	-5.36
11	Ptm1	737006	4551116	761.66	763.42	1.76
12	Pmz0	739682	4557080	723.64	732.22	8.58
13	Psd2	738436	4548595	779.20	780.65	1.45
14	Ptm2	737067	4551353	759.48	754.78	-4.70
15	Ppn1	738330	4554144	744.19	742.57	-1.62
16	Pcl1	739491	4556314	731.07	733.70	2.63
17	Pcl3	739660	4557062	723.71	731.56	7.85
18	Pcl4	738585	4553783	741.41	739.67	-1.74
19	Pcl5	738355	4552766	743.53	742.99	-0.54
20	Pcl6	738057	4551633	746.90	746.94	0.03
21	Pcl7	738427	4551375	746.83	746.89	0.06
22	Pcl8	738414	4552392	743.43	743.00	-0.43
23	Ptmsd	737110	4549835	761.93	757.82	-4.11
24	v1	740700	4555930	770.65	750.00	-20.65
25	v2	740770	4553530	780.55	788.00	7.45
26	v3	740875	4548700	820.36	808.50	-11.86
27	v4	737380	4547455	804.28	798.00	-6.28
28	v5	734650	4548400	819.22	824.00	4.78
29	v6	735000	4552500	810.44	803.50	-6.94
30	v7	736660	4553400	775.58	774.00	-1.58
31	v8	738780	4549645	773.96	769.00	-4.96
32	v1a	740475	4554350	770.93	765.00	-5.93
33	v2a	739855	4553023	773.07	767.00	-6.07
34	v3a	739770	4548783	806.04	804.35	-1.69
35	v9	735245	4555380	808.23	807.00	-1.23
36	v10	739770	4546690	809.35	809.00	-0.35
37	v11	734425	4550250	805.89	804.00	-1.89

Appendix I: Simulated chloride concentrations at the measured locations by the steady state solute model

No.	Location	UTM_X	UTM_Y	Simulated Cl(ppm)	Observed Cl (ppm)	Residual (ppm)
1	Gejo	736096	4557825	12.17	11.62	-0.55
2	Gjp	736503	4555731	6.62	4.96	-1.66
3	Gej	741035	4551574	18.75	19.24	0.49
4	Pmu1	739472	4547705	17.52	16.13	-1.39
5	Pmu2	738731	4548563	13.73	14.33	0.60
6	Pmu3	738703	4547895	23.07	27.56	4.49
7	Pnlb	738315	4554146	15.56	16.15	0.59
8	Sdn	736378	4548919	28.88	31.47	2.59
9	Trb	739508	4555882	12.68	8.50	-4.18
10	Tbgj	737842	4556719	10.83	10.28	-0.55
11	Ptm1	737006	4551116	21.55	22.00	0.45
12	Pmz0	739682	4557080	16.20	13.93	-2.27
13	Psd2	738436	4548595	13.06	9.70	-3.36
14	Ptm2	737067	4551353	21.71	22.00	0.29
15	Ppn1	738330	4554144	15.57	16.17	0.60
16	Pcl1	739491	4556314	18.95	22.80	3.85
17	Pcl3	739660	4557062	16.26	17.52	1.26
18	Pcl4	738585	4553783	15.36	14.32	-1.04
19	Pcl5	738355	4552766	20.14	20.21	0.07
20	Pcl6	738057	4551633	22.60	25.03	2.43
21	Pcl7	738427	4551375	17.14	13.99	-3.15
22	Pcl8	738414	4552392	21.02	21.38	0.36
23	Ptmsd	737110	4549835	21.65	21.00	-0.65
24	v1	740700	4555930	15.57	16.00	0.43
25	v2	740770	4553530	15.88	16.00	0.12
26	v3	740875	4548700	16.11	16.00	-0.11
27	v4	737380	4547455	22.91	23.00	0.09
28	v5	734650	4548400	21.14	21.00	-0.14
29	v6	735000	4552500	17.06	17.00	-0.06
30	v7	736660	4553400	17.57	18.00	0.43
31	v8	738780	4549645	12.84	13.00	0.16
32	v1a	740475	4554350	14.51	14.00	-0.51
33	v2a	739855	4553023	16.62	17.00	0.38
34	v3a	739770	4548783	13.96	14.00	0.04
35	v9	735245	4555380	12.34	12.00	-0.34
36	v10	739770	4546690	19.23	19.00	-0.23
37	v11	734425	4550250	18.72	19.00	0.29

Appendix J : First and final page of the weekly groundwater level used in the transient model calibration, 2003 - 2008

Days	Date (weekly)	WL Gejo	WL Gejuello	WL Muell1	WL Muell2	WL Sardon	WL Muell3	WL Ptm1	WL Ptbgj0	WL Psd2	WL Ppn0	WL Pgjtm0	WL Pmz0	TRB
7	09/14/03	806.10	804.28	795.28	779.31									735.48
14	09/21/03	806.08	804.24	795.23	779.26									735.48
21	09/28/03	806.06	804.21	795.18	779.22									
28	10/05/03	807.21	804.08	795.44	779.47									
35	10/12/03	807.35	804.11	795.75	779.49									
42	10/19/03	807.56	804.17	795.78	779.52									
49	10/26/03	807.69	804.24	796.09	779.57									
56	11/02/03	807.72	805.36	796.43	780.68									
63	11/09/03	807.71	805.38	796.84	780.69									
70	11/16/03	807.80	805.42	796.85	780.76									
77	11/23/03	807.80	805.45	796.85	780.79									
84	11/30/03	807.80	805.43	796.88	780.79									
91	12/07/03	807.75	805.37	796.87	780.73									
98	12/14/03	807.76	805.36	796.88	780.73									
105	12/21/03	807.75	805.33	796.87	780.74									
112	12/28/03	807.78	805.35	796.87	780.78									
119	01/04/04	807.72	805.27	796.87	780.73									
126	01/11/04	807.71	805.26	796.87	780.73									
133	01/18/04	807.67	805.24	796.88	780.72									
140	01/25/04	807.65	805.23	796.86	780.72									
147	02/01/04	807.75	805.30	796.88	780.76									
154	02/08/04	807.65	805.23	796.88	780.72									
161	02/15/04	807.57	805.18	796.88	780.71									
168	02/22/04	807.52	805.22	796.88	780.74									
175	02/29/04	807.45	805.20	796.91	780.72									
182	03/07/04	807.27	805.13	796.87	780.69									
189	03/14/04	807.37	805.22	796.88	780.70									
1624	17/02/08	806.99		796.88		803.47								737.11

1631	24/02/08	807.09		796.89		803.55								737.17
1638	02/03/08	807.03		796.89		803.57								737.18
1645	09/03/08	806.86		796.89		803.57								737.15
1652	16/03/08	806.58		796.88		803.56								737.11
1659	23/03/08	806.34		796.89		803.54								737.08
1666	30/03/08	806.17		796.89		803.54								737.06
1673	06/04/08	806.07		796.82		803.52								737.03
1680	13/04/08	806.39		796.91		803.58								737.10
1687	20/04/08	806.74		796.94		803.60								737.17
1694	27/04/08	807.17		796.90		803.59								737.28
1701	04/05/08	807.01		796.87		803.57								737.15
1708	11/05/08	806.74		796.92		803.60								737.07
1715	18/05/08	806.43		796.91		803.60								737.02
1722	25/05/08	806.21		796.95		803.62								736.97
1729	01/06/08	807.43		796.97		803.63								737.05
1736	08/06/08	807.71		796.88										737.21
1743	15/06/08	807.60	805.31	796.84			797.84	763.35	753.37	780.58	743.26	776.02	732.17	736.92
1750	22/06/08	807.44	805.17	796.79			797.74	763.34	753.28	780.52	743.21		732.14	736.77
1757	29/06/08	807.43	804.58	796.67			797.57	763.31	753.25	780.35	743.14		732.10	736.71
1764	06/07/08	807.18	804.47	796.60			797.39	763.15	753.10		743.12		732.05	736.46
1771	13/07/08	806.81	804.38	796.50			797.26	763.00	752.93		743.09		732.01	736.21
1778	20/07/08	806.58	804.30	796.44			797.16	762.89	752.80		743.11		731.98	736.03
1785	27/07/08	806.48	804.27	796.38			797.10	762.90	752.74		743.03		731.92	735.91
1792	03/08/08	806.41	804.23	796.30			797.04	762.86	752.65		742.94		731.82	735.82
1799	10/08/08	806.36	804.20	796.23			796.99	762.81	752.57		742.84		731.76	735.70
1806	17/08/08	806.31	804.18	796.16			796.96	762.74	752.51		742.77		731.73	735.55
1813	24/08/08	806.28	804.16	796.09			796.93	762.62	752.44		742.71		731.69	735.48
1820	31/08/08	806.24	804.15	796.00			796.90	762.52	752.37		742.68			735.48
1827	07/09/08	806.21		796.05			796.92	762.52			742.68			
1834	14/09/08	806.18		795.96			796.90	762.46			742.62			
1841	21/09/08	806.15		795.84			796.88	762.37						
1848	28/09/08	806.12		795.79		803.11		762.45						
1855	05/10/08	806.08		795.70		803.07		762.47						

Appendix K: Field activities and characteristics of the study area

Plate I.) Differential GPS survey and data download at Muelledes ADAS station

Plate II.) Piezometric constructions and chloride analysis

Plate III.) Sample logging and collection for analysis

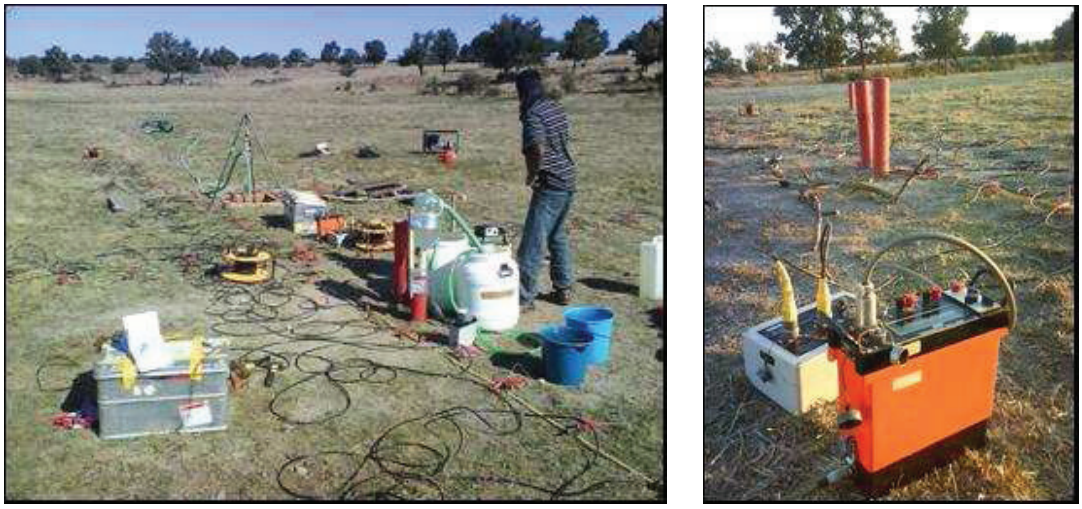

Plate IV.) Tracer test at Muelledes site in field programme September 2008

Plate V.) Two fracture network (NNE-SSW; NW-SE) and massif granite outcrops of the area